An-Najah National University

Faculty of Graduate Studies

Automatic Detection of Diabetic Retinopathy in Fundus Images by Using Fuzzy C-means (FCM) Clustering

By

Tahreer Nabeel Dwickat

Supervisor

Dr. Hadi Hamad

This Thesis is Submitted in Partial Fulfillment of the Requirements for the Degree of Master of Computational Mathematics, Faculty of Graduate Studies, An-Najah National University, Nablus, Palestine.

2018

Automatic Detection of Diabetic Retinopathy in Fundus Images by using Fuzzy C-means (FCM) Clustering

By

Tahreer Nabeel Dwickat

This thesis was defended successfully on 8/8/2018 and approved by:

Defense committee Members	**Signature**
– **Dr. Hadi Hamad/Supervisor**	**…..…….**
– **Dr. Radi Jarrar /External Examiner**	**……**
– **Dr. Ali Barakat /Internal Examiner**	**……**

Dedication

I dedicate this thesis and give special thanks to my parents, husband, brother, sisters, friends and family. Without their understanding, supporting, patience and most of all love nothing will be complete.

Thanks all.

Acknowledgments

First of all, thanks and praises to Allah for blessing me much more I deserve.

I would like to express my deep gratitude to my supervisor Dr. Hadi Hamad for his understanding, guidance, support and patience from the initial to the final stage; I really appreciate his advices and assistance for the success of this work.

Special thanks should be given to Dr. Mazen Khwaireh for his guidance, interest and valuable hints through the entire period of thesis.

And last, but not least important, very special thanks go to my beloved husband, parents, daughter who supported and encouraged me during stressful moments.

الإقرار

انا الموقع أدناه مقدم الرسالة التي تحمل عنوان :

Automatic Detection of Diabetic Retinopathy in Fundus Images by Using Fuzzy C-means (FCM) Clustering

أقر بأن ما اشتملت عليه هذه الرسالة انما هي نتاج جهدي الخاص، باستثناء ما تمت الاشارة اليه حيثما ورد، وأن هذه الرسالة ككل، أو أي جزء منها لم يقدم من قبل لنيل أي درجة علمية أو بحث علمي أو بحثي لدى أي مؤسسة تعليمية أو بحثية أخرى.

Declaration

The work provided in this thesis, unless otherwise referenced, is the researcher's own work, and has not been submitted elsewhere for any other degree or qualification.

Student's name: **اسم الطالبة: تحرير نبيل دويكات**

Signature: **التوقيع:**

Date: **التاريخ: 2018/8/8**

Table of Contents

List of Figures

List of Tables

List of Appendices

List of Abbreviation

Abbreviation	Explanation
BTH	Black top-hat transformation
CLAHE	Adaptive Histogram Equalization
DIARETDB1	Standard Diabetic Retinopathy Database Calibration Level 1
DR	Diabetic Retinopathy
FC	Fuzzy Clustering
FCM	Fuzzy C-mean
FL	Fuzzy Logic
FN	False Negative
FP	False Positive
GT	Ground Truth
HIS	Hue, Saturation and Intensity
MF	Membership Function
MM	Mathematical Morphology
N	Number of clusters
OD	Optic Disc
PLR	Positive Likelihood Ratio
PNG	Portable Network Graphics
PPV	Positive Predictive Value
RGB	Red, Green and Blue
SE	Structure Element
TN	True Negative
TP	True Positive
TT	Top-hat Transformation
WTH	White top-hat transformation

Automatic Detection of Diabetic Retinopathy in Fundus Images by using Fuzzy C-means (FCM) Clustering

By
Tahreer Nabeel Dwickat
Supervisor
Dr. Hadi Hamad

Abstract

Diabetic Retinopathy (DR) is the main cause of blindness for diabetic patients. As the exudates are the primary sign of DR, therefore early detection and timely treatment can prevent and delay the risk of vision loss. Automatic computerized screening could facilitate the screening process, reduce inspection time, and increase accuracy which is vital in ophthalmic treatment. In this thesis, we use an automatic method to detect exudates from retinal digital images with non-dilated pupils of retinopathy patients using a fuzzy c-means (FCM) clustering with a combination of morphology and pre-processing techniques.

The detection overall performance is evaluated through measuring sensitivity, specificity, positive predictive value (PPV), positive likelihood ratio (PLR) and accuracy. This measurement is done by comparing results to hand-drawn ground truth (GT) done by expert ophthalmologist; which are comparatively analyzed.

It is found that the proposed method detects exudates successfully with sensitivity, specificity, PPV, PLR and accuracy of 86.29%, 98.42%, 20.75%, 86.21 and 98.35% respectively on the testing studied database.

Chapter One
Preliminaries and Related Work

Chapter One

Preliminaries and Related Work

In this chapter, we discuss the main concepts concerning the structure and function of the eye, in addition to diabetic complications in the eye and their implications to vision. The most common diabetic eye disease is the diabetic retinopathy (DR)**.** The discussion includes some concepts and techniques used in image processing; segmentation, in addition to fuzzy logic, and fuzzy c-mean (FCM) clustering algorithm**.**

1.1 Introduction

The retina is one of the most important parts of the eyeball. It is seriously damaged by diabetes; the damage affects the tiny blood vessels in the retina of the eye, this disease is known as diabetic retinopathy (DR). DR causes changes in the retinal capillaries; the symptoms can blur or distort patients' vision, which are the main causes of vision loss. Hence, early detection is necessary to treat diabetic retinopathy and protect patients from blindness [7].

Diabetes is the fourth leading cause of death in Palestine after cardiovascular, cancer and cerebrovascular diseases [43]. Diabetes increases the risk of eye diseases; indeed, the main cause of blindness associated with diabetes is DR, where more than 80% of people with diabetes are at risk of developing DR [43]. Exudates is a primary sign of DR which is a common retinal complication associated with diabetes [69], it can be identified as random whitish or

yellowish colored areas with varying shapes, sizes and locations. They normally appear near the leaking capillaries within the retina [28].

Current methods for detection and evaluation of DR are expensive, manual, not accurate and time consuming. Therefore, we need an alternative method toward the detection; which is called Automatic Retinopathy detection system; that has attracted large popularity in recent years, where computer vision is employed in addition to image processing techniques to detect different features associated with retinopathy [8]. Automated methods of DR screening help to save time, cost and vision of patients compared to the manual methods of diagnosing [67].

Our proposed method based on clustering and fuzzy logic; where clustering is an unsupervised approach widely applied in image segmentation and statistics; it is useful in conditions where little former knowledge exists [52]. It can be used to organize a set of feature vectors into groups (clusters) based on resemblances of individual data items [63].

The main steps of clustering are: identifying salient features, detecting anomalies, and finally classifying data [63]. Clustering techniques use a centroid to represent each cluster based on the similarity with the centroid of the cluster features [24].

Another possible classification of clustering methods can be categorized into the following two types; crisp (hard) and fuzzy (soft) clustering algorithm [24], we will explain them in chapter two.

Hard clustering methods are based on classical set theory, this means a pixel belongs to one and only one cluster (see Fig.1.1.1: (a)). A popular and well known hard clustering algorithm is K-means clustering algorithm [57].

Fuzzy clustering is an unsupervised soft segmentation technique which has been implemented in image segmentation, the objects belong to several clusters having different degrees of membership [63] (see Fig.1.1.1).

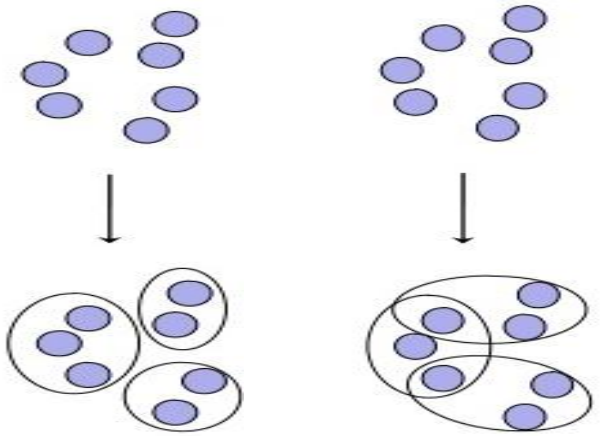

(a) (b)

Fig.1.1.1: Visual example of clustering types: (a) Hard, (b) Fuzzy [34].

Many clustering algorithms are based on Fuzzy logic (FL), for instance: FCM (fuzzy C- means), GK (Gustafson-Kessel), GMD (Gaussian mixture decomposition), FCV (Fuzzy C varieties) algorithms … etc. [33].

One of the most important clustering algorithms is FCM, which based on Fuzzy Logic.

FL was introduced by professor Zadeh in 1965 [52]. It offers several unique features that make it a particularly good alternative for many control problems. It poses the ability to mimic the human mind to effectively employ modes of reasoning that are approximate rather than exact [66].

FL techniques have been used in image-understanding applications such as detection of edges, feature extraction, classification, and clustering [32]. It can model nonlinear functions of arbitrary complexity to a desired degree of accuracy; it is a convenient way to map an input space to an output space [32]. It is inherently robust since it does not require precise, noise-free inputs [66].

1.1.1 Literature Review

Automatic exudates detection is a desire as it is an important step in improving human health. Hence many scientists worked to implement it in real life. In the following we would like to mention some of the related work.

A. Sopharak et al. [7] have proposed an automatic method to detect the exudates using FCM clustering algorithm. Firstly, applying contrast enhancement preprocessing, then extract the features from the modified image. These image features consist of intensity, standard deviation of the intensity, and hue. Numbers of edge pixels are used as input parameters to construct a coarse segmentation by using FCM clustering method. After that using some subsequent morphological reconstruction are implemented to obtain better segmentation results.

Finally, they validated there results by comparing them with ground truth (GT). They have used sensitivity, specificity, positive predictive value (PPV), positive likelihood ratio (PLR) and accuracy to evaluate the overall performance which came to be 87.28%, 99.24%, 42.77%, 224.26 and 99.11%, respectively.

M. Gandhietet et al. [40] proposed an automatic method for the detection of exudates using the FCM clustering technique and reconstruction through a superimposition process in the absence of dilating patient's eye. After that, they compared the results of the FCM clustering to the results of another clustering technique called Fuzzy K-Means segmentation. The sensitivity and specificity values for the exudates detection using the FCM algorithm were 87.38% and 96.94%, respectively. On the other hand, sensitivity and specificity values for exudates detection using the K-Means algorithm were 75.04% and 93.73%, respectively.

A. Osareh, et al. [22] published their work using FCM clustering to classify the segmented regions into exudates and non-exudates. An artificial neural network classifier was investigated. Their study indicates that automated evaluation of digital retinal images could be used to screen exudative diabetic retinopathy. The proposed system can achieve a diagnostic performance with 95.0% sensitivity and 88.9% specificity for the identification of images containing any evidence of retinopathy.

S. Babu, et al. [65] present a new, fast, fully automatic optic disc and fovea localization algorithm developed for DR screening. The DR disease detection involving the following fundamental stages: Pre-processing, feature extraction, fovea detection and disease identification. The accuracy and sensitivity of the diabetic retinopathy detection system are 98.5% and 98.7% respectively.

S. Rashid et al. [69] proposed an automated method to detect exudates from low-contrast digital images of retinopathy patients with non-dilated pupils

using feature based FCM clustering technique, it was implemented by a combination of morphological and pre-processing techniques, and these were used to improve the robustness of blood vessels and optic disk detection. Robustness and accuracy of the method have been evaluated on a database of different images. The accuracy values increase when the FCM clustering technique is combined with morphological techniques.

G. BabuKande et al. [23] proposed a system to detect optic disk and exudates from retinal images. They composed three steps to localize optic disc: estimate the center of the OD by finding a point that has maximum local variance. The color morphology in Lab space is used to have homogeneous OD region. The boundary of the OD is located using geometric active contour with variation formulation. For the other part, exudates identification, the processes involve pre-processing, OD elimination, and segmentation of exudates, that are extracted based on Spatially Weighted FCM clustering algorithm. It is formulated by incorporating the spatial neighborhood information into the standard FCM clustering algorithm. The performance of their proposed algorithm were: optic disc detection had 92.53% accuracy, while exudates detection sensitivity and specificity of the proposed algorithm were 86% and 98% respectively.

S. Habashy [67], detects the abnormalities in the retina such as the structure of blood vessels, micro-aneurysms, and exudates using image processing techniques. Identification of DR stages using Fuzzy C-means Classifier. This system intends to help ophthalmologists in the process of screening DR to

detect symptoms faster and more easily. The sensitivity, precision and accuracy were 98.01%, 99%, and 97% respectively.

In this research, we propose an automated method for the detection of exudates using the FCM clustering technique. This method is divided into four parts: first, detect and eliminate the OD and blood vessels from retinal image, after that apply pre-processing steps to detect candidate exudates, then implement the FCM clustering algorithm to the candidate results of the previous stage, finally using morphological reconstruction to complete identification of exudates.

This thesis is organized as follows: In chapter one, some concepts of eye anatomy, eye diseases, image processing and fuzzy logic are introduced. Chapters two, the fuzzy system properties and FCM clustering algorithm are reviewed. In chapter three, we discuss the algorithm used to eliminate the features of the retina (OD and blood vessels) to help us detect the exudates from retinal images. In chapter four, methodologies behind this approach are discussed; the discussion is divided into four parts; preprocessing step, different features employed for abnormality detection, explaining the FCM clustering algorithm and finally describing the system performance by using the accuracy measurement. Chapter five gives some numerical results, conclusions and reviews of future work.

1.2 Structure and Function of the Eye

The eye is the organ that allows us to see; it is a highly specialized organ of photoreception for processing light from the environment to produce potential actions in specialized nerve cells [14].

A picture of human eye can be seen in Fig.1.2.1. From the optical point of view, the black central circle, which is the pupil area, and the structured iris are the most interesting parts. Light reflected from an object is focused on the retina after passing through the cornea, pupil and lens respectively [35].

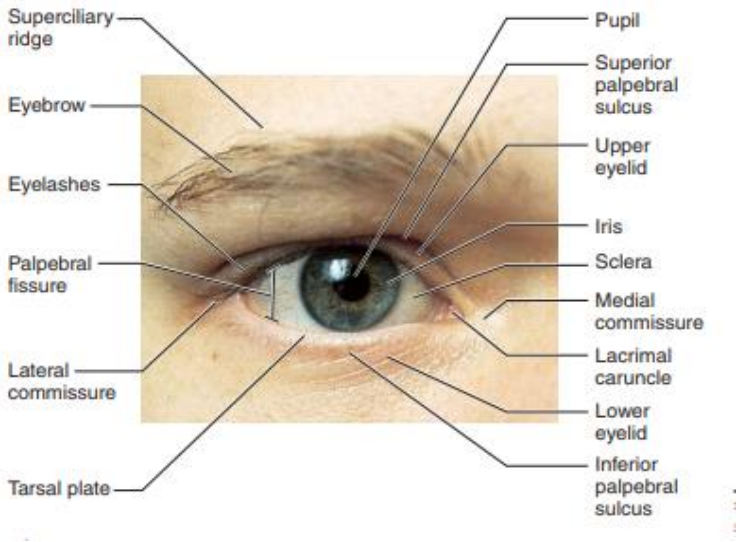

Fig.1.2.1: The external structure of the eye [35].

The eyeball consists of three main components which are shown in Fig1.2.2:

1. The tunics; which are three layers that make up the exterior wall of the eyeball, which are: the sclera, choroid, and retina.
2. The optical components of the eye; these are transparent elements that admit light rays, bend (refract) them, and focus images on the retina, also known as the refractile media components, which consist of: cornea,

aqueous humor, lens, and vitreous body that contains a fluid component called the vitreous humor, which admit and focus light on the retina.

3. The neural components; which consist of the retina and the optic nerve.

One important part of the eye that should be described for its particular importance is the "retina", that is the third and the most inner layer of the eye [35].

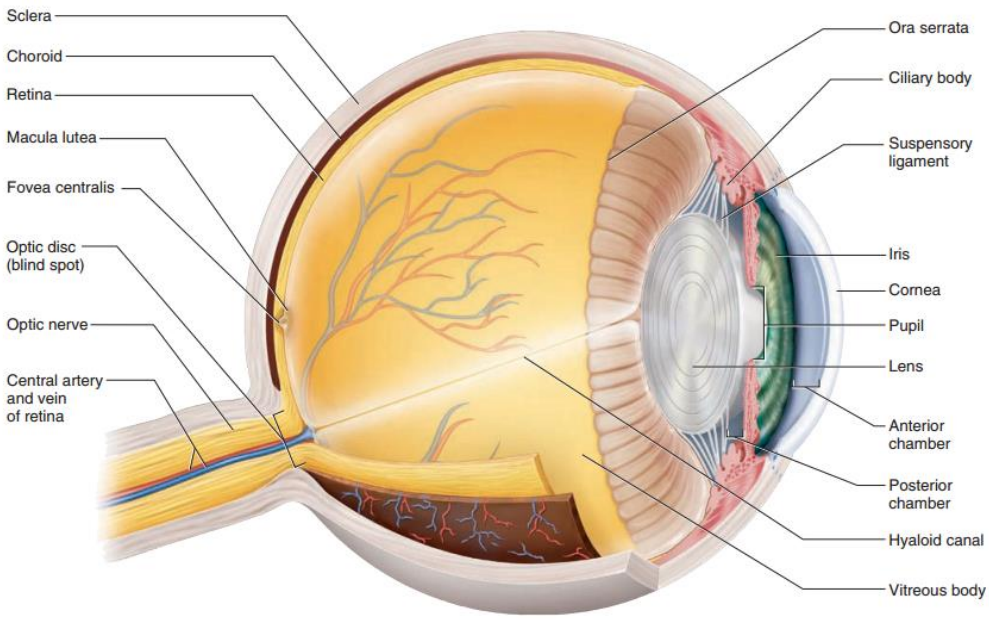

Fig.1.2.2: Cross-sectional anatomy of the eye [35].

1.3 Structure and Function of the Retina

The retina is a thin layer of tissue at the back of the eyeball which converts the received light to electrical nervous signals and sends it to the brain, retina is the “seeing tissue” of the eye [28].

The retina contains photoreceptor cells called rod cells and cone cells; turning visible light into neuronal signals, which are sent to the brain. This process is called transduction. The cone cells are about 6 million cones in the retina, that

are sensitive to different wavelengths of light, providing color sensitivity which is of most use in the daytime. The lack of cones which are sensitive to red, blue, and green light causes various kinds of color blindness [39].

The rod cells are the most numerous of 120 million and very sensitive to light and do not distinguish color, which means the rods are more effective in low light conditions than cones, and are crucial for seeing at night.

Retina has some particular features, these features are optic disc, blood vessels and fovea [15] Fig.1.3.1 shows the anatomy and features of the human retina, these features are discussed below:

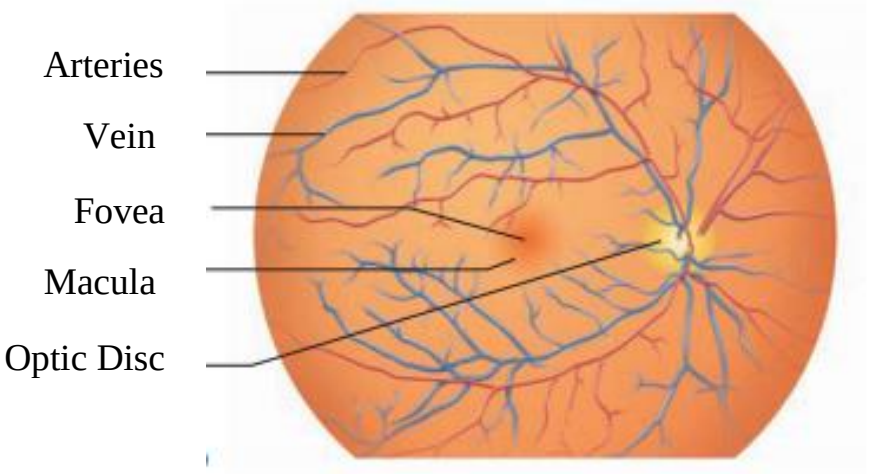

Fig.1.3.1: Retina surface anatomy [35]

1.3.1 Optic Disc (OD)

The optic disc (OD) is the brightest region on the retina at which the optic nerve axons enter and leave the eye, it contains no receptor cells, so it represents a blind spot in the visual field of each eye. The OD location is a very important matter and can be used as an origin to determine the position of other parts such as Fovea and blood vessels.

Any change in shape, size, and color of OD is an important indicator of various pathologies related to eye [29].

1.3.2 Blood Vessels

Retina is surfaced by blood vessels; there are two types of vessels, arteries and veins that are visible within Fig.1.3.1. Arteries are brighter as they transport blood rich in oxygen to the organs of the body, while the veins afterwards transport the blood to the lungs and the liver, which is at low oxygen level and thus darker.

Information about blood vessels in retinal images can be used to detect severe retinal diseases such as DR from an abnormal retinal image [13, 16].

1.3.3 Macula

The macula in the human eye is a small functional area, measuring about 5 mm in diameter. It centers the retina see Fig.1.3.1 and it is the place where light is focused by the structures in the front of the eye (cornea & lens). The macula is very important as it gives us the vision needed for detailed activities such as reading, and the ability to differentiate colors [39].

1.3.4 Fovea

Fovea or the “yellow spot” is a minute area at the center of the macula, that is most sensitive to light and is responsible for our sharp central vision, and there are no rods in the fovea [39, 3].

1.4 Fundus Image

Medical image analysis is a research area that currently attracts a lot of interest from both scientists and physicians. The objective of this field is to develop computational tools which will assist quantification and visualization of interesting pathology and anatomical structures [51]. In this research, these tools work with digital fundus image of the eye.

The procedure of taking fundus images start by either non-dilating or dilating the pupil with pharmaceutical eye drops, by using specialized fundus cameras that consist of an intricate microscope attached to a flashed enabled camera used in fundus photography, this is illustrated in Fig.1.4.1. The patient is asked to stare at a fixation device in order to steady the eyes. While taking the pictures, the patient will see a series of bright flashes. The entire process takes about five to ten minutes. A fundus is shown in Fig.1.4.1. The eye fundus images of diabetic patients must be examined at least once a year, to ensure that DR treatment is received on time [51].

Fig.1.4.1: Fundus photography [62].

Retinal images obtained by the fundus camera are used to diagnose DR. Every healthy retina has some normal features; these normal features are optic disc, blood vessels and fovea. Apart from these, an unhealthy retina might have some abnormal features like hemorrhages, micro-aneurysms and exudates [15, 76].

1.5 Eye Diseases

In this section, we discussed the diabetic complications, diseases and symptoms in the eye and their implications to vision. Diabetic retinopathy (DR) is the most common diabetic eye disease, the current and future prospects of early detection are discussed. The discussion includes the shortcomings of the current diagnosis and the potential benefits of automated eye fundus image analysis.

Current methods of detection and assessment of DR are manual, expensive, and require trained ophthalmologists. Automated methods of DR screening help to save time, cost and vision of patients, compared to manual diagnosing methods [4].

The screening of diabetic patients for the development of DR can potentially reduce the risk of blindness in these patients by 50%. An early detection of DR is important, because treatment methods can slow down the progression of the disease. Nevertheless, early detections enable laser therapy to be performed to prevent or delay visual loss and may be used to encourage improvement in diabetic control [9].

1.5.1 Diabetic Eye Diseases

Diabetes is a condition where the amount of glucose in blood is too high, this happened when the pancreas doesn't produce any enough insulin to help glucose enter in the body cells, then glucose stays in the blood and it is not consumed by cells. Consequently, blood glucose levels get too high and can cause diabetes, where glucose is the main type of sugar found in blood considered as the main source of energy [47, 76].

This disease affects slowly the circulatory system including that of the retina, and it is one of the leading causes of irreversible blindness worldwide [76], diabetic eye disease also encompasses a wide range of other eye problems such as cataract, nonvascular glaucoma, DR, and diabetic neuropathies [48].

Cataract is a clouding of the lens, it is also developed at an earlier age in people with diabetes [48].

Glaucoma is one of the many eye diseases which can lead to blindness if it is not detected and treated in proper time, this disease causes an increase in pressure of the eye, which leads to optic nerve damage [18].

The most serious eye condition associated with diabetes involves the blood vessels network supplying the retina. This condition is called DR. Some of the effects of the diabetic eye disease on vision are illustrated in Fig.1.5.1.

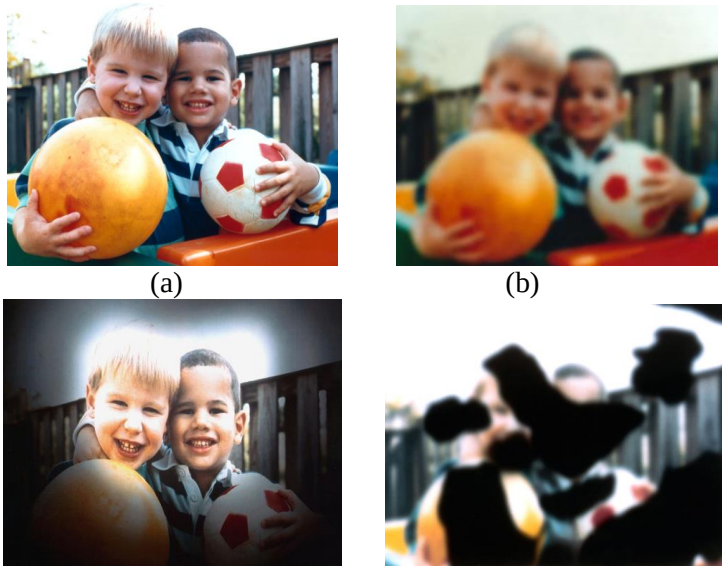

(a) (b)

(c) (d)

Fig.1.5.1: Influence of diabetes on vision: (a) Normal vision, (b) Cataract, (c) Neovascular glaucoma, (d) Diabetic retinopathy [48].

1.5.2 Diabetic Retinopathy (DR)

The most serious complication of diabetes for eye is DR. It blurs the vision, if left undiagnosed and untreated it can eventually lead to blindness [65]. Retina is fed by a network of blood vessels and any change in these blood vessels can cause difficulties with vision. DR occurs when the small blood vessels have a high level of glucose in the retina causing a change in the retina, which occurs over a period of time under diabetics [67].

The symptoms can blur or distort the patient's vision, **exudates** are one of the primary signs of DR, and it is vital symptoms of DR. They appear as yellowish areas with varying sizes, shapes, and locations about areas of leakage, as shown in Fig.1.5.2: (a) Exudates are made up from serum lipoproteins and usually occur when lipid or fat leaks from abnormal blood

vessels or aneurysms, they normally appear near the leaking capillaries within the retina [16].

In extreme stages of DR, certain spots called the **cotton wool spots** are identified. They appear as fluffy white patches on the retina, see Fig.1.5.2: (b). They are caused by the damage of nerve fibers as a result of accumulations of axoplasmic material within the nerve fiber layer because of the ischemia. This causes the nerve fibers to be damaged by swelling in the surface layer of the retina [9].

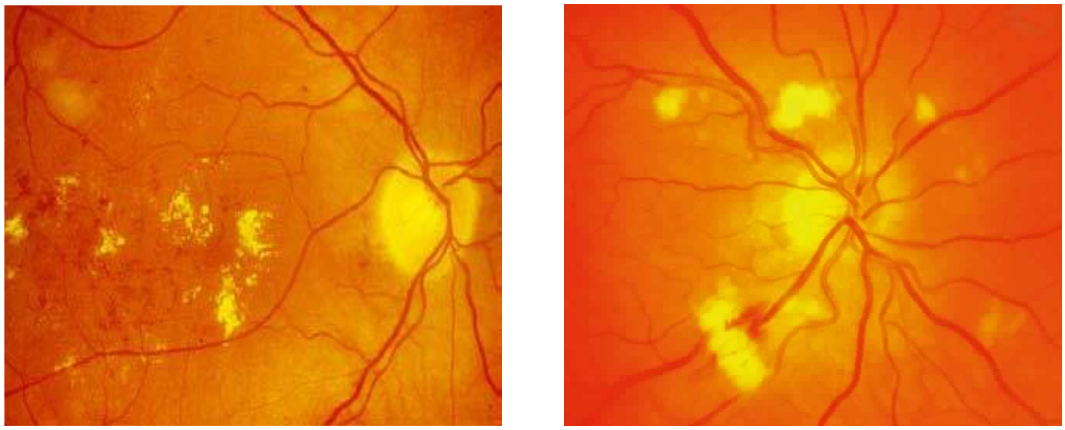

(a) (b)

Fig.1.5.2: A retinal image with (a) Exudates, and (b) Cotton wool spots [28].

Micro-aneurysms are almost always the first clinical sign of DR, they are the focal dilations of retinal capillaries, where it appears as small, round and deep red spots 15 to 60 μm in diameter [9]. Micro-aneurysms occur when walls of the blood vessels become fragile and then start to break, leaking blood around them [67], rupture of micro-aneurysms and increased capillary permeability give rise to intra retinal hemorrhage [28], an example is shown in Fig.1.5.3.

Hemorrhage occurs when blood leaks from the retinal vessels. It can be caused by hypertension, blockage of arterial vein or diabetes mellitus [67]. Retinal hemorrhages appear either as small red dots or blots indistinguishable from micro-aneurysms or as larger flame-shaped hemorrhages [28].

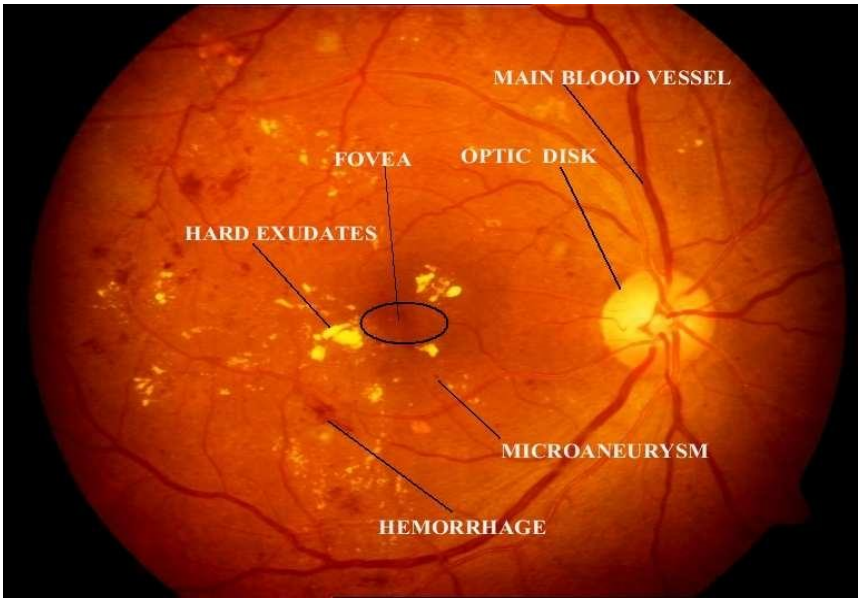

Fig.1.5.3: DR effect on a fundus image; showing normal features (OD, blood vessels and fovea), and abnormal features (hemorrhages, micro-aneurysms and exudates) [19].

1.6 Image Processing

Image processing, analysis and computer vision techniques are increasingly used in all fields of medical science and are especially pertinent to modern ophthalmology. Retinal image analysis is one of the promising topics in medical image processing [58].

Medical image processing is a process of converting an image or photo into a digital form and performing some steps and procedures so that the image can be enhanced to extract more information from it [58].

The aim of processing an image normally falls into one of the three broad categories: enhancement (e.g. improved contrast and content), restoration (e.g. de-blurring of an image) and segmentation (e.g. isolating particular areas of interest within the image) [46].

Transforming the image into different formats is another technique used in image processing; it involves manipulation of the entire image so that pixel's vales are represented in a different but equivalent form. This may allow more efficient and powerful processing before the image is reverted to its original mode of representation [58, 46].

1.6.1 Image Segmentation

Image segmentation is a process of partitioning its pixels into a set of non-overlapping regions or categories whose union is the original image.

In other words; image segmentation is the process of assigning a label to every pixel in an image such that pixels with the same label share certain characteristics. Every pixel in a segmented image is allocated to one of a number of these categories, segmentation stops when all objects of interest have been isolated [6]. Consequently, the process of image segmentation is equivalent to the process of clustering; that is grouping image parts with similar features into regions (clusters) [12].

Image segmentation approaches are currently divided into the following categories:

1. **Detecting Discontinuities**

   It means to divide an image based on abrupt changes in intensity, such as edge detection segmentation algorithms [24]

2. **Detecting Similarities**

   It means to divide an image into regions that are similar according to a set of predefined criteria, like thresholding, region splitting, region growing and merging image segmentation algorithms [57].

   In the following we introduce some of the most important general approaches of segmentation:

1.6.1.1 Edge-Based Segmentation

Edge detection is a fundamental tool for image segmentation; it is used for object detection which serves various applications like medical image processing, biometrics … etc. The major property of the edge detection technique is its ability to extract the exact edge line with good orientation [60]. Edge carries a lot of information about the various regions in an image. They provide an outline of the object and can be used to measure the size of objects or to recognize and isolate objects [46].

An edge is said to be a set of connected pixels that lies on the boundary between two regions that differ in color intensity. These pixels on the edge are called edge points. Edge detection technique is boundary identification

where the information of the edge is detected and edge pixels with adjacent neighbor connectivity are tracked, this is illustrated in Fig.1.6.1**:** (b) [46].

An edge detection operation is basically an operation to perceive important local changes in the intensity level of an image. It is measured by gradient of the image, this can be done by the application of specialized filters of varying complexity and utility [58]. Applying the threshold technique to the resultant image creates a binary image of the edges [46].

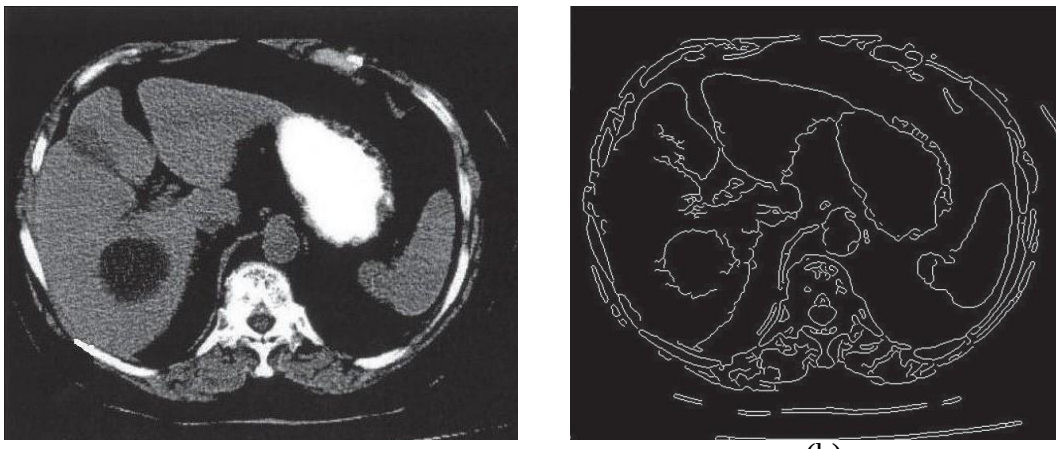

(a) (b)

Fig.1.6.1: Segmentation of abdomen image (a) Original abdomen image, (b) Result of Edge-based segmentation [75].

There are many edge detection techniques, the main common ones are: Roberts, Sobel, Prewitt, Kirsh, Robinson, Marr-Hildreth, LoG and Canny edge detection techniques [60].

1.6.1.2 Threshold Based Segmentation

Thresholding is the simplest, most powerful and commonly used method of image segmentation; it is used when images having light objects on dark background, the process of thresholding may be particularly useful to

remove unnecessary details or variations through high lighting details that are of interest [57].

Thresholding operation converts a multilevel image into a binary image (only two values: 0 or 1), this involves separating the image into white or black pixels on the basis of whether their intensity value is greater or less than a certain threshold level *t* [46].

The thresholding operation is defined by equation (1.6.1) [58]:

$$\boldsymbol{f}(x) = \begin{cases} \mathbf{0}, x < t \\ \mathbf{1}, x \geq t \end{cases} \tag{1.6.1}$$

where $\boldsymbol{f}$ is the thresholded image, x represents a grey value, and t is the threshold value. After the thresholding operation, the image has been segmented into two segments, identified by pixel values 0 or 1, see Fig.1.6.2: (b) [58].

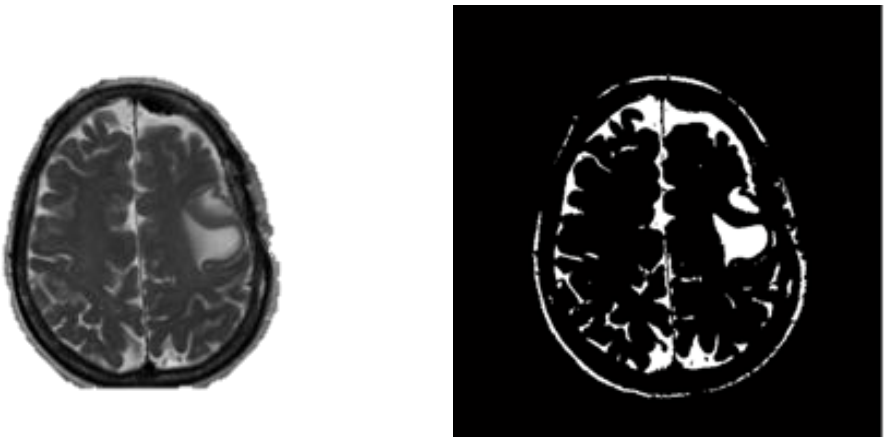

(a) (b)

Fig.1.6.2: Thresholding segmentation (a) Original brain image, (b) threshold based segmentation [75].

Thresholding method has a set of limitation. One of which is that cannot be applied to multichannel images and only two classes are generated. In

addition, thresholding does not take into account the spatial characteristics of an image. As a result, it is sensitive to noise, as both of these artifacts corrupt the histogram of the image, making separation more difficult [57].

1.6.1.3 Region Based Segmentation

Region based segmentation algorithms are relatively simple and more immune to noise [63]. These methods separate an image into regions of connected homogenous subsets with respect to some criterion such as gray level, texture, or the group of connected pixels with similar properties, as shown in Fig.1.6.3: (b) below [57]. In the region-based segmentation, pixels which correspond to a particular object are grouped together and marked using appropriate thresholding techniques. The significant principles upon which it depends are value similarity and spatial proximity [63].

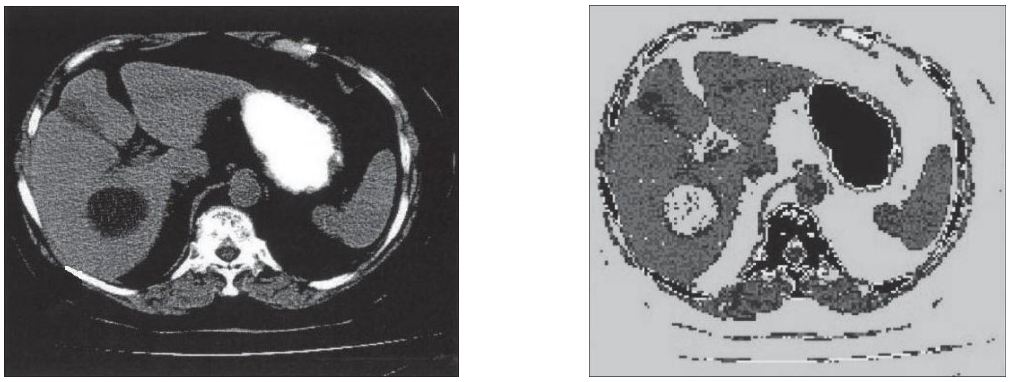

(a) (b)

Fig.1.6.3: Based segmentation (a) Original abdomen image, (b) region based segmentation [75].

1.7 Fuzzy C-means (FCM) Clustering

FCM is based on soft computing and overlapping clustering algorithms [71], which allows each point to belong to one or more cluster with different degrees of membership. This method is frequently used in pattern recognition [4, 6].

FCM technique is a popular method used in image segmentation because it can preserve more information from the original image. Its robust characteristics for ambiguity and can retain more information than hard segmentation methods do [63]. It was developed by Dunn and improved by Bezdek [7].

Features with close similarity values in an image are grouped into the same cluster. The similarity is defined by the distance between features vectors to clusters centers by using the Euclidean distance, where data will be associated to an appropriate membership value having grades between 0 and 1. The clusters centers are updated until the differences, as displayed in equation (1.7.1), are close to zero or practically less than a predefined small constant, the equation is described as the adjacent objective function [67,71,8]:

$$J(\boldsymbol{u}, \boldsymbol{c}, \boldsymbol{x}) = \sum_{i=1}^{N} \sum_{j=1}^{C} u_{ij}^{m} \left\| x_i - c_j \right\|^2 \qquad (1.7.1)$$

$$u_{ij} = \frac{1}{\sum_{k=1}^{C} \left(\frac{\left\| x_i - c_j \right\|}{\left\| x_j - c_k \right\|} \right)^{\frac{2}{m-1}}} \qquad (1.7.2)$$

$$c_j = \frac{\sum_{i=1}^{N} u_{ij}^{m} \; x_i}{\sum_{i=1}^{N} u_{ij}^{m}} \tag{1.7.3}$$

where *m* is an exponential weighting function, that controls the fuzziness of the membership function, it has any real number greater than 1, it is set to 2 by Bezdek [71], *J* be the objective function of the FCM, *N* is the number of features, x_i is the i^{th} element of *d*-dimensional measured data, u_{ij} is the degree of membership of x_i in cluster *j*, *C* is the number of clusters, c_j is the *d*-dimension center of cluster *j*, and ||*|| is any norm expressing the similarity between any measured data and the center. The update of membership u_{ij} and the cluster centers c_j are carried by equations (1.7.2) and (1.7.3), respectively. This iteration will stop when equation (1.7.4) is satisfied:

$$\max_{ij}\left\{\left|u_{ij}^{K+1} - u_{ij}^{K}\right|\right\} < \epsilon \tag{1.7.4}$$

where ϵ is a termination criterion, *K* is the maximum iteration step [4, 64]. Under the normalization constraint the following condition should be maintained:

$$\sum_{i=1}^{C} u_{ij}^{m} = 1 \;,\; \forall j = 1, \dots, N \tag{1.7.5}$$

Finally, Lagrangian multipliers are introduced to solve this constrained optimization problem, where the Lagrange function $\underline{L}$ is given by [52, 42]:

$$\underline{L}(\boldsymbol{u}, \boldsymbol{c}) = J - \sum_{i=1}^{N} \alpha_i \left(\sum_{j=1}^{C} u_{ij}^{m} - 1\right) \tag{1.7.6}$$

where α_i is the Lagrange multiplier. The algorithm will be explained in detail later.

Chapter Two
Fuzzy Logic

Chapter Two

Fuzzy Logic

This chapter presents the fundamental concepts of Fuzzy Logic such as fuzzy sets, fuzzy logic properties and FCM clustering.

2.1 Fuzzy Logic (FL)

The idea of FL was introduced by Professor L. A. Zadeh from the University of California in 1965 [41], it attempts to reflect the human way of thinking. It is so often utilized in our routine life, for instance, to answer some questions in certain surveys, most time one could answer with 'Not Very Satisfied' or 'Quite Satisfied', which are also fuzzy (ambiguous) answers [61].

FL is an extension of Boolean logic, based on the mathematical theory of fuzzy sets, which is a generalization of the classical set theory [32].

2.1.1 Classical Set

The classical set is defined by crisp boundaries [21]. To make it clearer we introduce some examples; {4, 9, 8, 6} is a set of integers. {1, 2, 3, 4, 5, 6, 7, 8} is the set of integers between 0 and 9. {"Book", "Run", "Eye", "see"} is a set of words, and ∅ is defined as the empty set which contains no element.

In Fig.2.1.1 below, we can see the graphical representation of a set $\boldsymbol{A}$, typically represented by circles, $\boldsymbol{A} = \{4, 9, 8, 6\}$, where $\boldsymbol{A}$ is a subset of $\boldsymbol{S}$ which is the universal set.

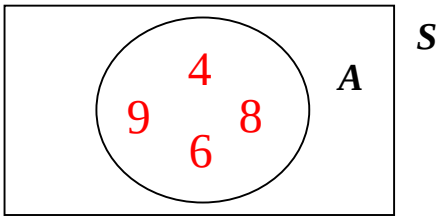

Fig.2.1.1: Graphical representation of set A (Vinn diagrams).

In a crisp set, membership or non-membership of element x in set $\boldsymbol{A}$ is described by a characteristic function $\boldsymbol{\mu_A}(x)$, where

$$\boldsymbol{\mu_A}(x) = \begin{cases} 1\,, x \in \boldsymbol{A} \\ 0\,, x \notin \boldsymbol{A} \end{cases}$$

where {0,1} is called valuation set; where 1 indicates membership, while 0 indicates non-membership [54], Fig.2.1.2 illustrates the membership function for a crisp set.

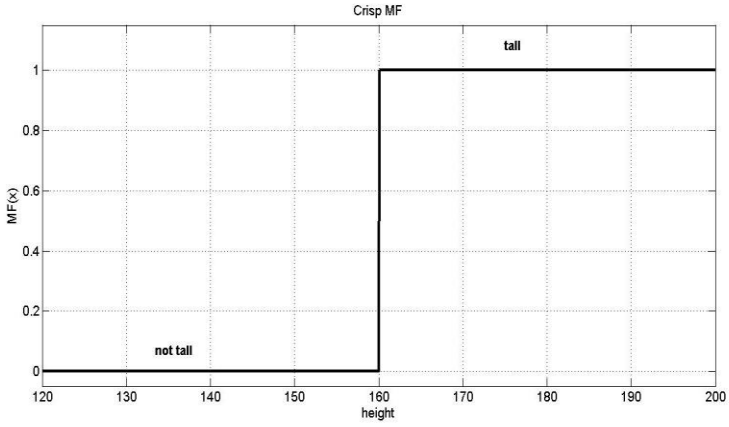

Fig.2.1.2: Crisp membership function (MF).

Some properties of classical set operations are defined in Table 2.1.1, assuming $\boldsymbol{S}$ is the universal set which means a collection of objects that have the same main characteristics [61], $\boldsymbol{A}$ and $\boldsymbol{B}$ are two classical sets, $\overline{\boldsymbol{A}}$ complement set of $\boldsymbol{A}$ and $\emptyset$ is the empty set [25], where the set $\emptyset$ is defined as [54]:

$$\boldsymbol{\mu_\emptyset}(x) = 0, \qquad \forall x \in \boldsymbol{S},$$

Table 2.1.1: Properties of Classical Set Operations

Name of property	Properties
	$\boldsymbol{A \cup A = A}$
	$\boldsymbol{A \cap (A \cup B) = A}$
	$\boldsymbol{A \cup (A \cap B) = A}$
	$\boldsymbol{A \cap (\overline{A} \cup B) = A \cap B}$
	$\boldsymbol{A \cup (\overline{A} \cap B) = A \cup B}$
	$\boldsymbol{A \cup S = S}$
	$\boldsymbol{A \cap S = A}$
	$\boldsymbol{A \cup \emptyset = A}$
	$\boldsymbol{A \cap \emptyset = \emptyset}$
	$\boldsymbol{A \cup \overline{A} = S}$
	$\boldsymbol{A \cap \overline{A} = \emptyset}$
Involutive law	$\boldsymbol{\overline{\overline{A}} = A}$
Commutative law	$\boldsymbol{A \cup B = B \cup A}$ $\boldsymbol{A \cap B = B \cap A}$
Associative law	$\boldsymbol{(A \cup B) \cup C = A \cup (B \cup C)}$ $\boldsymbol{(A \cap B) \cap C = A \cap (B \cap C)}$
Distributive law	$\boldsymbol{A \cap (B \cup C) = (A \cap B) \cup (A \cap C)}$ $\boldsymbol{A \cup (B \cap C) = (A \cup B) \cap (A \cup C)}$
DeMorgan's law	$\boldsymbol{\overline{A \cap B} = \overline{A} \cup \overline{B}}$ $\boldsymbol{\overline{A \cup B} = \overline{A} \cap \overline{B}}$

Defining a set of operations using Vinn diagrams, which are very intuitive, such as the union and intersection operations on the classical set are shown in Fig.2.1.3: (a), (b) respectively [21].

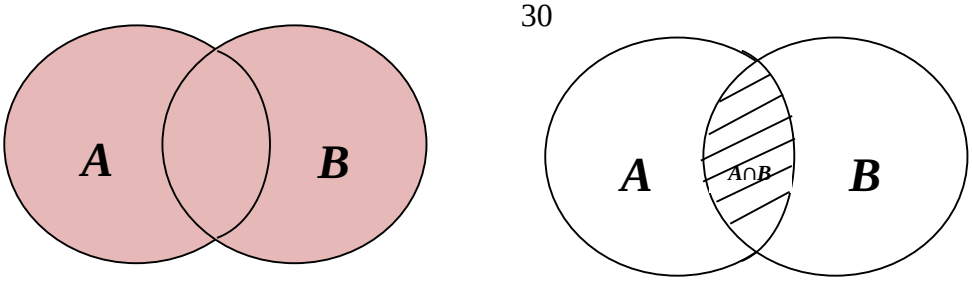

(a) (b)

Fig.2.1.3: The shaded area represents the union and intersection of two sets respectively (a) Union, $A \cup B$, (b) Intersection, $A \cap B$.

2.2 Fuzzy Sets and Operations

The theory of fuzzy sets is a generalization of the classical (crisp) set theory, which means that the classical set is a special case of fuzzy sets theory, this concept is illustrated in Fig.2.2.1.

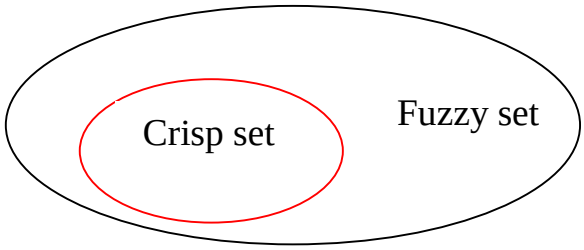

Fig.2.2.1: The classical set is a subset of fuzzy sets.

In order to introduce the concept of fuzzy sets, we first review the elementary set theory of classical mathematics.

The fuzzy set theory is a very natural extension of the classical set theory [32], which is considered as a subset of the fuzzy set. It extends this concept by defining partial membership. Fuzzy sets represent common sense linguistic labels like small, large, medium, high, tall, etc. A given element can be a member of more than one fuzzy set at a time [54, 25].

After defining the classical (crisp) set in the previous section, fuzzy sets are defined in the following, in addition to their properties and operations.

2.2.1 Definition and Properties of Fuzzy Sets [54, 74, 17]

Definition 1. Let $\boldsymbol{X}$ be a universal set. A fuzzy subset $\boldsymbol{A}$ of $\boldsymbol{X}$ is characterized by a membership function:

$$\boldsymbol{\mu_A}(x)\boldsymbol{:}\ \boldsymbol{X} \rightarrow\ [\mathbf{0}, \mathbf{1}]$$

of $\boldsymbol{A}$ and defines the fuzzy set $\boldsymbol{A}$ of $\boldsymbol{X}$. Where $(x\ , \boldsymbol{\mu_A}(x))$ with $x \in \boldsymbol{X}$ is the set of all pairs [54].

To give more motivation for this concept of partial membership, let us consider the following example:

Consider a fuzzy set of the property tall; suppose $\boldsymbol{S}$ is a subset from universe set $\boldsymbol{U}$, it represents the heights from 120 cm to 200 cm. With a crisp set, all people with height more than 160 cm are considered tall. Fig.2.2.2: (a). illustrates the crisp set membership function for the set tall, the curve which is indeed a generalization of the classical characteristic function $\mu(x)$ (it can be used to conclude a person who either "is" or "is not" a member of the set $\boldsymbol{S}$), is called a ***membership function (MF)*** associated with the set $\boldsymbol{S}$ [25].

The corresponding fuzzy set with a smooth membership function is shown in Fig.2.2.2 (b). The curve defines the transition from not tall and shows the degree of membership for a given height [25].

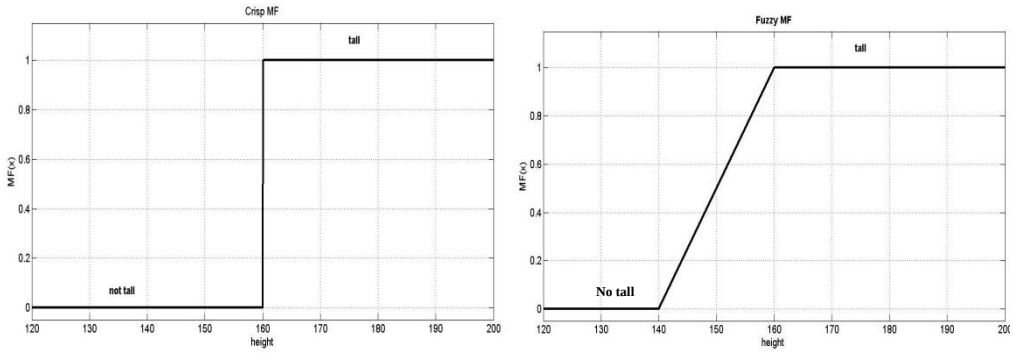

(a) (b)

Fig.2.2.2: Crisp/Fuzzy membership function (a) Crisp, (b) Fuzzy.

There is no fixed or even unique universal rule or criterion for choosing a membership function for a particular fuzzy subset; in general, a correct and good membership function is determined by the user based on his scientific knowledge, working experience, and actual need for the particular application. The most commonly used shapes for membership functions are triangular, trapezoidal, s-shaped, bell-shaped, sigmoid, piecewise linear and Gaussian curves [66,32,25]. A summary of the graphical and analytical representation of frequently used membership functions (MF), are shown in Table 2.2.1.

Table 2.2.1. Typical membership functions (MF).

Type of membership function	Analytical Representation	Graphical Representation
Triangular	$\mu_A(x) = \begin{cases} 0 \; for \; x < a \\ \frac{x-a}{b-a} \; for \; a \le x < b \\ \frac{c-x}{c-b} \; for \; b \le x \le c \\ 0 \; for \; x > c \end{cases}$	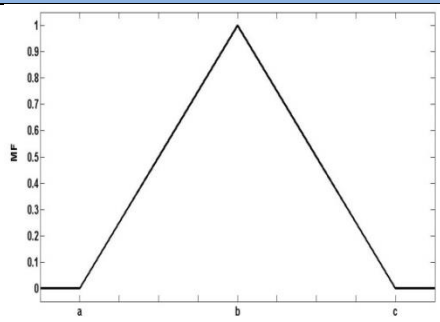
Trapezoidal	$\mu_A(x) = \begin{cases} 0 \; for \; x < a \\ \frac{x-a}{b-a} \; for \; a \le x < b \\ 1 \; for \; b \le x < c \\ \frac{d-x}{d-c} \; for \; c \le x < d \\ 0 \; for \; d \le x \end{cases}$	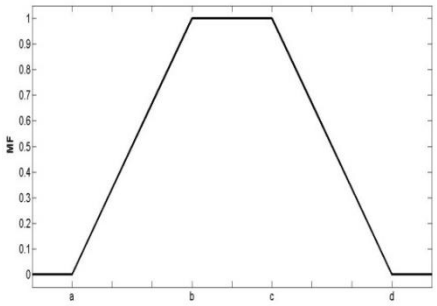
Gaussian curves	$\mu_A(x) = \frac{1}{e^{\left(\frac{(x-c)^2}{2.\sigma^2}\right)}}$	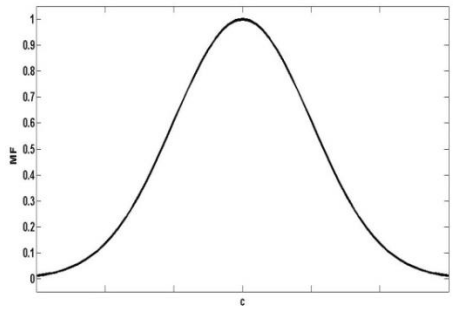
Sigmoid	$\mu_A(x) = \frac{1}{1+e^{-a(x-b)}}$	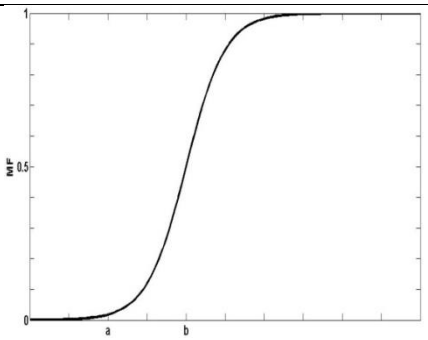
Bell-shaped	$\mu_A(x) = \frac{1}{1+\left\|\frac{x-c}{a}\right\|^{2b}}$	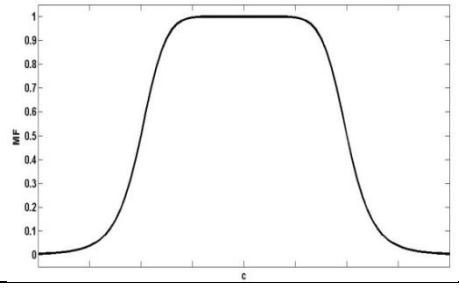

Triangular curves depend on three parameters *a, b* and *c*. Trapezoidal curves depend on four parameters; *a, b, c* and *d*. Gaussian curves depend on two parameters σ and *c*; where *c* and σ represent the mean and the standard deviation of the distribution respectively. While the sigmoid function equals 0.5, at $x = b$. Furthermore, Bell-Shaped curve depends on *a, b* and *c* parameters.

Fuzzy sets have a number of properties and definitions; here are some of the most important definitions:

1) Equality of Fuzzy Sets

Two fuzzy sets $\boldsymbol{A}$ and $\boldsymbol{B}$ are *equal*, $\boldsymbol{A = B}$, if and only if

$$\boldsymbol{\mu_A}(x) = \boldsymbol{\mu_B}(x) \ \forall x \in \boldsymbol{X}.$$

2) The Support, the Crossover Point and the Singleton of a Fuzzy Set.

The support of the fuzzy set $\boldsymbol{A}$ is the ordinary subset of $\boldsymbol{X}$ that has nonzero membership in $\boldsymbol{A}$, this is shown in Fig.2.2.3:

$$\boldsymbol{suppA = A^{+0}} = \{x \in \boldsymbol{X}, \boldsymbol{\mu_A}(x) > 0\}$$

The elements of *x* such as $\boldsymbol{\mu_A}(x) = \boldsymbol{1/2}$ are the crossover points of $\boldsymbol{A}$. A fuzzy set that has only one point in $\boldsymbol{X}$ with $\boldsymbol{\mu_A}(\boldsymbol{x}) = \boldsymbol{1}$ as its support is called a singleton. To illustrate the properties, see Fig.2.2.3 below.

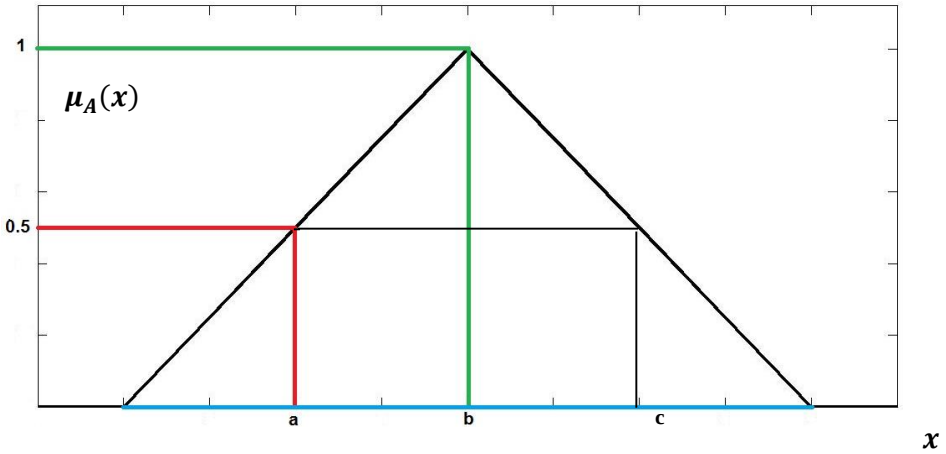

Fig.2.2.3: The crossover and singleton points: a & c refer to the crossover point, and the point b refer to singleton point.

3) The Height of a Fuzzy Set (Normal and Subnormal Sets).

The height of $\boldsymbol{A}$ is the least upper bound (supremum) of $\boldsymbol{\mu_A}(x)$.

$$\boldsymbol{hgt}(\boldsymbol{A}) = \boldsymbol{sup}_{x \in \boldsymbol{X}} \boldsymbol{\mu_A}(x)$$

Now, defining the normalize sets, where $\boldsymbol{A}$ is called to be normalized ***iff*** $\exists x \in \boldsymbol{X}$, $\boldsymbol{\mu_A}(x) = \boldsymbol{1}$. This definition implies $\boldsymbol{hgt}(\boldsymbol{A}) = 1$. Otherwise A is called subnormal fuzzy set.

4) $\boldsymbol{\alpha}$-level Fuzzy Sets.

An important way of representing fuzzy sets is $\boldsymbol{\alpha - cut}$ method. The $\boldsymbol{\alpha - cut}$ of $\boldsymbol{A}$, denoted by $\boldsymbol{A_\alpha}$, is a set consisting of those elements of the universe $\boldsymbol{X}$ whose membership values exceed the threshold level $\boldsymbol{\alpha}$; the $\boldsymbol{\alpha - cut}$ of $\boldsymbol{A}$ is illustrate in Fig.2.2.4.

Hence; defining a fuzzy set $\boldsymbol{A_\alpha}$ as:

$$\boldsymbol{A_\alpha}(x) = \boldsymbol{\alpha A^\alpha}(x)$$

Then the original fuzzy set $\boldsymbol{A}$ may be defined as

$$\boldsymbol{A} = \bigcup_{\boldsymbol{\alpha} \in [\boldsymbol{0},\boldsymbol{1}]} (\boldsymbol{\alpha A_\alpha})$$

This means that any fuzzy set $\boldsymbol{A}$ can be decomposed into a series of its $\boldsymbol{\alpha - cut}$, ∪ denotes the standard fuzzy union.

The lower the level of $\boldsymbol{\alpha}$, the more elements are admitted to the corresponding $\boldsymbol{\alpha - cut}$, that is, if $\boldsymbol{\alpha_1 > \alpha_2}$ then $\boldsymbol{A_{\alpha 1} \subset A_{\alpha 2}}$.

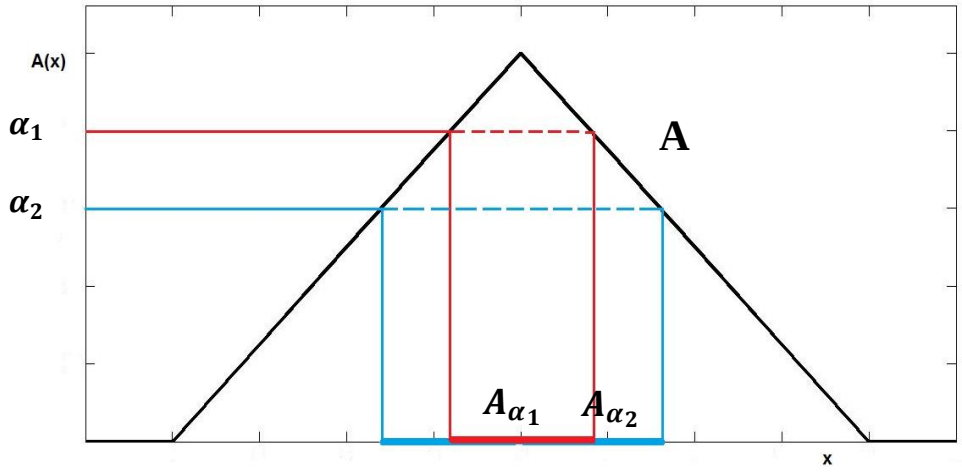

Fig.2.2.4: The $\boldsymbol{\alpha - cut}$ for two values where $\boldsymbol{\alpha_1 > \alpha_2}$.

5) Convexity of Fuzzy Sets.

A fuzzy set $\boldsymbol{A}$ of $\boldsymbol{X}$ is called convex iff

$$\boldsymbol{\mu_A(\lambda x_1 + (1-\lambda)x_2) > \min(\mu_A(x_1), \mu_A(x_2))}$$

for all $x_1, x_2 \in \boldsymbol{R}$, $\boldsymbol{\lambda \in [0,1]}$, min denotes the minimum operator. In other words, a fuzzy set $\boldsymbol{A}$ on $\boldsymbol{R}$ is convex iff all its $\boldsymbol{\alpha}$-level sets are convex in the classical sense.

6) The Cardinality of Fuzzy Sets.

The scalar cardinality of a fuzzy set $\boldsymbol{A}$ on $\boldsymbol{X}$ denoted by $\boldsymbol{|A|}$ is defined as (when $\boldsymbol{X}$ is a finite set):

$$\boldsymbol{|A| = \sum_{x \in A} \mu_A(x)}$$

when $\boldsymbol{X}$ is infinite, $|\boldsymbol{A}|$ is defined as:

$$|\boldsymbol{A}| = \int_{\boldsymbol{X}} \boldsymbol{\mu_A}(\boldsymbol{x})\, dx$$

Sometimes $|\boldsymbol{A}|$ is called the power of $\boldsymbol{A}$. The relative cardinality denoted by $\|\boldsymbol{A}\|$ is defined as:

$$\|\boldsymbol{A}\| = |\boldsymbol{A}|/|\boldsymbol{X}|$$

7) Inclusion of Fuzzy Sets to Fuzzy Sets

$\boldsymbol{A}$ is said to be inclusion in $\boldsymbol{B}$, presented as $\boldsymbol{A} \subseteq \boldsymbol{B}$, or $\boldsymbol{A}$ is a subset of $\boldsymbol{B}$, if $\forall x \in \boldsymbol{X}$, $\boldsymbol{\mu_A}(x) \leq \boldsymbol{\mu_B}(x)$.

2.2.2 Operations on Fuzzy Sets

Before defining the operations on fuzzy sets, we will illustrate a fuzzy number to understand the operations on fuzzy sets.

Definition 2. A fuzzy number $\boldsymbol{A}$ is a fuzzy set of the real line $\boldsymbol{R}$ with a normal, convex and continuous membership function of bounded support. The family of fuzzy numbers will be denoted by $\boldsymbol{F}$ [57, 74].

On the other hand, a fuzzy number is a fuzzy subset of the real line $\boldsymbol{R}$ whose highest membership values are clustered around a given real number called the mean value; where the membership function is monotonic on both sides of this mean value [17]. The most common shapes for fuzzy numbers are triangular, trapezoidal, S-shaped, Bell-shaped, sigmoid function, piecewise linear and Gaussian curves fuzzy numbers [66, 32, 25]. All types are summarized and defined in Table 2.2.1.

In order to easily manipulate fuzzy sets, redefine the operators of the classical set theory, such as intersection, union, and complement, to fit the specific membership functions of fuzzy logic for values strictly between 0 and 1[54].

Actually, L. A. Zadeh suggested the minimum operator for the intersection and the maximum operator for the union of two fuzzy sets [38], this is illustrated in the following definition.

Let $\boldsymbol{A}$ and $\boldsymbol{B}$ be two fuzzy sets in $\boldsymbol{X}$ with membership functions $\boldsymbol{\mu_A}(x)$ and $\boldsymbol{\mu_B}(x)$ respectively. The operations of union, intersection and complement for fuzzy sets are defined theoretically as given below.

Definition 3. **Fuzzy Standard Intersection.**

The intersection **(∩)** of fuzzy sets $\boldsymbol{A}$ and $\boldsymbol{B}$ contains only elements common to both sets, since the membership values chosen are the minimum values from the two elements. The intersection can be calculated by the following formulas:

$$\forall x \in \boldsymbol{X} \quad \boldsymbol{\mu_{A\cap B}}(x) = \mathbf{min}(\boldsymbol{\mu_A}(x), \boldsymbol{\mu_B}(x))$$

Or, in abbreviated form:

$$\boldsymbol{\mu_{A\cap B}}(x) = \boldsymbol{\mu_A}(x) \wedge \boldsymbol{\mu_B}(x)$$

where $\boldsymbol{\mu_{A\cap B}}(\boldsymbol{x})$is the membership function of $\boldsymbol{A} \cap \boldsymbol{B}$. If one set does not contain an element (empty set), the minimum value will therefore be zero; this means $\boldsymbol{A} \cap \boldsymbol{B}$ is empty, then A and B are disjoint [54, 38].

Definition 4. **Fuzzy Standard Union.** The union **(∪)** of sets $\boldsymbol{A}$ and $\boldsymbol{B}$ will contain all elements in both sets. Therefore, the union of two fuzzy sets

contains all elements in both sets and will select the maximum value given for each element. The Union can be calculated by the following formulas:

$$\forall x \in \boldsymbol{X}, \qquad \boldsymbol{\mu_{A\cup B}}(x) = \boldsymbol{max}(\boldsymbol{\mu_A}(x), \boldsymbol{\mu_B}(x))$$

Or, in abbreviated form:

$$\boldsymbol{\mu_{A\cup B}}(x) = \boldsymbol{\mu_A}(x) \vee \boldsymbol{\mu_B}(x)$$

where $\boldsymbol{\mu_{A\cup B}}(x)$ is the membership function of $\boldsymbol{A} \cup \boldsymbol{B}$ [54, 38].

Definition 5. **Fuzzy Standard Complement.**

The complement of a fuzzy $\boldsymbol{A}$ is denoted by $\overline{\boldsymbol{A}}$ and is defined by

$$\boldsymbol{\mu_{\bar{A}}}(x) = \mathbf{1} - \boldsymbol{\mu_A}(x)$$

where $\boldsymbol{\mu_{\bar{A}}}(x)$ is the membership function of $\overline{\boldsymbol{A}}$ [54, 38].

The intersection, union and complement of fuzzy sets in R^1, are illustrated in Fig.2.2.5.

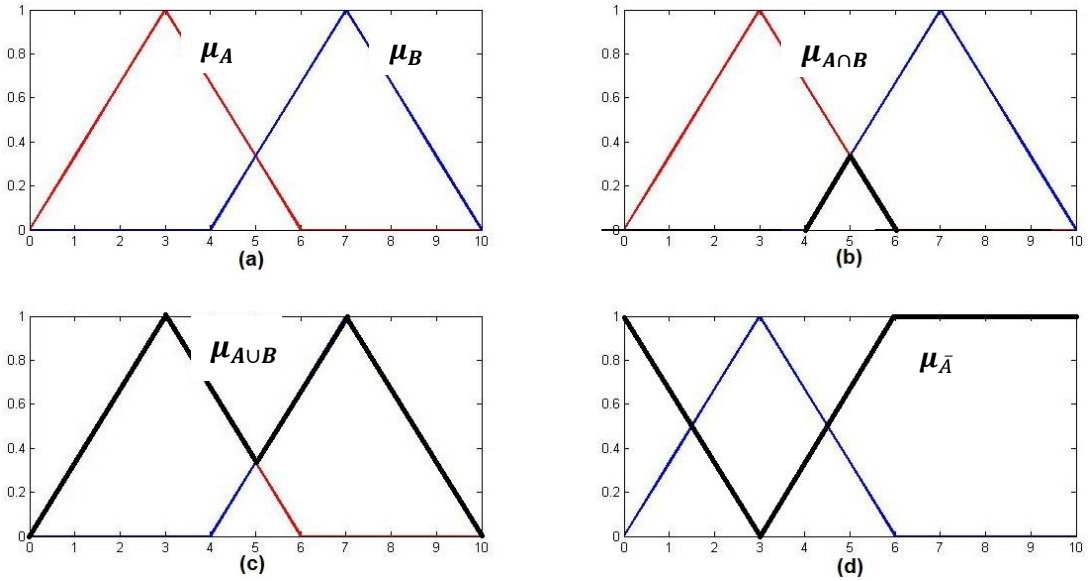

Fig.2.2.5: The intersection, union and complement of fuzzy sets (a) Two fuzzy sets A and B respectively, (b) Intersection of two fuzzy sets, A∩B, (c) Union of two fuzzy sets, A∪B, (d) Complement of fuzzy set, $\overline{\boldsymbol{A}}$.

2.2.2.1 Properties of Fuzzy Sets Operations

After defining the operations of fuzzy sets; intersection, union, and complement, we note that the following rules which are common in classical set theory, like commutative, associative, involutive, distributive, and DeMorgan's law, which are defined in Table 2.1.1**,** also holds for standard fuzzy operations in general.

But the standard fuzzy operations do not satisfy the law of excluded middle $\boldsymbol{A} \cup \overline{\boldsymbol{A}} = \boldsymbol{X}$, and the law of contradiction $\boldsymbol{A} \cap \overline{\boldsymbol{A}} = \emptyset$ of classical set theory [54].

2.3 Clustering Methods

This section presents an overview of the main clustering methods. The aim is to introduce the theories and the mathematics underlying clustering techniques, also discuss the usefulness of soft-computing methods in clustering tasks. The section begins by providing measures and criteria that are used for determining whether two objects are similar or dissimilar. Presenting clustering methods which are divided into two types: hard (crisp), and soft-computing (fuzzy) methods.

2.3.1 Overview of Clustering Methods

Clustering is a process of partitioning or grouping a given set of input data vectors or image pixels into a number of clusters such that similar objects are allocated to one cluster [10]. Clustering is one approach to perform image segmentation on digital images.

Clustering techniques are among the unsupervised methods; which means they do not use prior class identifiers. The main potential of clustering is to detect the basic structure in data, not only for classification and pattern recognition, but also for optimization [49].

Before defining the types of clustering, another type of data partitioning, that is classification, is introduced here.

Clustering and classification are both fundamental tasks in Data Mining [31]. Classification is used mostly as a supervised learning method, while clustering is used as an unsupervised learning (some clustering models are for both). The goal of classification is predictive, while that of clustering is descriptive. Since the aim of clustering is to detect a new set of categories, the new classes are of interest in themselves, and their assessment is intrinsic. In classification tasks, however, an important part of the assessment is extrinsic, since the groups must reflect some reference set of classes [31].

Definition 6. The clustering structure is represented as a set of subsets $\boldsymbol{C} = \boldsymbol{C_1}, \ldots, \boldsymbol{C_k}$ of $\boldsymbol{S}$, such that: $\boldsymbol{S} = \bigcup_{\boldsymbol{i=1}}^{\boldsymbol{k}} \boldsymbol{C_i}$ and $\boldsymbol{C_i} \cap \boldsymbol{C_j} = \emptyset$ for $\boldsymbol{i} \neq \boldsymbol{j}$. Consequently, any instance in $\boldsymbol{S}$ belongs to exactly one and only one subset [31].

Since clustering is the grouping of similar objects, the term similarity should be understood from a mathematical scope. For instance in metric spaces, similarity is often defined by means of a distance norm. Distance can be measured among the data vectors themselves, or as a distance from a data vector to some prototypical object of the cluster. The prototypes may be vectors of the same dimension as the data objects, but they can also be

defined as “higher-level” geometrical objects, such as linear or nonlinear subspaces or functions [11, 31]. In this thesis we will focus and use a clustering method to detect features related to DR diseases in the retina.

2.3.2 Similarity Measures

Clustering is based on a similarity measure to group similar data objects together. This similarity measure is based on distance functions (for example; Euclidean distance, Manhattan distance, Minkowski distance, Cosine similarity, etc.) to group objects in clusters and has given good result [31].

In this part, the mathematical definition of distance measure is introduced, it is useful to denote the distance between two objects x_i and x_j as: $\boldsymbol{d}(x_i, x_j)$. The distance measure is called a distance metric if it satisfies the symmetry and triangular inequality properties.

Definition 7. Let $\boldsymbol{d}$ (distance) be defined as $\boldsymbol{d}: \mathbb{R}^{\boldsymbol{m}} \times \mathbb{R}^{\boldsymbol{n}} \rightarrow \mathbb{R}_{\boldsymbol{0}}^{+}$ be a distance function if it satisfies [59]:

$\forall x_i, x_j, x_k \in \mathbb{R}^{\boldsymbol{m}}$:

$\boldsymbol{d}(x_i, x_j) \geq 0$ **(Non-negativity)**

$\boldsymbol{d}(x_i, x_j) = 0 \iff x_i = x_j$ **(Identity of indiscernible)**

$\boldsymbol{d}(x_i, x_j) = \boldsymbol{d}(x_j, x_i)$ **(Symmetry)**

$\boldsymbol{d}(x_i, x_k) \leq \boldsymbol{d}(x_i, x_j) + \boldsymbol{d}(x_j, x_k)$ (**Triangular inequality**)

After defining the distance function, brief overviews of similarity measure functions which are commonly used for clustering are shown in the following:

1. Minkowski Distance

Minkowski Distance also known as the generalized distance metric, is a generalization of several other canonical distances and is also known as the L_p norm distance. We note in equation (2.3.1) below the metric has a free parameter ***p*** which must be defined:

$$D_{\text{Minkowski}}(x_i, x_j) = \sqrt[p]{\sum_{k=1}^{n} |x_{ik} - x_{jk}|^p} \tag{2.3.1}$$

Note that if ***p = 1*** this yields the Manhattan distance, in case ***p = 2*** we obtain the Euclidean distance and finally when $\boldsymbol{p} = \infty$ we obtain the Chebychev distance. However, we can also pick different values for ***p*** [59].

2. Manhattan Distance

The Manhattan distance, also called a city block distance or $\boldsymbol{L_1}$ distance, is a second type of distance function that calculates the absolute differences between the two points x_i and x_j as shown in equation (2.3.2) given below [31]:

$$D_{\text{Manhattan}}(x_i, x_j) = \sum_{k=1}^{n} |x_{ik} - x_{jk}| \tag{2.3.2}$$

Manhattan distance between two points is the sum of the absolute differences of their Cartesian coordinates as shown in equation (2.3.2), as illustrated in Fig.2.3.1 below:

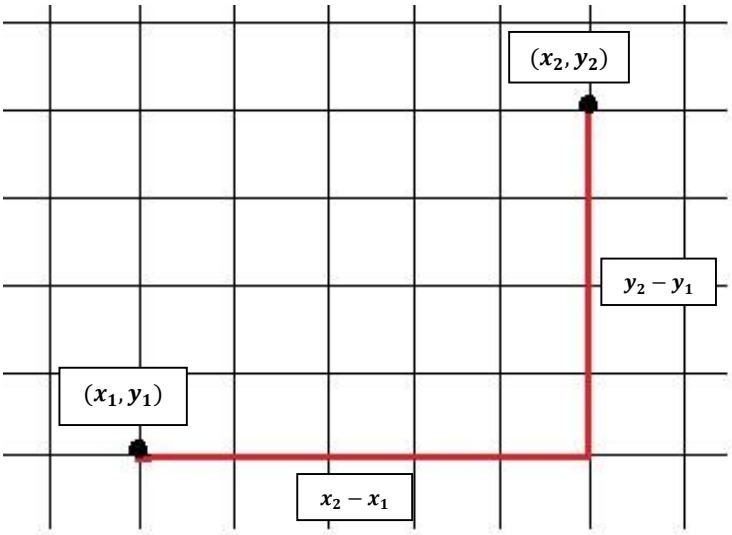

Fig.2.3.1: The Manhattan distance between two points.

$$d = |x_2 - x_1| + |y_2 - y_1| \tag{2.3.3}$$

More formally, it is the sum of the lengths of the projections of the line segments between the points onto the coordinate axes of the coordinate system [59].

3. Euclidean Distance

Euclidean distance is the most well-known and widely used distance function, it is considered as the standard metric for geometrical problems, and this metric is extensively used in clustering problems. It is simply the ordinary distance between two points, also used as the default distance measure in the FCM algorithm. The Euclidean distance is the root of square differences between the coordinates of a pair of objects as shown in equation (2.3.4) given below:

$$D_{Euclidean}(x_i, x_j) = \sqrt{(x_i - x_j)^2} = \sqrt{\sum_{k=1}^{n} (x_{ik} - x_{jk})^2} \tag{2.3.4}$$

The Euclidean distance between two points (x_1, y_1) and(x_2, y_2) are in two dimensional spaces as shown in Fig.2.3.2 below where the Euclidean distance between them is given by equation (2.3.5)

$$d = \sqrt{(x_2 - x_1)^2 + (y_2 - y_1)^2} \tag{2.3.5}$$

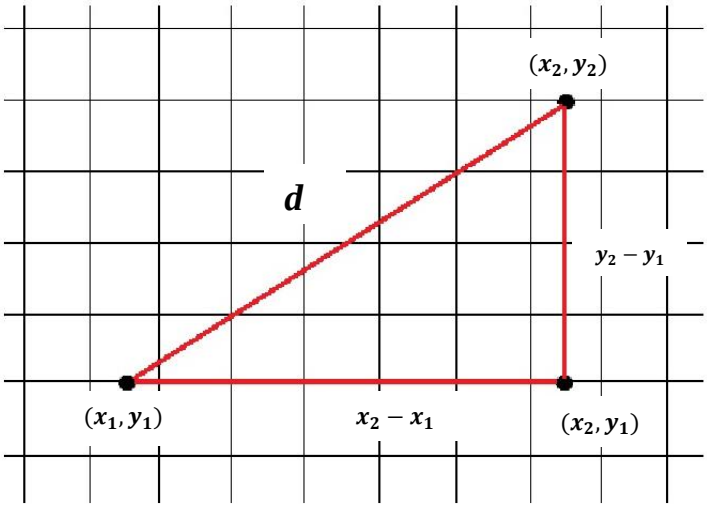

Fig.2.3.2: The Euclidian distance between two points (x_1, y_1) & (x_2, y_2)

The Euclidean distance is also known as the L_2 distance (or the squared L_2 norm) [59].

4. Chebyshev Distance

Chebyshev distance, also called the maximum value distance, is the maximum absolute magnitude of the differences between the points in any single dimension as given in equation (2.3.6) [31]:

$$D_{\text{Chebyshev}}(x_i, x_j) = \max_k |x_{ik} - x_{jk}| \tag{2.3.6}$$

This distance measure is a special case of the L_∞ norm. It may be appropriate if the difference between points is reflected more by differences in individual dimensions rather than all the dimensions considered together [59].

After defining some similarity measure functions which are commonly used for clustering, we want to introduce and discuss clustering types:

There are two types of clustering: hard clustering and fuzzy clustering, in section 2.3.3 a detailed explanation of these two types is introduced.

2.3.3 Types of Clustering Methods

Clustering methods are performed by using two main approaches: crisp (hard) clustering and fuzzy (soft) clustering, each of which has its own special characteristics. Crisp (hard) clustering is to process the data to find the boundary between clusters [38]. As a consequence, with this approach the segmentation results are often very crisp, i.e., each pixel of the image belongs to exactly just one class.

However, issues such as limited spatial resolution, overlapping intensities, poor contrast, noise and intensity in homogeneities variation make this hard (crisp) segmentation a difficult task. Fuzzy clustering is a good approach to solve this kind of problems where object can belong to more than one cluster [38].

2.3.3.1 Hard Clustering

The objective of clustering is to partition the data set $\boldsymbol{Z}$ into $\boldsymbol{c}$ clusters (groups); where $\boldsymbol{Z}$ is typically a number of observations of some process consists of $\boldsymbol{n}$ measured variables, grouped into an n-dimensional column

vector $z_k = [z_{1k}, \ldots, z_{nk}]^T$, $z_k \in \mathbb{R}^n$. An $\boldsymbol{N}$ observations data set is denoted by $\boldsymbol{Z} = \{z_k \mid k = 1, 2, \ldots, N\}$ (see section 5.1.1.1), supposing that $\boldsymbol{c}$ is known based on prior knowledge.

Using classical sets, a hard partition of $\boldsymbol{Z}$ can be defined as a family of subsets $\{A_i \mid 1 \leq i \leq c\} \subset \boldsymbol{S}$, where $\boldsymbol{S}$ is the universe set, with the following properties:

$$\bigcup_{i=1}^{c} A_i = \boldsymbol{Z}, \tag{2.3.7}$$

$$A_i \cap A_j = \emptyset, \quad 1 \leq i \neq j \leq c, \tag{2.3.8}$$

$$\emptyset \subset A_i \subset \boldsymbol{Z}, \qquad 1 \leq i \leq c. \tag{2.3.9}$$

These conditions mean that the subsets A_i contain all the data in $\boldsymbol{Z}$, they must be disjoint and none of them is empty nor contains all the data in $\boldsymbol{Z}$.

Clusters are expressed in terms of *membership functions* like this:

$$\bigvee_{\mathrm{i}=1}^{c} \mu_{A_i} = 1\,, \tag{2.3.10}$$

$$0 < \mu_{A_i} < 1, \qquad 1 \leq i \leq c. \tag{2.3.11}$$

Here $\bigvee$ is the **OR** operation, $\bigwedge$ is the **AND** operation, and μ_{A_i} is the membership (characteristic) function of the subset A_i and its value can be zero or one. To simplify the notations, to make things easier μ_i is used instead of μ_{A_i}, partitions can be represented in a matrix notation. A partition can be conveniently represented by the partition matrix: $[\mu_{ik}]_{\boldsymbol{c}\times\boldsymbol{N}}$. The i^{th} row of this matrix contains values of the membership function μ_i of the i^{th} subset A_i of $\boldsymbol{Z}$.

The partition matrix represents a hard partition if and only if its elements satisfy the following conditions:

$$\mu_{ik} \in \{0,1\}, 1 \leq i \leq c, 1 \leq k \leq N, \quad (2.3.12)$$

$$\sum_{i=1}^{c} \mu_{ik} = 1,\ 1 \leq k \leq N, \quad (2.3.13)$$

$$0 < \sum_{k=1}^{N} \mu_{ik} < N,\ 1 \leq i \leq c. \quad (2.3.14)$$

Hence, the hard partition matrices of $\boldsymbol{Z}$ are called the hard partitioning space.

Definition 7: Let $\boldsymbol{Z} = [z_1, z_2, \dots, z_N]$ be a finite set and let $2 \leq c < N$ be an integer. The hard partitioning space for $\boldsymbol{Z}$ is the set [11]:

$$M_{hc} = \left\{ \boldsymbol{U} \in \mathbb{R}^{c \times N} | \boldsymbol{\mu_{ik}} \in \{0,1\}, \forall i, k;\ \textstyle\sum_{i=1}^{c} \boldsymbol{\mu_{ik}} = 1, \forall k; 0 < \sum_{k=1}^{N} \boldsymbol{\mu_{ik}} < N, \forall i \right\} \quad (2.3.15)$$

2.3.3.2 Fuzzy Clustering (FC)

The idea of fuzzy clustering (FC) comes from the fuzzy set theory, which produced the idea of partial membership of belonging described by a membership function [76].

FC algorithm has always been a hot area of research in academia because it is widely applicable in real life [64], for instance: FC as a soft segmentation method has been widely studied and successfully applied in image segmentation [79].

FC algorithms allow the objects to belong to several clusters, where every data object has a membership degree. These degrees are valued between 0 and 1, with a high degree value will be representing a high similarity between the object and the group [10], in other words the data item belongs by a degree of membership to each cluster of the predefined clusters, and the summation of all membership values for one of the data items is equal to one [30].

Hence, larger membership values indicate higher confidence in the assignment of the object to the cluster or group. However, hard clustering can be obtained from a fuzzy partition by using a threshold of the membership value. The most well-known FCM algorithm is the fuzzy c-means (FCM) algorithm [10].

But before discussing FCM clustering, we will explain FC from the mathematical point of view.

Fuzzy partitioning can be seen as a generalization of hard clustering, allows μ_{ik} attaining real values in $[0,1]$. The conditions of the fuzzy partitions matrix $\boldsymbol{U}$ are given by:

$$\mu_{ik} \in [0,1], 1 \leq i \leq c, 1 \leq k \leq N, \tag{2.3.16}$$

$$\sum_{i=1}^{c} \mu_{ik} = 1,\ 1 \leq k \leq N, \tag{2.3.17}$$

$$0 < \sum_{k=1}^{N} \mu_{ik} < N,\ 1 \leq i \leq c. \tag{2.3.18}$$

Hence; i^{th} row of the fuzzy partition matrix $\boldsymbol{U} = [\mu_{ik}]_{c\times N}$ contains values of the i^{th} membership function of the fuzzy subset A_i of $\boldsymbol{Z}$.

In equation (2.3.17) the sum of each column equals one, and thus the total membership of each z_k in $\boldsymbol{Z}$ equals one.

Definition 8: Let $\boldsymbol{Z} = [z_1, z_2, \dots, z_N]$ be a finite set and let $2 \leq c < N$, where c be an integer. The fuzzy partitioning space for $\boldsymbol{Z}$ is the set:

$$M_{fc} = \left\{ U \in \mathbb{R}^{c\times N} | \mu_{ik} \in [0,1], \forall i, k;\ \sum_{i=1}^{c} \mu_{ik} = 1, \forall k; 0 < \sum_{k=1}^{N} \mu_{ik} < N, \forall i \right\} \tag{2.3.19}$$

2.3.4 Segmentation Using FCM Clustering

For medical images segmentation, FC is a suitable clustering type. In this section, description of the most well-known fuzzy clustering algorithm: The Fuzzy C-Means (FCM). The FCM algorithm is unsupervised clustering algorithms that is widely used in image processing and computer vision because it is easy to implement and has good clustering performance [73]; it divides the image into various cluster regions with similar pixels [30].

It is one of the most popular methods used in image segmentation as it has robust characteristics for ambiguity and can retain much more information than hard segmentation methods do [79].

Segmentation using FCM clustering is an overlapping clustering algorithm, where each point may belong to one or more cluster with different degrees of membership. The similarity is defined by the distance of the features vector to clusters centers. Euclidean distance might be implemented to measure this distance and each feature will be associated to an appropriate membership value [67].

Most analytical fuzzy clustering algorithms are based on optimization of the basic C-means objective function, or some modification of it. Hence we start discussion with presenting the fuzzy C-mean functional.

The FCM algorithm is based on the minimization of an objective function called c-means functional, it is defined by Dunn [11] as:

$$\boldsymbol{J}(\boldsymbol{Z};\boldsymbol{U},\boldsymbol{V}) = \sum_{i=1}^{c}\sum_{k=1}^{N}(\mu_{ik})^{m}\|z_k - v_i\|_A^2 \qquad (2.3.20)$$

where

$$\boldsymbol{U} = [\mu_{ik}] \in M_{fc} \tag{2.3.21}$$

is a fuzzy partition matrix of $\boldsymbol{Z}$, also:

$$\boldsymbol{V} = [v_1, v_2, \dots, v_c], \qquad v_i \in \mathbb{R}^n \tag{2.3.22}$$

is a vector of cluster (centers), which have to be determined:

$$D_{ikA}^2 = \|z_k - v_i\|_A^2 = (z_k - v_i)^T A (z_k - v_i) \tag{2.3.23}$$

is a squared inner-product distance norm.

The matrix A is the distance measure (2.3.23); a common choice is

$$A = I. \tag{2.3.24}$$

Also,

$$m \in [1, \infty)$$

is a parameter which determines the fuzziness of the resulting clusters. The value of the objective function (2.3.20) can be seen as a measure of the total variance of z_k from v_i.

2.3.4.1 Optimizing the Objective Function with Constraints

The minimization of the c-means functional equation (2.3.20) represents a nonlinear optimization problem that cannot be minimized directly, so the alternating optimization will be used; which means optimize membership degrees ($\boldsymbol{U}$) for fixed cluster parameters ($\boldsymbol{V}$), then optimize cluster parameters ($\boldsymbol{V}$) for fixed membership degrees($\boldsymbol{U}$); which called Lagrange multipliers, for more information see appendix **A-3**.

The stationary points of the objective function of equation (2.3.20) can be found by adjoining the constraint equation (2.3.17) to $\boldsymbol{J}$ by means of Lagrange multipliers λ_k , $0 \leq k \leq N$, and obtain:

$$L(\boldsymbol{Z};\boldsymbol{U},\boldsymbol{V},\lambda) = \sum_{i=1}^{c}\sum_{k=1}^{N}(\mu_{ik})^m D_{ikA}^2 + \sum_{k=1}^{N}\lambda_k\left[1 - \sum_{i=1}^{c}\mu_{ik}\right], \quad (2.3.25)$$

and by setting the gradients of L with respect to $\boldsymbol{U}$, $\boldsymbol{V}$ and λ to zero; which means:

$$\frac{\partial}{\partial \mu_{ik}} L(\boldsymbol{Z};\boldsymbol{U},\boldsymbol{V},\lambda) = 0\,, \quad (2.3.26)$$

and

$$\frac{\partial}{\partial v_i} L(\boldsymbol{Z};\boldsymbol{U},\boldsymbol{V},\lambda) = 0, \quad (2.3.27)$$

First, finding the μ_{ik} which minimizes the objective function $\boldsymbol{J}$; a necessary condition for the minimum is that the partial derivatives of the Lagrange function with respect to the membership degrees should satisfy:

$$\frac{\partial}{\partial \mu_{ik}} L(\boldsymbol{Z};\boldsymbol{U},\boldsymbol{V},\lambda) = \sum_{i=1}^{c}\sum_{k=1}^{N} m(\mu_{ik})^{m-1} D_{ikA}^2 - \sum_{k=1}^{N}\lambda_k\left[\sum_{i=1}^{c} 1\right] = 0 \quad (2.3.28)$$

Then solving the equation (3.3.28); where

$$\sum_{i=1}^{c} 1 = c \text{ and } \sum_{k=1}^{N}\lambda_k\, c = N\,\lambda_k\, c$$

then

$$\sum_{i=1}^{c}\sum_{k=1}^{N} m(\mu_{ik})^{m-1} D_{ikA}^2 = N\,\lambda_k\, c \quad (2.3.29)$$

$$m\,N\,c\sum_{i=1}^{c}\sum_{k=1}^{N}(\mu_{ik})^{m-1}\, D_{ikA}^2 = N\,\lambda_k\, c \quad (2.3.30)$$

After solving (2.3.28); we obtain:

$$\forall i; 1 \le i \le c, \forall k; 1 \le k \le N: \ \mu_{ik} = (\frac{\lambda_k}{m\ D_{ikA}^2})^{\frac{1}{m-1}} \qquad (2.3.31)$$

Now; substitute equation (2.3.31) over clusters constraints (2.3.17), it gives equation (2.3.32):

$$\sum_{i=1}^{c} \mu_{ik} = \sum_{i=1}^{c} \left(\frac{\lambda_k}{m\ D_{ikA}^2}\right)^{\frac{1}{m-1}} = 1 \qquad (2.3.32)$$

Consequently, the λ_k where $1 \le k \le N$, are:

$$\lambda_k = \left(\sum_{i=1}^{c} \left(m\ D_{ikA}^2\right)^{\frac{1}{1-m}}\right)^{1-m} \qquad (2.3.33)$$

After finding the result of λ_k equation (2.3.33), substitute it into membership degrees equation (2.3.31); it can be shown that if $D_{ikA}^2 > 0, \forall i, k$ and m $>$ 1, then $(\boldsymbol{U}, \boldsymbol{V}) \in \mathrm{M_{fc}} \times \mathbb{R}^{\mathrm{n}\times\mathrm{c}}$ may minimize equation (2.3.21) only if:

$$\mu_{ik} = \frac{1}{\sum_{j=1}^{c} \left(\frac{D_{ikA}}{D_{jkA}}\right)^{2/(m-1)}}, 1 \le i \le c, 1 \le k \le N \qquad (2.3.34)$$

Now, take the partial derivative for the objective function with respect to cluster centers; which means $\frac{\partial}{\partial v_i}\mathrm{L}(\boldsymbol{Z}; \boldsymbol{U}, \boldsymbol{V}, \lambda) = 0$, but the $D_{ikA}^2 = \|z_k - v_i\|_A^2 = (z_k - v_i)^T A (z_k - v_i)$, then the resulting update rule for the cluster centers is shown in equation (2.3.35) :

$$v_i = \frac{\sum_{k=1}^{N} (\mu_{ik})^m\, z_k}{\sum_{k=1}^{N} (\mu_{ik})^m} \ ; \ \ 1 \le i \le c \qquad (2.3.35)$$

This solution in equations (2.3.34 and 2.3.35) also satisfies the remaining constraints equations (2.3.16 and 2.3.18). Equations (2.3.29 and 2.3.30) are

first-order necessary conditions for stationary points of the functional equation (2.3.20).

We note that if $D_{isA} = 0$ for some z_k and one or more cluster prototypes v_s, $s \in S \subset \{1,2,\dots,c\}$, in this case, the membership degree in (2.3.34) cannot be computed; then a singularity occurs in FCM.

When singularity happens, zero membership is assigned to each μ_{ik} [34].

Chapter Three
Localization and Detection of Optic Disc and Blood Vessels

Chapter Three

Localization and Detection of Optic Disc and Blood Vessels

3.1 Preview

In this chapter the major parts of a fundus retinal image were defined such as the optic disc (OD), fovea and blood vessels. Identification of the regions of this kind of fundus images may help analysis for other diseases [15]. Also, methods and algorithms used automatically to detect optic disc and blood vessels are discussed.

The aim of processing an image is dividing into three categories: enhancement, restoration and segmentation [46].

Adaptive local contrast enhancement and noise removal was applied [9]. Afterwards, we introduced various algorithms for OD extraction with combination of mathematical morphology.

3.1.1 Converting Color Maps from RGB to HSI

In digital world, input images can be an RGB (Red, Green, and Blue), see Fig.3.1.1. An RGB image can be described as $M \times N \times 3$ array representing colored pixels. The three channels translate each pixel to 24 bits of color information, 8 bits for each channel images, and the range of intensity value for each component from 0 to 255 [58].

The first preprocessing step is transforming the original RGB image into HSI (Hue, Saturation and Intensity) image; the components are shown below in Fig.3.1.1. The HSI model is suitable for image enhancement; because we can separate the intensity component from the other components [7]. The

equations used to convert RGB to HSI are described here; Hue component is obtained using the equation (3.1.1) [15,49]:

$$H = \begin{cases} \theta & , B \leq G \\ 360 - \theta, & B > G \end{cases} \tag{3.1.1}$$

where θ is:

$$\theta = \cos^{-1}\left\{\frac{\frac{1}{2}[(R-G)+(R-B)]}{[(R-G)^2+(R-B)(G-B)]^{\frac{1}{2}}}\right\} \tag{3.1.2}$$

The saturation component is obtained by equation (3.1.3):

$$S = 1 - \frac{3}{(R+G+B)}[min(R,G,B)] \tag{3.1.3}$$

The intensity component is obtained by equation (3.1.4):

$$I = \frac{1}{3} * (R+G+B) \tag{3.1.4}$$

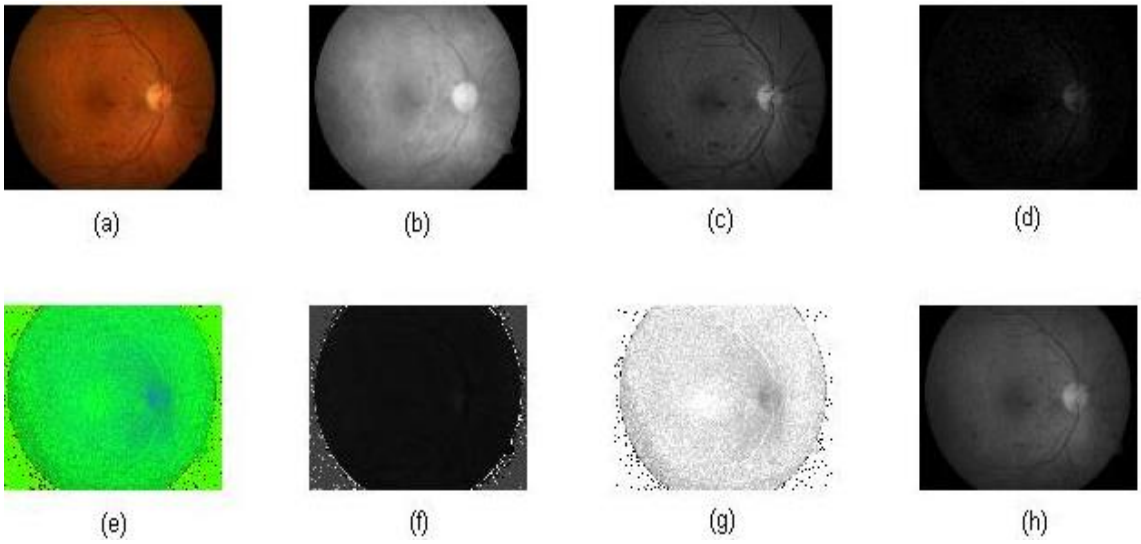

Fig.3.1.1: RGB and HSI image formats: (a) RGB image, (b-d) Red, Green and Blue channels respectively, (e) The input image in HSI, (f-h) Hue, Saturation and Intensity channels respectively.

3.1.2 Local contrast enhancement

A contrast limited adaptive histogram equalization (CLAHE) was applied for contrast enhancement, but also increases the noise, it is one of the main parts of the pre-processing stage, it is applied to distribute the values of pixels around the local mean [8], the CLAHE technique is used to enhance the separability between the OD and the background. It subdivides the image into non-overlapping rectangular regions, then applying their local equalization histogram [7].

The adaptive local contrast enhancement transformation is obtained by equation (3.1.5) [36].

$$g(x,y) = 255\ \frac{[\psi_W(f) - \psi_W(f_{min})]}{[\psi_W(f_{max}) - \psi_W(f_{min})]} \tag{3.1.5}$$

where W is the image of size $M \times M$ pixels indexed by (i,j), $1 \leq i \leq M, 1 \leq j \leq M, f_{min}$ and f_{max} are the minimum and maximum intensities of the whole image respectively, and ψ_W represents the sigmoidal function which is defined as shown in equation (3.1.6):

$$\psi_W = [1 + \exp\left(\frac{\langle f \rangle_W - f}{\sigma_W}\right)]^{-1} \tag{3.1.6}$$

where $\langle f \rangle_W$ and σ_W denote the mean and standard deviation of the intensity within W. The objective is to define a transformation point dependent on W such that the distribution is localized around the mean of the intensity and covers the entire intensity range [15].

The mean and standard deviation are defined in equations (3.1.7) and (3.1.8).

$$\langle f \rangle_W = \frac{1}{M^2} \sum_{(k,l) \in W(i,j)} f(k,l) \tag{3.1.7}$$

$$\sigma_W = \sqrt{\frac{1}{M^2} \sum_{(k,l) \in W(i,j)} (f(k,l) - \langle f \rangle_W)^2} \tag{3.1.8}$$

For a small value of σ (low contrast), the contrast enhancement is large, on the other hand, little contrast enhancement will take place for an initially large σ (high contrast) [36].

3.1.3 Median, Gaussian and Label Filters

A **median filter** is a nonlinear digital filtering technique applied on the image, used to remove noise from an image, it preserves edges while removing noise, and this is illustrated in Fig.3.1.2

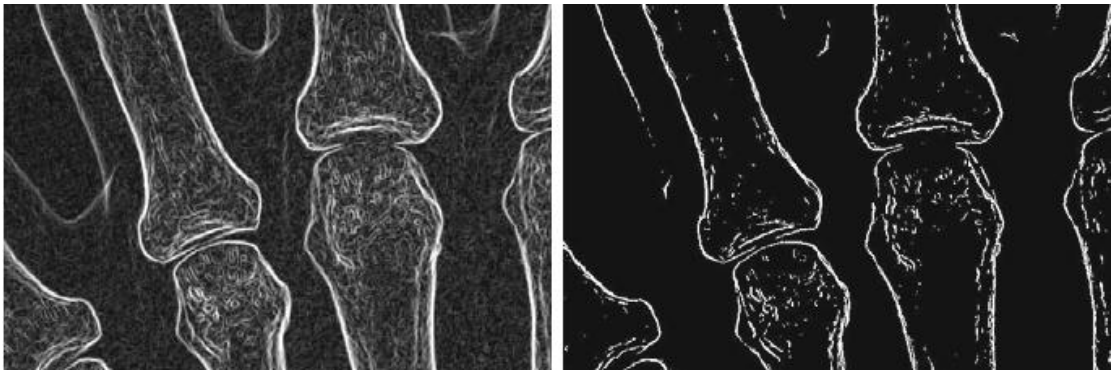

(a) (b)

Fig.3.1.2: Median filter (a) Original image, (b) Image after applying a median filter [75].

Median filters replace the center pixel values with the median of the intensity value available in the local neighborhood.

Gaussian filtering is used to remove noise and details that are not belonging to vessels by blurring images.

Applying a Gaussian filtering operation to an image is accomplished in two steps: firstly, is removing bright details smaller than a threshold by applying

area opening, and secondly by applying a Gaussian filter for noise reduction (see Fig.3.1.3) [45], it is defined in equation (3.1.9):

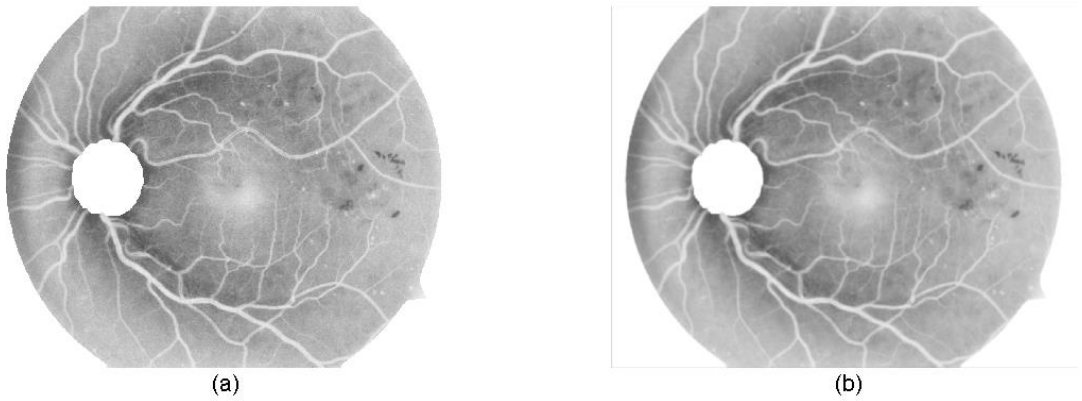

Fig3.1.3: Gaussian filter (a) Original image, (b) Image after apply Gaussian filtering.

$$G(x,y) = \frac{1}{2\pi\sigma^2} e^{-\left(\frac{x^2+y^2}{2\sigma^2}\right)} \tag{3.1.9}$$

where *x* is the distance from the origin in the horizontal axis, *y* is the distance from the origin in the vertical axis, and $\boldsymbol{\sigma}$ is the standard deviation of the Gaussian distribution, istandard deviation plays an important role in Gaussian function behavior, see Fig.3.1.4. We note that 68% of values are located within $\pm 1\sigma$, while 95% of the values are within $\pm 2\sigma$ of the mean, and 99.7% of the values are located within $\pm 3\sigma$.

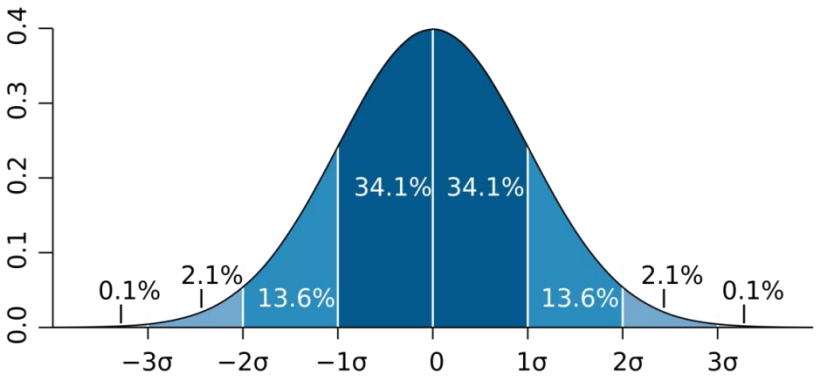

Fig.3.1.4: Distribution values of the Gaussian function [75].

While applying a Gaussian filter in Matlab make sure the size of the filter to be at least $6 \times \sigma$, to cover all the maximum values of the function.

Label filtering is used to remove isolated pixels by using the concept of labeling connected pixels. It tries to isolate the individual objects by using the eight connected neighborhood and label propagation [16]. The process of recognizing depends on the number of pixels for these components.

3.1.4 Morphological Image Processing

Mathematical Morphology (MM) is powerful tools for image processing and analysis, MM is mostly used to analyze the shape of the image [53], and remove imperfections from the image by accounting for the form and structure of the image [45]. The fundamental operations on MM are: dilation and erosion [20].

Before explaining MM types, we will clarify some important relevant concepts, for instance: pixel neighborhoods and structure element.

Pixel neighborhood; which means each pixel $P(i, j)$ of the image has a set of neighbor pixels called neighborhood. Two types of neighborhood are defined; 4-neighborhood and 8-neighborhood, which are illustrated in Fig.3.1.5: (a), (b).

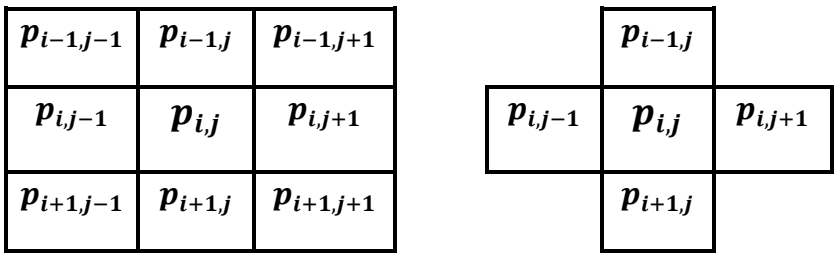

Fig.3.1.5: Pixels neighborhood of a pixel $\mathbf{p_{i,j}}$ (a) 8-connected, (b) 4- connecter [44].

A **structuring element** (SE) is a binary image (mask) that allows us to define arbitrary neighborhood structures, MM probe an image with SE, such that the SE is positioned at all possible locations and it is compared with the corresponding neighborhood pixels. The results are obtained: either the SE **fits** within the neighborhood, **hits** and **miss** the neighborhood, these results in Fig.3.1.6:

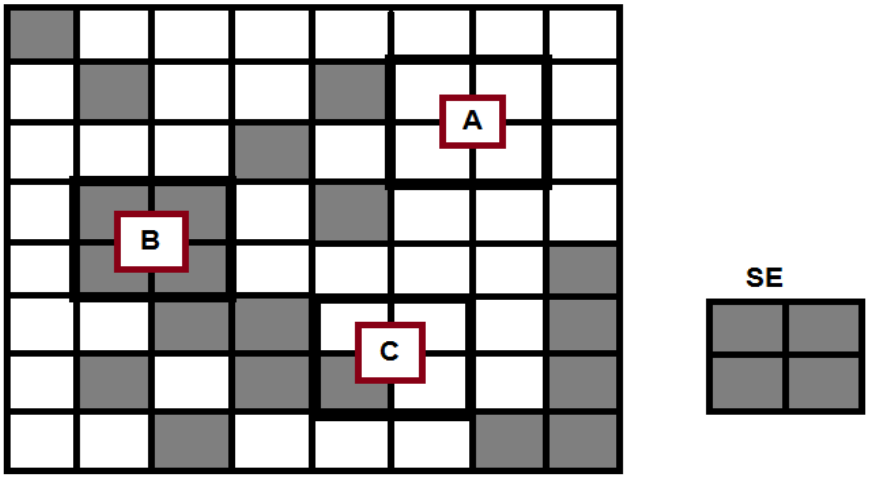

Fig.3.1.6: Probing an image with a SE, B: fits, C: hits and A: miss, where grey and white pixels have non-zero and zero values, respectively [44].

If for each of its pixels is set to one the corresponding image pixel is also one, the SE is said to **fit** the image, see Fig.3.1.6. And, if at least one of its pixels set

to one the corresponding image pixel is also one in this case a SE is said to **hit (intersect)** an image, for example the SE **hits** the image in C. The last case is **miss** the image, it happens when no pixels in the image is covered by any pixels in the SE, see Fig.3.1.6 in A.

3.1.4.1 Mathematical Morphology (MM) Types

Now, the dilation is an operation that grows or thickens objects in a binary image. The SE shape controls the extent of this thickening [20].

The **dilation** of an image f by a structuring element B produces a new binary image $g = f \oplus B$, as shown in equation (3.1.15), B hits the image f, then $g(x, y) = 1$, and 0 otherwise, repeating for all pixel coordinates (x, y), this is illustrated in Fig.3.1.7

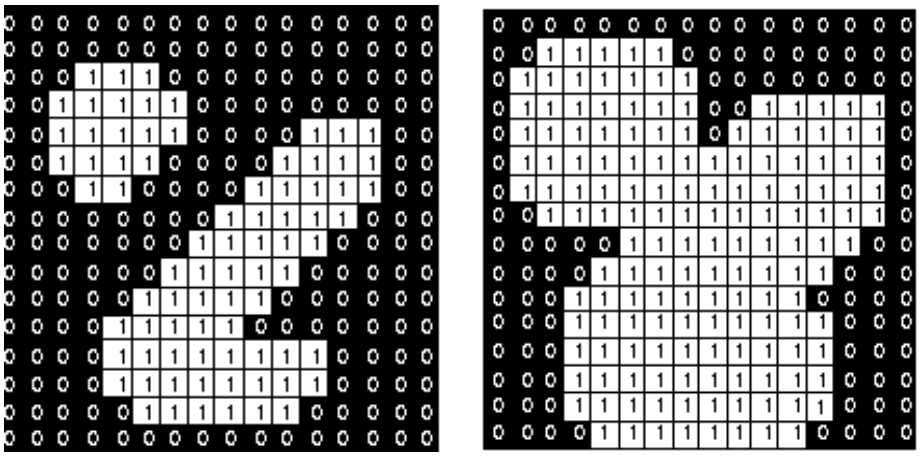

(a) (b)

Fig.3.1.7: Dilating an image: (a) Image, (b) Image dilation by a 3×3 SE [44].

To clarify the concept, we applied the dilation on binary retinal image, this is illustrated in Fig.3.1.8.

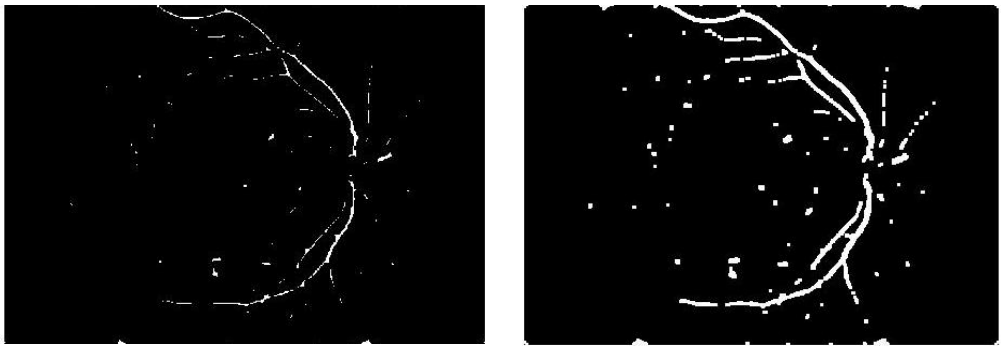

(a) (b)

Fig.3.1.8: Dilation of a retinal image (a) Input image, (b) Image $\boldsymbol{g}$ after dilation.

The second type is **erosion**, which shrinks or thins objects in a binary image. The manner and extent of shrinking is controlled by a SE [72]. The erosion of a binary image f by a structuring element B produces a new binary image $g = f \ominus B$, as shown in equation (3.1.14). B fits the image f with ones in all locations (x, y) of a B's origin, repeating for all pixel coordinates, this is illustrated in Fig.3.1.9 and Fig.3.1.10:

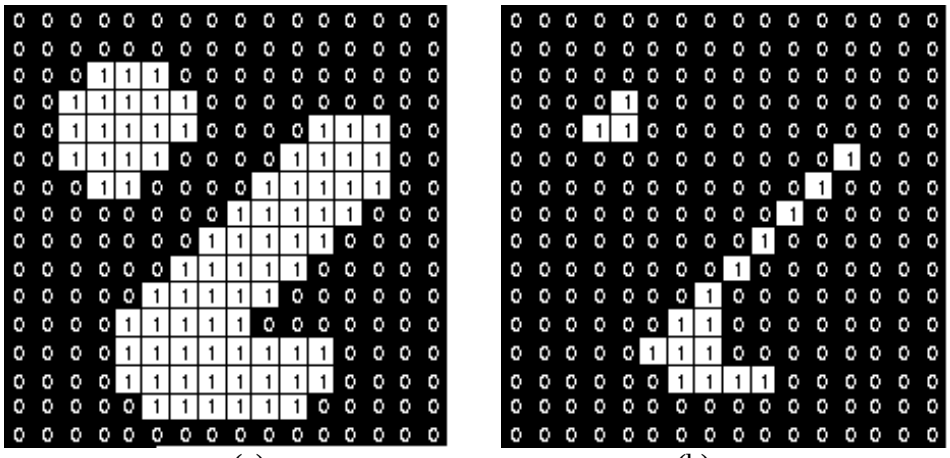

(a) (b)

Fig.3.1.9: Image Erosion: (a) Input $\boldsymbol{f}$, (b) Output $\boldsymbol{g}$ after erosion by a 3×3 SE [44].

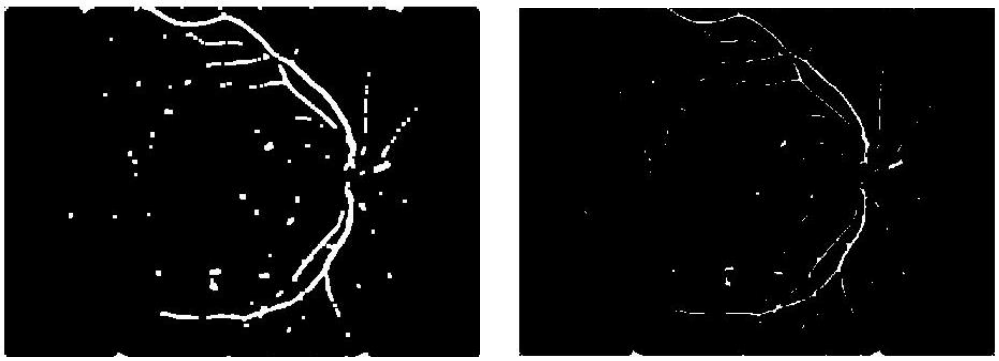

(a) (b)

Fig.3.1.10: Erosion of a retinal image (a) Original image, (b) After erosion.

The opening operation is considered essentially as maintaining pixel values, while eliminating more intense image regions with sizes smaller than the SE size [53]. The opening of an image f by a structuring element B is an erosion followed by a dilation, to understand the operation see equation (3.1.12) and Fig.3.1.11:

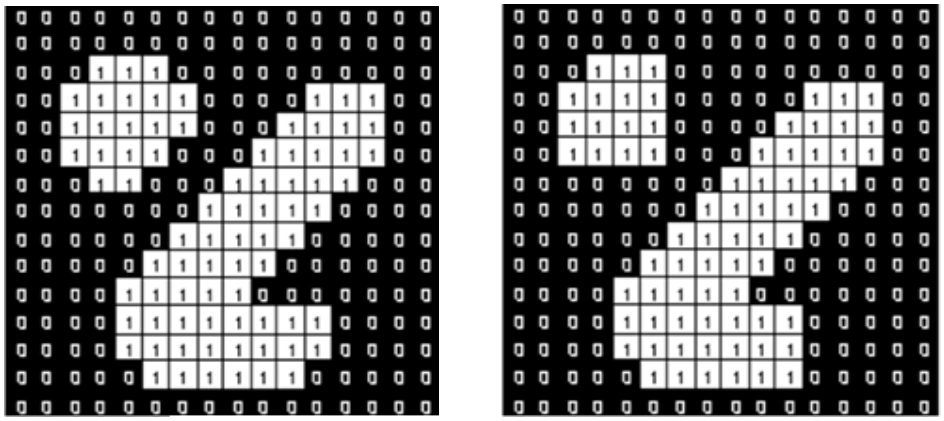

(a) (b)

Fig.3.1.11: Image Opening: (a) Input image, (b) Image $\boldsymbol{g}$ after opening by 3×3 SE [44].

The last operation is **closing**, it is considered to generate a smooth version of the original data, the SE are replaced by higher nearby intensities when the details are smaller than it, and this is shown in Fig.3.1.12.

The closing of an image f by a SE B is a dilation followed by an erosion, see equation (3.1.13)

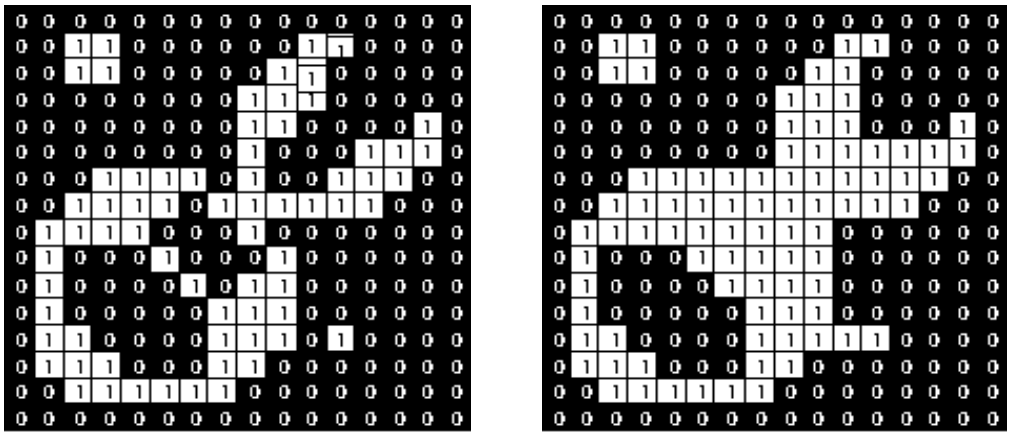

(a) (b)

Fig. 3.1.12: Image Closing: (a) Input image, (b) $\boldsymbol{g}$ after closing by 3×3 SE [44].

Now, we will discuss one of the most important operations that extract small elements and details from image, this is Top-Hat Transforms.

3.1.4.2 Top-Hat Transforms (TT)

Top-hat transformation is the important operations for target detection, image segmentation, image enhancement, feature extraction, background equalization and so on [77]. In MM and digital image processing, TT is a process that extracts small elements and details from given images [45].

Two types of top-hat transform are existing: white top-hat transformation (WTH) and black top-hat transformation (BTH), these are defined as follows [77]:

Let $f(x,y)$ and $B(i,j)$ represent the grayscale filtered image and SE, respectively. Then applying the WTH and BTH will be shown by:

$$WTH(f) = f - f\mathrm{o}\,B \tag{3.1.10}$$

$$BTH(f) = f \bullet B - f \tag{3.1.11}$$

where,

$$f\mathrm{o}\,B = (f \ominus B) \oplus B \tag{3.1.12}$$

$$f \bullet B = (f \oplus B) \ominus B \tag{3.1.13}$$

$$f \ominus B = \min_{ij}\big(f(x+i, y+j)\big) \tag{3.1.14}$$

$$f \oplus B = \max_{ij}(f(x-i, y-j)) \tag{3.1.15}$$

where o, $\bullet$, $\ominus$, and $\oplus$ are opening, closing, erosion and dilation operations. WTH is defined as the difference between the input image and its opening by some SE, see equations (3.1.10) and (3.1.12), the BTH transform which is defined dually as the difference between the closing and the input image, see equations (3.1.11) and (3.1.13) [53, 77].

3.2 Localization and Detection of the OD

In this section we will explain the procedures followed in this work to detect the OD.

The OD is one of the major parts of the retinal image. It appears as a bright yellowish or white circular area; the OD was considered to be a region having large cluster of bright pixels [36]. Hence, determining the location of the OD is an important anatomical landmark in automated analysis of retinal diseases in color fundus photographs [65].

Retinal images are often poorly and noisy illuminated because of unknown noise, camera motion, incorrect settings, in addition to eye particular structure, so we used a preprocessing to improve the image quality prior to the detection step.

The overall procedures for OD detection are presented in Fig.3.2.1. In the block diagram, the first step is to convert RGB image into HSI; because the HSI model is suitable for image enhancement [7], then using the intensity channel (see Fig.3.2.2: (b)) to be used in other process.

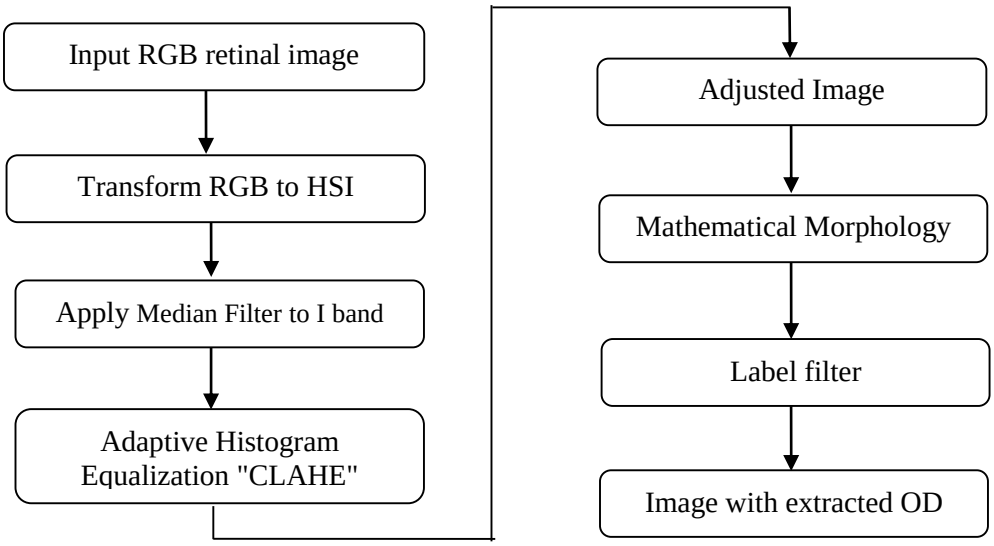

Fig.3.2.1. A block diagram outlining the proposed method for OD detection.

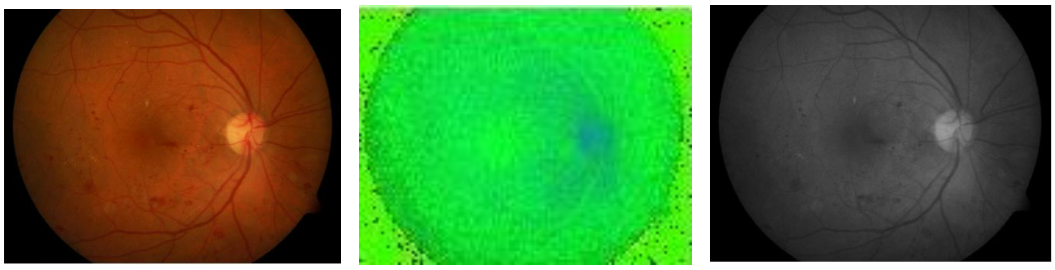

(a) (b) (c)

Fig.3.2.2: Intensity channel extraction: (a) RGB Retinal Image (b) HSI image, (c) Intensity Channel of the HSI image**.**

Apply a median filter on the I channel (Fig.3.2.3: (b)) to reduce the noise and preserve edges. After that, a CLAHE was applied for contrast enhancement. This technique is used to improve the contrast of the image and enhance the separability between the OD and the background [8]. The result is appeared in Fig.3.2.3: (c), the dark and bright areas are clearer hence the image shows more detail [15].

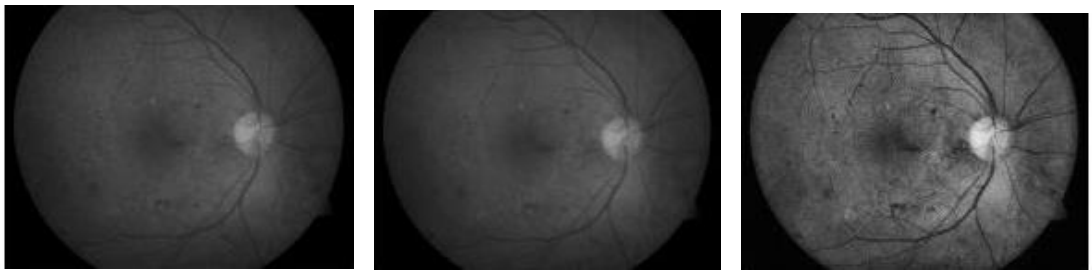

(a) (b) (c)

Fig.3.2.3: Influence of median filter and CLAHE (a) Intensity image, (b) Apply median filter, (c) Apply CLAHE.

These steps are followed by morphological closing for the CLAHE image to remove and close blood vessels, consequently creating a fairly constant OD region.

This stage, creates a flat, disc-shaped SE by Matlab command: *strel ('disk', R)*, where *R* specifies a non-negative integer radius, after experimenting different values, a flat SE of 15 is used. The result of closing for the CLAHE images on the intensity band is shown in Fig.3.2.4 [36].

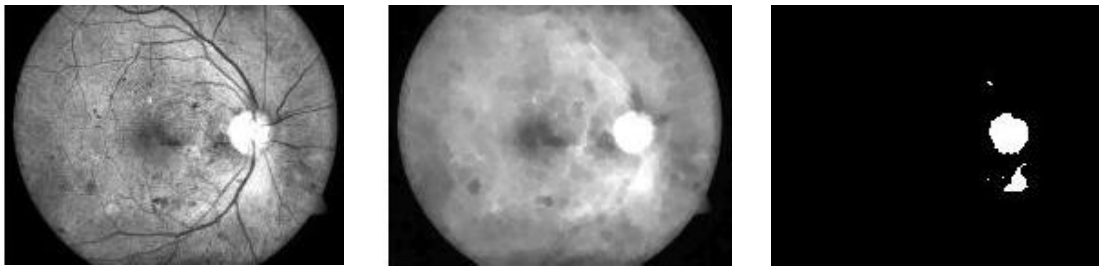

(a) (b) (c)

Fig.3.2.4: Locating OD (a) An adjusted image (b) Appling closing, (c) Thresholding

We note that some areas are not properly representing the OD, see Fig.3.2.4: (c), so we need to discard these areas. To solve this problem, the label filtering can be used to remove isolated pixels by using the concept of connected pixels labeling. It tries to isolate the individual objects by using the eight-connected neighborhood and label propagation [16]. The process of recognizing the OD depends on the number of pixels for these components. After labeling the connected areas in the image, deleting all components having a number of pixels which is less than a certain value, for instance in this code we accommodated the number of pixels to be equal to 700, so any area contains less than 700 pixels is removed. The result after applying label filtering is shown in Fig. 3.2.5, we note that small areas about the OD are deleted and hence the OD is detected a lone.

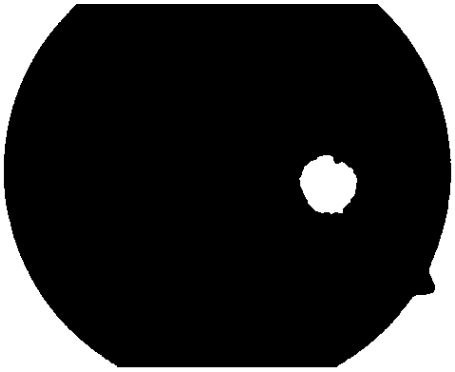

Fig.3.2.5: OD detection after applying label filtering.

3.3 Blood Vessels Detection

Changes in shape and size of retinal blood vessels may be an important indicator of the disorder of the eye, for example, in advanced stages of DR it is known that the retina has more blood vessels due to eye damages rather than normal one. This indication shows that the DR exists and reveals its degree [67].

Automatic segmentation of retinal vessels is an important step to identify and diagnose diseases early, such as DR, glaucoma and arteriosclerosis [53]. The main goal of this section is blood vessels detection in retinal images. The algorithm was developed based on fundus images obtained from DIARATDB1 database. The method presented here can be described by the functional block diagram described in Fig.3.3.1, the proposed algorithm and its details will be explained below.

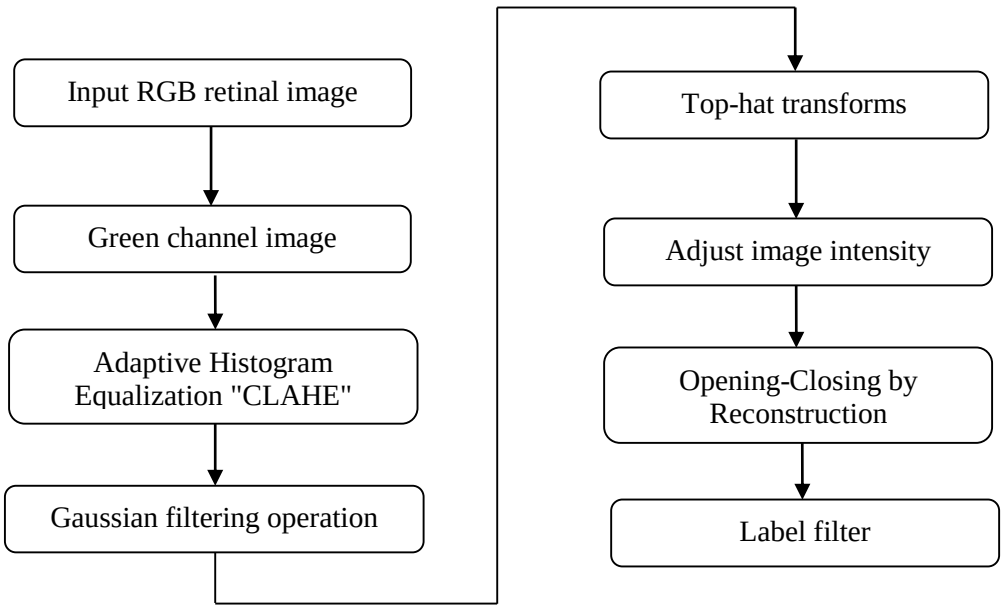

Fig.3.3.1: A block diagram showing blood vessel extraction methodology.

3.3.1 Preprocessing for vessels extraction

In general, a fundus image is an RGB color image. In this section we will focus only on the green channel as the retinal image distribution is clearer and gives best contrast of blood vessels; darker blood vessels on a brighter background [53]. While the red channel contains too much noise. Finally, the blue channel is characterized by low contrast, so not feasible to use it [45], an example of the three channels is shown in Fig.3.3.2.

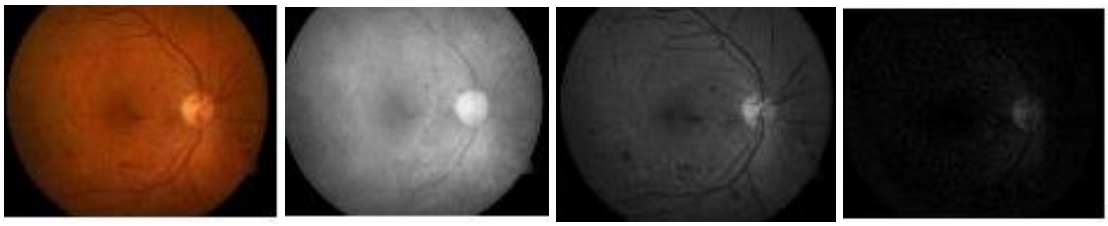

(a) (b) (c) (d)

Fig.3.3.2: RGB image format: (a) RGB image, (b-d) Red, Green and Blue channels respectively.

Hence, using only the green channel in the processing, see Fig.3.3.3: (b).

The first step towards automatic analysis of retinal images is image enhancement. The “CLAHE” technique is applied to the green channel for contrast enhancement [65], this makes the image have well contrast inversion as shown in Fig.3.3.3**:** (c).

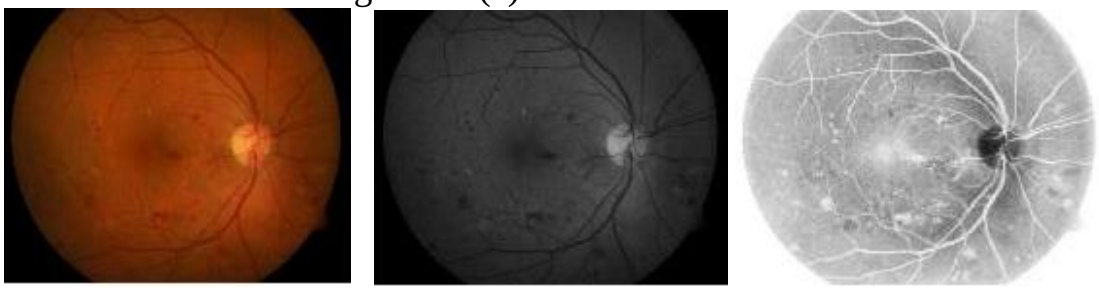

(a) (b) (c)

Fig.3.3.3: Implementing CLAHE (a) RGB image, (b) Green channel, (c) The image after applying contrast-limited adaptive histogram equalization (CLAHE).

After that, the Gaussian filtering is applied to the CLAHE image, this step is done to remove noise and unnecessary details that are not belonging to vessels, this implementation can be seen in Fig.3.3.4.

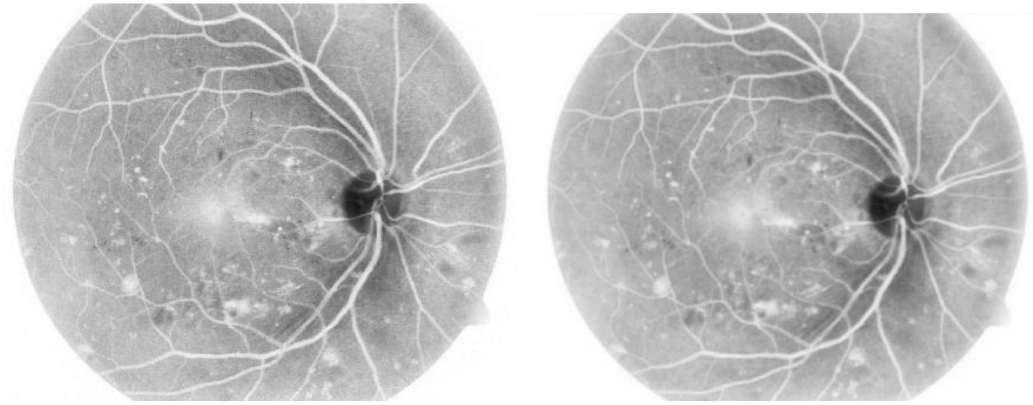

(a) (b)

Fig.3.3.4: Gaussian filtering enhancement (a) The CLAHE image, (b) Implementing Gaussian filtering.

And now, applying the top-hat transformation on the filtered image with a disc SE. In this work, a disc SE of radius 3 and 15 are used to fill all holes in blood vessels.

The top-hat returns an image, as shown in Fig.3.3.5: (a), containing the parts that are smaller than the SE and are darker than their surroundings. It worth to say that, blood vessels appear as clear elongated objects while the background spreads to be black [45].

Now, to increase the contrast of the output image resulted from the top-hat transformation, perform an adjustment on it, this modification will give a new version of the image as shown in Fig.3.3.5: (b). To remove unnecessary details from Fig.3.3.5: (b), thresholding is applied on it, the resulted image is a binary one shown in Fig.3.3.5: (c).

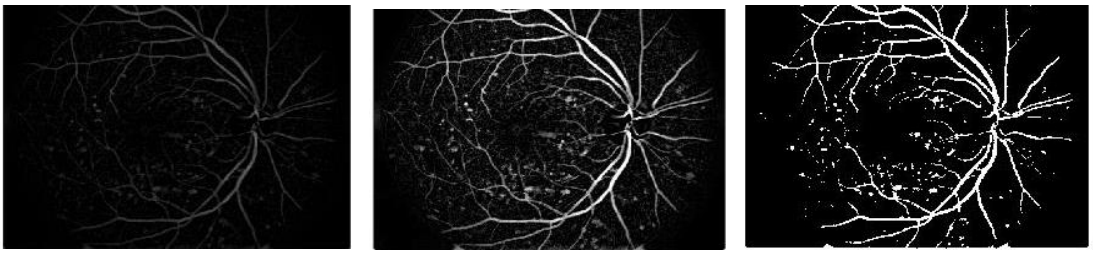

(a) (b) (c)

Fig.3.3.5: Thresholding vessels: (a) Top-hat transformation (b) Adjust intensity. (c) Thresholding.

3.3.2 Morphological Techniques for Blood Vessels Extraction

Mathematical morphology is mostly used to analyze the shape of the image [53], and to remove imperfections by accounting for the form and structure of the image [45].

In this part we used opening and opening-closing by reconstruction to clean up the image, but before these steps, a median filter is applied to reduce the noise; this is illustrated in Fig 3.3.6: (a). Reconstruction is a morphological transformation involving two images and a structuring element; one of them is marker and the other is the mask.

The normal morphological opening is erosion followed by dilation. Erosion typically removes small objects, and the subsequent dilation tends to restore the shape of the objects that remain, as shown in Fig.3.3.6: (b), while opening by reconstruction restores the original shapes of the objects that remain after erosion [56].

The final step is to complement the output of the morphological reconstruction as shown in Fig.3.3.6: (c). We notice that the reconstruction based on opening and closing are more effective than standard opening and

closing for removing small blemishes without affecting the overall shapes of the objects [45, 72].

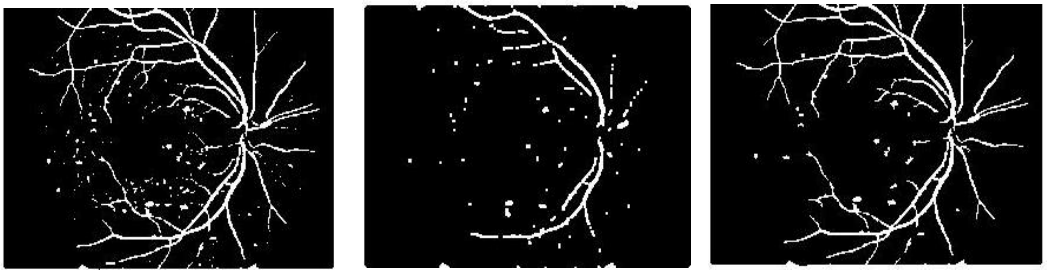

(a) (b) (c)

Fig.3.3.6: (a) Image after applying median filter, (b) Opening, (c) Opening-closing by reconstruction.

In Fig.3.3.6: (c) after applying Opening-closing by reconstruction, we note that some areas are not of blood vessels, in order to resolve this problem, the label filter is used.

Label filtering is used to remove isolated pixels by using the concept of connected pixels labeling (refer to section 3.1). The process of recognizing blood vessels depends on the number of pixels for these components. After labeling the connected areas in the image, deletion of all components that have a number of pixels less than a certain value. In this code, any area containing less than 300 pixels was removed. The final result for blood vessels network after implementing the label filtering is shown in Fig.3.3.7.

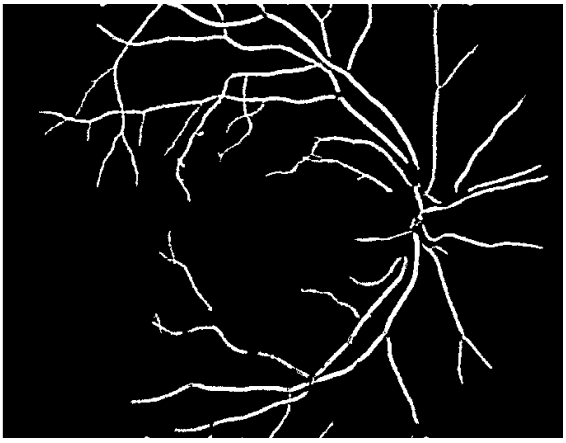

Fig.3.3.7: Blood vessels network after implementing label filter.

After applying the algorithm to extract the OD and blood vessels, the final result is superimposed on the original RGB image (see Fig.3.3.8). Consequently, the image is ready to be used to detect the exudates in side it by the FCM clustering procedures which will be discussed in chapter 4.

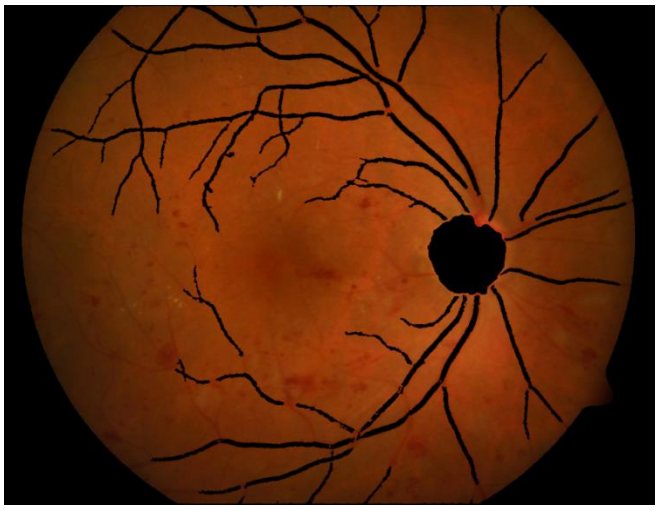

Fig.3.3.8: Masking OD and Blood vessel network in a retinal image.

Chapter Four
Methodology

Chapter Four

Methodology

4.1 Overview

Exudate is one of earliest indicators for diabetic retinopathy (DR). These can be identified as white or yellowish color random areas with varying shapes, sizes and locations. They appear near the leaking capillaries within the retina [28], examples are shown in Fig.4.1.1.

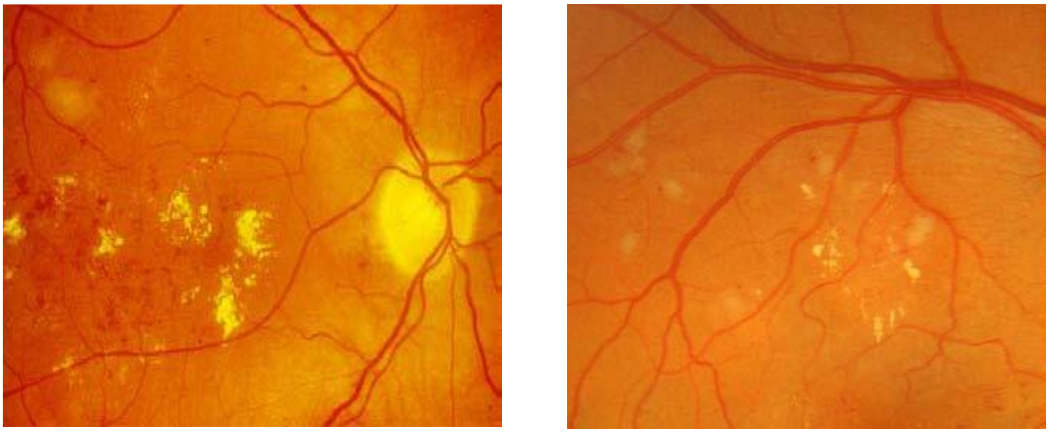

(a) (b)

Fig.4.1.1: Retinal images with exudates (a) and (b) are two examples [28].

Our proposed method is used to automatically discriminate the exudates from normal background in retinal image, based on Fuzzy C-means (FCM) technique. After eliminating the OD and blood vessels network, a preprocessing of contrast enhancement is applied to enhance the quality of the input image.

Afterwards, four features: Hue, entropy for intensity, standard deviation for intensity and Y-channel are extracted to provide FCM method with this input

data. Finally, an evaluation of the system performance is performed by comparing the detected results with the ground truth (GT) images that are drawn from expert ophthalmologists. Fig.4.1.2 shows a block diagram for exudates detection process.

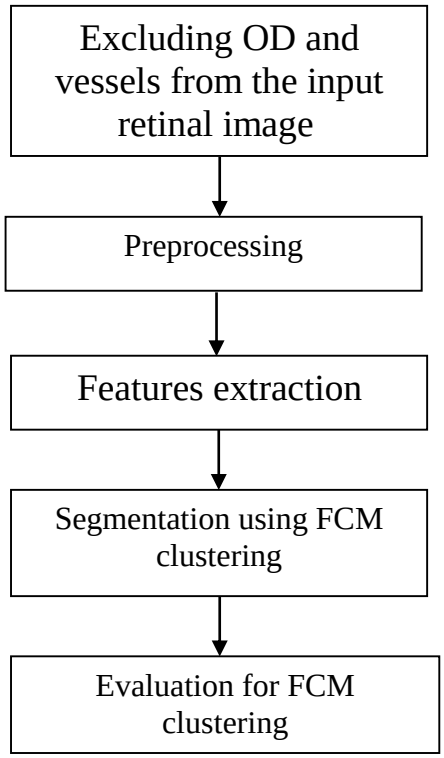

Fig.4.1.2: A block diagram for the implemented exudates detection method.

In this chapter, the methodology behind this approach is discussed; which is divided into five parts: in this first section (4.1) an overview is given, the second section (4.2) illustrates steps involved in the preprocessing, the third section (4.3) discusses in details the different features employed for abnormality detection, the fourth section (4.4) explains the FCM clustering algorithm, and finally section (4.5) describes the system performance by using the accuracy measurement.

4.2 Preprocessing Overview

Ten digital color retinal images five for training and another five for testing from DIARETDB1 (Standard Diabetic Retinopathy Database Calibration Level 1) dataset are obtained from digital fundus camera with varying imaging settings with a 50° field of view. The images were stored in a *Portable Network Graphics* (PNG) image format (.png) files. The resolution is 1152×1500 at 24 bit RGB color.

The aim of the preprocessing step is to compensate, one of the main obstacles for identification of retinal exudates, that is the wide variability in the color of the fundus image from different patients, because the variations are strongly correlated to skin pigmentation and iris color [28,5], so we used ten images only from 89 images in dataset.

Another problem appears in the exudates detection is exudates lesions which may appear dimmer in some regions of an image rather than the background color of other regions. So, the exudates can wrongly be classified as the background.

In fact, image variation is divided into two type; one of them is intra image variability which appears within the same image because of differences in light diffusion, fundus thickness, variation in reflectivity, and the presence of abnormalities, the second type is inter image variability that appears between different images which happens as a result of retinal pigmentation, differences in cameras, acquisition angle and illumination [55].

4.2.1 Detecting Expected Exudates

To reduce retinal image variation problem, we applied some preprocessing steps; the block diagram in Fig.4.2.1 illustrates the preprocessing steps on retinal image to extract expected exudate areas.

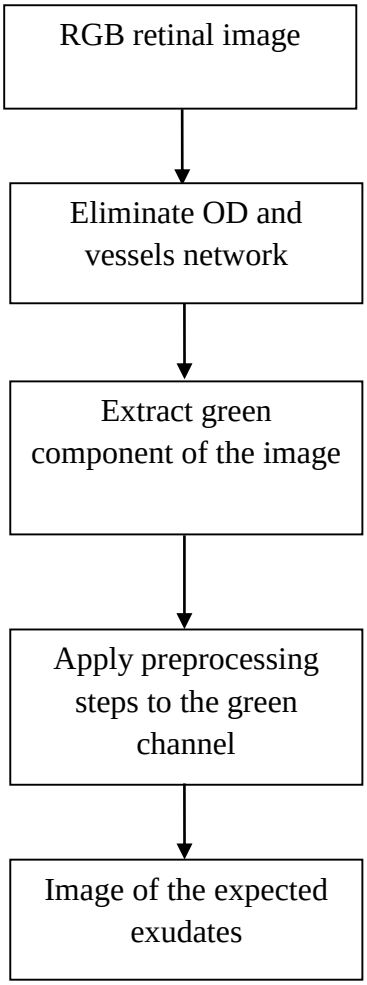

Fig.4.2.1: A Block diagram for the preprocessing steps to find the expected exudates.

In the first step, eliminate the OD and blood vessels network (Fig.4.2.2: (b)). The detection of the OD in fundus images is a very important task because of its similarity in brightness, color and contrast to the exudates [68], we note that the area around the OD has the same or nearly the same color and doesn't actually contain the exudates, we exclude these areas to reduce the area

which is not exudate but having the same color and features. Then use the green channel from the modified RGB image (Fig.4.2.2: (c)), because it gives the best contrast between background and exudates (see Fig.4.2.2**:** (g)), note that exudates appear brighter than the background in the green channel, but in red and blue channels exudates look less clear.

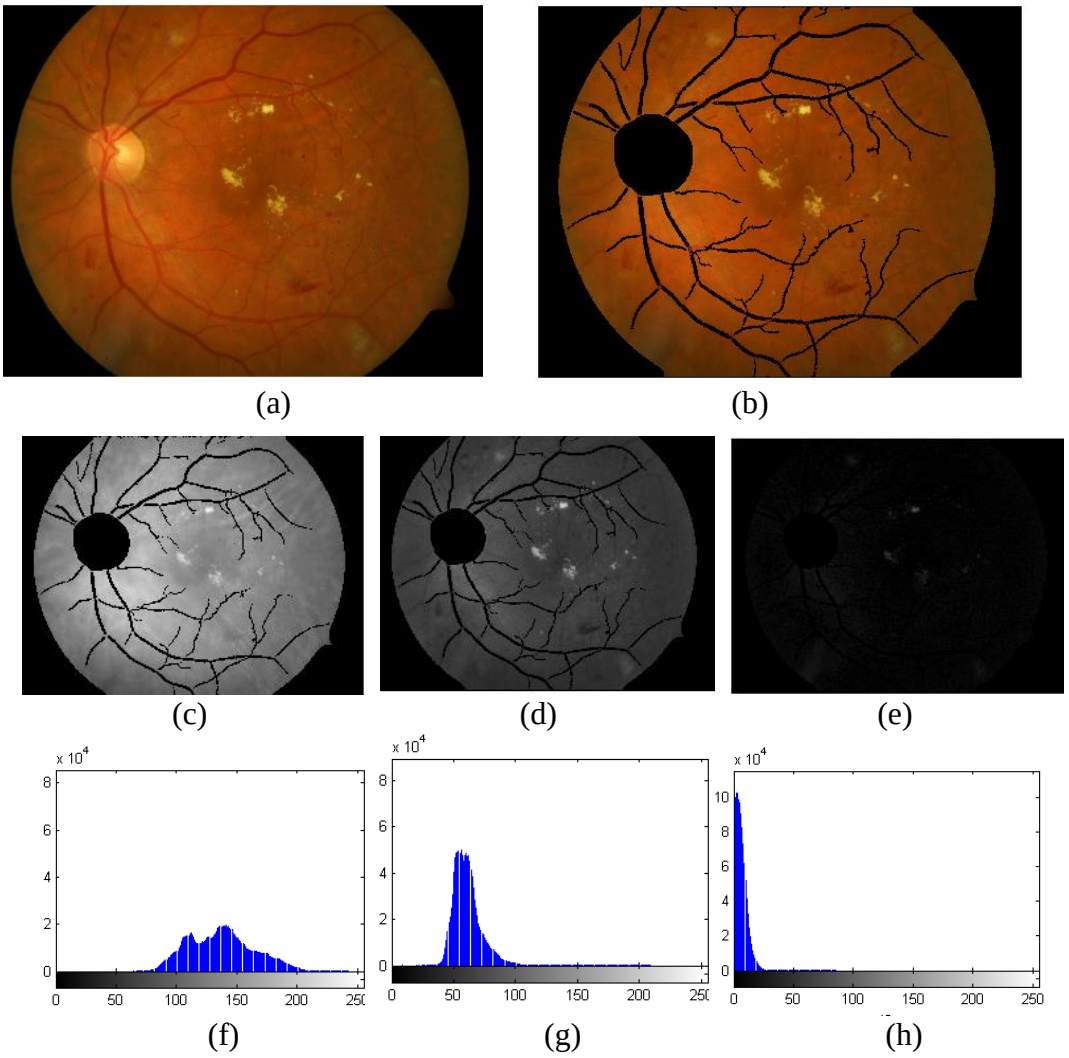

Fig.4.2.2: Illustrating the expected exudates in the pre-detection step (a) Input RGB; (b) Eliminating OD and blood vessels, (c) Red; (d) Green; (e) Blue; (g-h) Corresponding intensity distribution red, green and blue respectively.

4.2.2 Extracting Expected Exudate Areas

In this part we propose a method to extract expected exudate areas from retinal images, these will be entered as input for FCM clustering. However, this reduction of data will reduce the time of processing.

Suppose I_G is the green channel in an RGB image. In the first stage square the pixels values in the green channel, then change it into double type and let us call it I_d , after that applying the sobel edge filter on the I_d image to detect the edges, call the result image as I_s , the result contains the edge of OD, blood vessels and exudate regions (see Fig.4.2.3: (a-c)).

The second stage in this process is taking the complement of the I_d image, name it as I_c , we note that the result contains only the OD and blood vessels, we need to eliminate the OD and blood vessels so applying the sobel edge filter on the I_c image to detect the edges, the result (I_{sc}) contains only the edges of OD and blood vessels (Fig.4.2.3: (d-g)).

The object of this process is to detect the expected exudates by applying the dilation and complement for I_{sc}, the result is called I_{di}, after that take the AND between I_s and I_{di}, construct the result in I_{AND} which contains the expected exudates from retinal image as illustrated in Fig.4.2.3: (h).

After that, close and dilation operations are performed on the output image (I_{AND}) to preserve the data (Fig.4.2.3: (i)). The process of extracting expected exudates is illustrated in Algorithm (4.1) and Fig.4.2.3:

ALGORITHM 4.1

Input: Retinal image $I_{m,n}$.

Output: Retinal image contains the candidate exudate areas that can be considered as expected exudates.

Step (1): Extract Green channel image I_G.

Step (2): The pixel's values are squared in the green channel (I_{sq}), then change the resulted matrix to the type double (I_d).

Step (3): Apply the sobel edge filter on the (I_d) image giving the image I_s.

Step (4): Take the complement of the (I_d) image, name it as (I_c).

Step (5): Apply the sobel edge filter on the (I_c) image, the result is called (I_{sc}).

Step (6): Apply the dilation and complement on the (I_{sc}) image, then the result is (I_{di}).

Step (7): Take the "AND" between (I_s) and (I_{di}), name it as (I_{AND}).

Step (8): Perform the close operation on the (I_{AND}) image, the result is (I_{close}),then apply the dilation operations on the (I_{close}) image, the result is (I_{out}).

After applying the mentioned preprocessing stages the output result contains the candidate exudate areas that can be considered as expected exudates (see Fig.4.2.4: (b)).

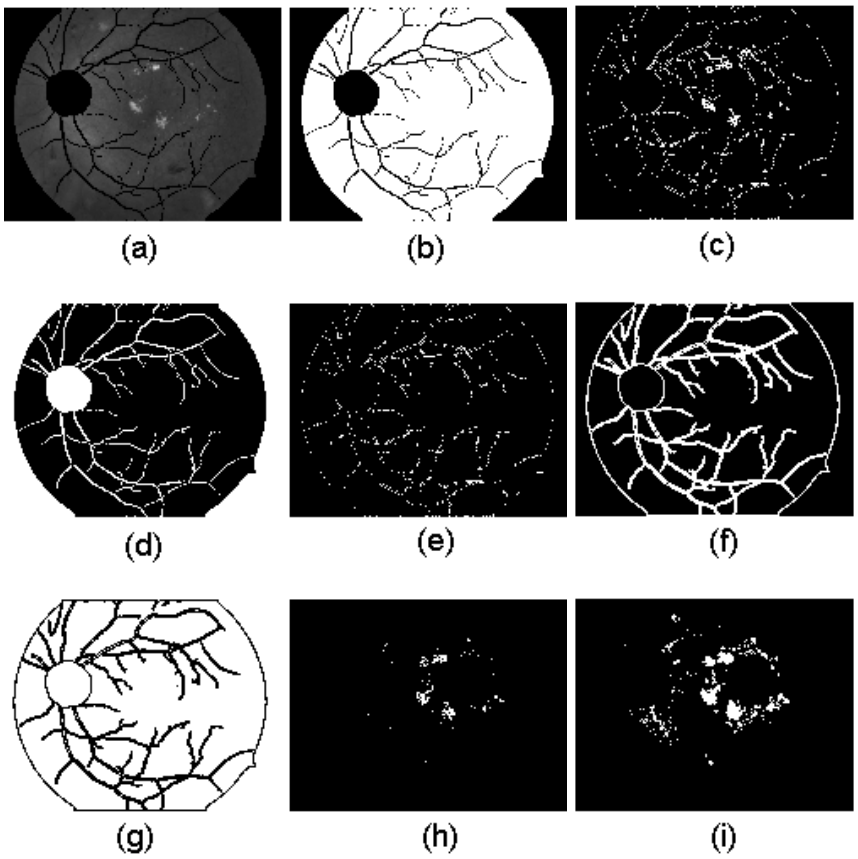

Fig.4.2.3: Preprocessing stages for expected exudates: (a) A green channel excluding OD and vessels, (b) Double type normalized image ($\mathbf{I_d}$), (c) Sobel edge image ($\mathbf{I_s}$), (d) Complement image ($\mathbf{I_c}$) of $\mathbf{I_s}$, (e) Sobel edge image ($\mathbf{I_{sc}}$), (f-g) Dilation complement image ($\mathbf{I_{di}}$) , (h) And operation image ($\mathbf{I_{AND}}$), (i) Dilation image ($\mathbf{I_{out}}$) contains the expected exudates.

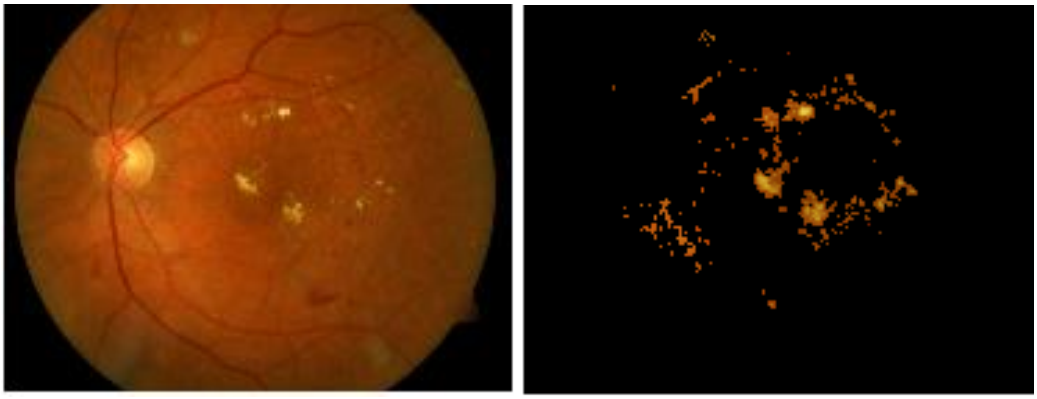

(a) (b)

Fig.4.2.4: Expected exudates after preprocessing stages (a) Input retinal RGB image, (b) Expected exudates.

We note in Fig.4.2.4: (b) that some areas are included in the extracted exudates around the OD which are not really exudates, and some of them around or even connected to exudates are not exudates. Therefore, to solve this problem we must use a method to detect the actual exudates exactly, in this work we are using FCM clustering method.

The expected exudate output of the preprocessing process will be used in the next section to extract the features that will be implemented as an input for the FCM clustering.

4.3 Features Extraction

Features extraction is a process to convert the preprocessed image into a set of features that efficiently represent the interested parts of an image. Proper features in this case depend on the properties of exudates. Traditionally, exudates are defined by ophthalmologists, where exudates appear as bright yellow spots with variable shapes and size, but they have sharp and strong

edges. These different features and others are used as an input data for the FCM clustering algorithm.

Many features were tested and finally four features are experimentally selected to be used in FCM, these are: hue, entropy and standard deviation for intensity and Y-channel. The reason for selecting these features and their details are explained in the following.

Firstly, we will discuss all the features used and tested, then we clarify the reason for choosing those particular four features.

4.3.1 Color Spaces Overview

Color spaces are different types of color modes, used in image processing. The most important types of color space are RGB, XYZ, HSI, Lab and Luv which can be used as features for FCM clustering [78].

For further information and clarification, refer to appendix A-2.

4.3.2 Variance, Standard Deviation and Entropy

The variance (which we denote by σ^2) is a measure of how spread out a data set is; in other words, it is the average squared deviation of values from the mean [22].

The variance of a set of values is defined as:

$$\sigma^2 = \frac{1}{\mathrm{N}} \sum_{i=1}^{\mathrm{N}} (x_i - \mu)^2 \qquad (4.3.1)$$

where x_i is the data value, N is the number data value, μ is the mean for the data, it is calculated by this formula:

$$\mu = \frac{1}{\mathrm{N}} \sum_{\mathrm{i}=1}^{\mathrm{N}} x_i \qquad (4.3.2)$$

and $\sum_{\mathrm{i}=1}^{\mathrm{N}} (x_i - \mu)^2$ means the summation of the squared of the difference between the mean and each data value [22].

In this thesis, the variance is calculated between pixels by partitioning the preprocessing image of size $(n \times n)$ to sub matrices of size $(m \times m)$, calculate the mean for these sub matrices using equation (4.3.2), then compute the variance by using equation (4.3.1), the result is a matrix of size $(n \times n)$ that contains the variance value for each pixel compared with the pixels around it, this is shown in Fig.4.3.1.

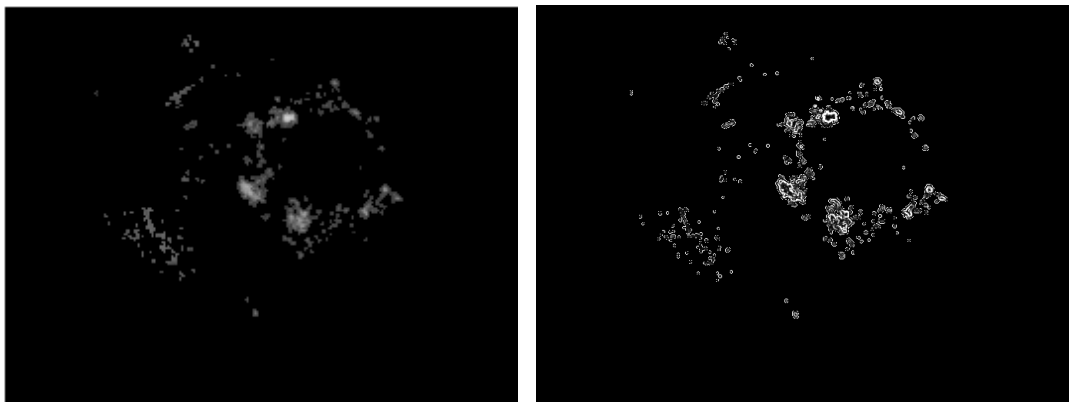

(a) (b)

Fig.4.3.1: Image variance (a) Green original image, (b) Image variance.

We note in calculating the image variance, the values of color are between 0 and 255, which means between black and white colors, the white refers to the high variance, but the black pixels refer to zero variance which means the data in the sub-matrix are of the same color, and the values in between have low contrast between the calculated pixels.

Another important feature is the standard deviation (σ), it is a useful measure of data spreading, commonly used as a statistical measure. It is useful when

comparing the spread of two separate data sets, so we used this feature in our work to compare between exudate and non-exudate pixels [7, 16, 22].

Standard deviation is calculated by taking the square root of the variance of a sub matrix as shown in equation (4.3.3).

$$\sigma = \sqrt{\frac{1}{\mathrm{N}}\sum_{\mathrm{i}=1}^{\mathrm{N}}(x_i - \mu)^2} \qquad (4.3.3)$$

Standard deviation shows how much variation exists from the mean. A small value of standard deviation indicates that the pixel values tend to be very close to the mean, whereas high value of standard deviation indicates that the pixel values are spread out over a large range of values, which means pixels are different.

We note in Fig.4.3.2: (a) that pixels with smaller standard deviation has a narrower spread of measurements around the mean. An item selected at random from a data set whose standard deviation is low having a better chance of being close to the mean than an item from a data set whose standard deviation is higher.

The entropy is a statistic measurement of randomness that can be used to characterize the texture of the input image. The concept of entropy tries to describe how much randomness is there in an image. When the value of entropy is high the pixel is different from the pixels around it, and low entropy images according to very little contrast and large runs of pixels with the same intensity. An image that is perfectly flat will have zero entropy [69,1]. Entropy is defined as:

$$H(x) = -\sum_{i \in W(x)} p_i \log_2 p_i \qquad (4.3.4)$$

where x is a set of all pixels in a sub-window $W(x)$, p_i is the histogram count in sub-window i. A window size of 3×3 pixels was used; the result is shown in Fig.4.3.2: (b):

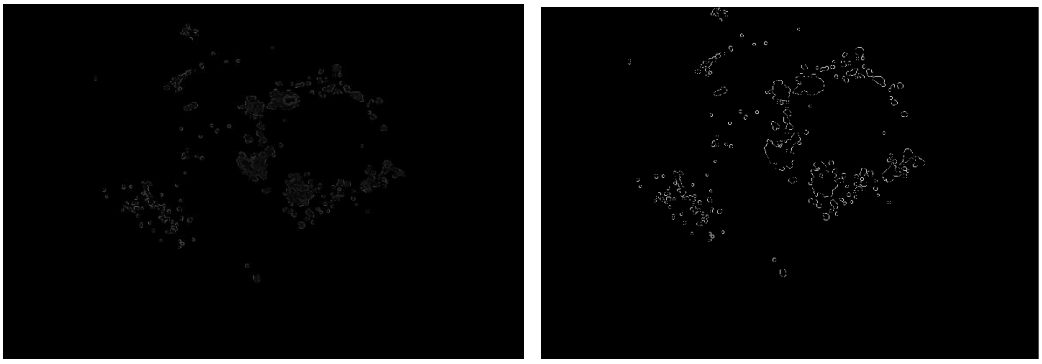

(a) (b)

Fig.4.3.2: A comparison between standard deviation and entropy (a) Standard deviation, (b) Entropy of a green channel image

4.4 Segmentation Using FCM Clustering

After the features are extracted from the expected exudates image, these features are considered as the data ($\boldsymbol{Z}$) which will be fitted as input for the FCM clustering algorithm.

4.4.1 FCM clustering overview

FCM is an overlapping clustering algorithm which can be used for segmentation. Each pixel may belong to one or more clusters with different degrees of membership. It assigns any unclassified pixel to the closest cluster

based on similarity measures; which means the distance of the features vector to the cluster centers ($\boldsymbol{V}$) (e.g., exudates and non-exudates).

The Euclidean distance is used to measure the distance and data will be associated to an appropriate membership value [11, 30]

The FCM clustering algorithm is briefly illustrated below (you can refer to chapter 2 for extra details):

The input data is a matrix containing the features for the candidate exudates which are extracted (as explained in section 4.3),

$$\boldsymbol{Z} = [z_1, z_2, \dots, z_M], \qquad z_i \in \mathbb{R}^N \tag{4.4.1}$$

The objective function is given by:

$$\boldsymbol{J}(\boldsymbol{Z}; \boldsymbol{U}, \boldsymbol{V}) = \sum_{i=1}^{M} \sum_{k=1}^{c} (\mu_{ik})^2 \|z_k - v_i\|^2 \ , \tag{4.4.2}$$

$$\mu_{ik} = \left[\sum_{j=1}^{c} \left(\frac{\|z_i - v_k\|}{\|z_i - v_j\|} \right)^2 \right]^{-1} , \tag{4.4.3}$$

$$v_k = \frac{\sum_{i=1}^{M} (\mu_{ik})^2 \, z_i}{\sum_{i=1}^{M} (\mu_{ik})^2} , \tag{4.4.4}$$

where M is the number of features used as input for FCM to identify the exudates accurately (four in our case), N is the number of pixels in an image that contains the candidate exudates, c is the number of clusters (in our case, experimentally we tried two and three), μ_{ik} is the degree of membership of z_i in the cluster k, z_i is the i^{th} item of the d-dimensional measured data, v_j is the center of the cluster, and $\|*\|$ is any norm expressing the similarity between any measured feature and the center.

Fuzzy partitioning is carried out through an iterative optimization of the objective function by updating μ_{ik} and v_k. The iteration stops when

$$\max_{ik}\{|\mu_{ik}{}^{(l+1)} - \mu_{ik}{}^{(l)}|\} < \varepsilon \qquad (4.4.5)$$

where ε was set to 0.00001, and l is the iteration number which is set to a maximum of 100 based on the default setting in matlab (in this implementation).

4.4.2 Executing the FCM Clustering Algorithm

The FCM algorithm is composed of the following steps, with the selected set of features as input data for the algorithm:

Step 1: Initialize the fuzzy membership (partition) matrix

$$\boldsymbol{U} = [\mu_{ik}](\boldsymbol{U}^{(0)})$$

by generating random numbers in the range 0 to 1 subject to equation (4.4.6):

$$\sum_{i=1}^{M}\sum_{k=1}^{c}\mu_{ik} = 1 \qquad (4.4.6)$$

Step 2: where c is the number of clusters and M is the number of features, at j-step compute the centers vectors

$$V^{(j)} = [v_k]$$

according to equation (4.4.4).

Step 3: Update the fuzzy partition (membership) matrix $\boldsymbol{U}^{(j)}$ to obtain $\boldsymbol{U}^{(j+1)}$ by the new computed μ_{ik}, refer to equation (4.4.3).

Step 4: Compute the objective function ($\boldsymbol{J}$), refer to equation (4.4.2). If the difference between $\boldsymbol{U}^{(j+1)}$ and $\boldsymbol{U}^{(j)}$ is less than or equal (ε). In other words, the difference satisfies equation (4.4.5) then stop the iteration, otherwise return to step 2.

In the end of process, the output from the FCM is defines cluster centers and membership grade for each pixel, a pixel will be assigned to the cluster corresponding to the highest membership grade.

4.5 Evaluating the FCM Clustering

Image segmentation can vary based on image quality and user experience. Hence several standard parameters are used to evaluate the segmentation performance.

Performance is measured by comparing the automated detected results with hand-drawn ground truth (GT) provided by expert ophthalmologists for retinal images [7], see Fig.4.5.1, where retinal colored images with corresponding GT segmentations showing exudates.

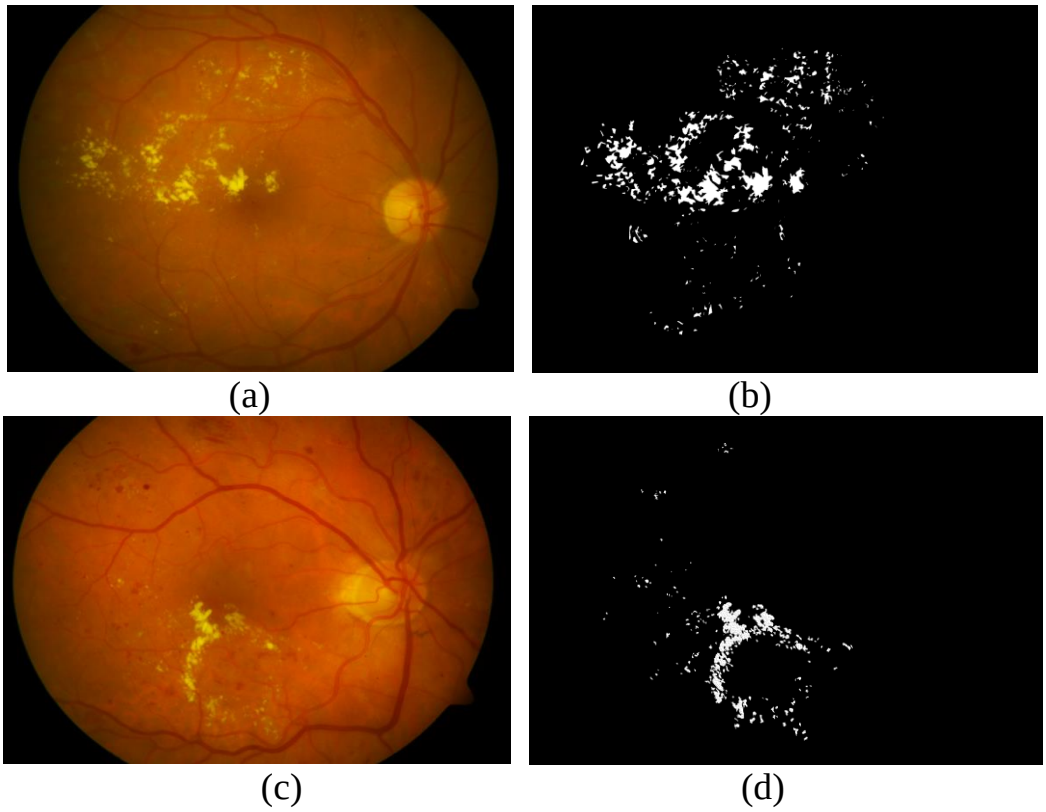

Fig.4.5.1: RGB retinal image with GT segmentation of exudates: (a) & (c) RGB retinal images, (b) & (d) GT exudates respectively.

True positive (TP), false positive (FP), false negative (FN), true negative (TN), sensitivity, specificity, accuracy, positive predictive value (PPV) and positive likelihood ratio (PLR) are used to analyze the performance of the FCM clustering. Their definitions are given in the following:

- TP: is the number of pixels detected as exudates in both GT and result image.
- FP: is the number of pixels detected as exudates in result image, but it is non-exudates in GT image.
- FN: is the number of non-exudate pixels detected in result image, but are identified as exudates in GT image.
- TN: is the number of non-exudate pixels which are correctly identified as non-exudate pixels.

In the next figure (Fig.4.5.2) confusion matrix shows the relation between GT versus output results.

		Result of FCM clustering	
		Exudates	Non-Exudates
GT	Exudates	TP	FN
	Non-Exudates	FP	TN

Fig.4.5.2: Confusion Matrix of Performance Evaluation.

To understand the results; some other parameters are used and computed, such as sensitivity, specificity, accuracy, PPV and PLR. And here are their definitions related to our work:

- Sensitivity (or true positive rate): measures the potential of FCM clustering to positively detect the exudates, on other words, the ability to identify exudate pixels correctly, and is hence given by:

$$\text{Sensitivety} = \frac{\text{TP}}{\text{TP} + \text{FN}} \tag{4.5.1}$$

- Specificity (or true negative rate): measures the potential of FCM clustering to correctly detect the non-exudate pixels, or the ability to identify non-exudate pixels correctly, and is given by:

$$\text{Specificity} = \frac{\text{TN}}{\text{TN} + \text{FP}} \tag{4.5.2}$$

- Accuracy: measures the potential of FCM clustering to get accurate results while detecting exudates and non-exudates, it is given by:

$$\text{Accuracy} = \frac{\text{TP} + \text{TN}}{\text{TP} + \text{FP} + \text{FN} + \text{TN}} \tag{4.5.3}$$

- Positive Predictive Value (PPV): is the ratio of exudates and non-exudate pixels which are positively detected, or is the probability to detect correct exudate pixels out of all detected exudate pixels by the method. Mathematically can be expressed as:

$$\text{PPV} = \frac{\text{TP}}{\text{TP} + \text{FP}} \tag{4.5.4}$$

- Positive Likelihood Ratio (PLR): is defined as follows:

$$\text{PLR} = \frac{\text{Sensitivety}}{1 - \text{specificity}} = \frac{\text{TP} * (\text{TN} + \text{FP})}{\text{FP} * (\text{TP} + \text{FN})} \tag{4.5.5}$$

We note in (4.5.1), (4.5.4) and (4.5.5) the high value of TP value will increase the PPV, PLR and sensitivity values; this means the high value of TP indicates the correct identify for exudates will happen, then the PPV and PLR values are indicators of an another performance of the exudates detection system [28,7,8,37].

Chapter Five
Results and Discussion

Chapter Five

Results and Discussion

In this research, we have used five images for training and another five for testing to evaluate the performance of the proposed method; we used DIARETDB1 dataset [19]. The used images are a subset of the DIARETDB1 Project's dataset which consists of 89 color fundus images, because of the wide variability in the color of the fundus images for different patients, and these images contain normal and abnormal with symptoms of retinopathy, we managed to choose only ten abnormal images out of them. The images have a size of 1500×1152 pixels stored in PNG format.

The proposed algorithm is implemented using MATLAB version R2017a and run on a Laptop with 4GB Ram and 2.2GHz Intel Core i3.

The method includes: extracting both the OD and blood vessels by using preprocessing, after that another preprocessing process is applied to define expected exudates as a first stage, and then FCM based segmentation is implemented as a second stage to refine the exudates identification. Finally, a testing of the algorithm on the dataset has been performed.

5.1 Experimental Results

In chapters three and four, we discussed and explained the preprocessing steps; the features extracted used as input for the proposed algorithm (FCM clustering) and finally how to evaluate the method.

In this section we review the performance results to evaluate the system by comparing the GT images with the clustering results using equations 4.5.1, 4.5.2, 4.5.3 and 4.5.4 in chapter four.

Many features are extracted for each image as shown in section (4.3) to be used as input for FCM clustering algorithm, but not all features are useful. So we used evaluation system to determine which are the best features to be used. However, we firstly evaluated the system by using each feature separately, then using two features together, after that, three features together and so on.

The suggested features are about one hundred, hence the number of combination possibilities are $\binom{n}{m}$, where *n* is the overall number of features and *m* is the number of input features, so the total number of possibilities is huge, it is not helpful to display all results. Practically; we note that using four features gave the best sensitivity results compared to using two or three features.

Hence, we display only the results for each feature separately and the four features that are experimentally selected and these are shown in Tables 5.1.1 and 5.2.1.

Table 5.1.1.The sensitivity of exudates detection for the suggested features using FCM on the training images.

	Image 1	Image 2	Image 3	Image 4	Image 5	Mean of Sensitivity
Red channel (R)	52.97	54.18	48.47	69.89	79.83	61.07
Green channel (G)	53.76	58.22	59.87	80.81	63.26	63.18
Blue channel (B)	58.26	47.43	40.32	49.73	62.06	51.56
X-channel	58.61	45.52	56.82	78.70	60.70	60.07
Y-channel	59.31	44.80	62.88	80.41	50.25	59.53
Z-channel	55.97	58.64	49.08	57.77	55.86	55.46
H-channel	55.34	59.53	69.58	71.33	96.00	70.36
Intensity channel	58.50	47.57	58.58	77.20	98.05	67.98
L-channel	63.24	53.62	63.48	81.63	50.85	62.56
a-channel	66.82	74.93	72.87	84.22	97.90	79.35
b-channel	69.39	47.24	41.51	68.62	82.68	61.89
l-channel	58.61	47.43	56.82	78.70	60.71	60.45
u-channel	59.31	45.52	62.88	80.41	50.25	59.67
v-channel	55.97	58.64	49.08	57.77	55.86	55.46
Contrast G channel	64.89	58.51	64.75	80.01	56.96	65.02
Variance for G channel	85.48	84.18	75.62	82.40	97.81	85.10
Standard deviation for G channel	94.51	87.36	75.93	86.24	97.60	88.33
Variance without border for G channel	86.83	86.09	78.62	86.56	93.89	86.40
Standard deviation without border for G channel	95.78	89.76	78.94	90.22	97.95	90.53
Entropy G channel	94.51	87.36	75.89	86.24	97.60	88.32
Contrast Red channel	67.93	66.24	48.30	69.36	78.88	66.14
Variance for Red channel	92.72	87.36	75.89	86.24	97.25	87.89
Standard deviation for Red channel	94.51	87.36	75.94	86.24	97.61	88.33
Entropy for Red channel	94.51	87.36	75.89	86.24	97.60	88.32
Contrast Blue channel	67.61	60.71	44.87	46.79	51.95	54.39

Variance for Blue channel	80.10	80.71	49.51	73.67	88.19	74.44
Standard deviation for Blue channel	54.42	58.10	60.76	53.58	78.28	61.03
Entropy for Blue channel	81.89	77.71	41.53	55.87	86.04	68.61
Contrast X- channel	71.68	60.90	59.10	75.31	62.56	65.91
Variance for X-channel	91.86	87.36	75.88	86.21	97.15	87.69
Standard deviation for X-channel	94.51	87.36	75.91	86.24	97.65	88.33
Entropy for X- channel	94.51	87.36	75.89	86.24	97.60	88.32
Contrast Y- channel	68.67	58.23	61.90	78.32	53.75	64.17
Variance for Y-channel	88.55	86.42	75.82	85.24	95.15	86.24
Standard deviation for Y-channel	94.48	87.36	75.91	86.24	97.60	88.32
Entropy for Y-channel	94.51	87.36	75.89	86.24	97.60	88.32
Contrast Z- channel	67.95	55.46	52.32	66.97	51.15	58.77
Variance for Z-channel	89.98	87.48	70.82	86.19	97.30	86.35
Standard deviation for Z-channel	72.81	87.21	56.82	80.44	90.34	77.52
Entropy for Z-channel	94.51	87.36	75.89	86.24	97.60	88.32
Contrast H-channel	96.01	90.31	91.06	91.07	98.05	93.30
Variance for H-channel	91.56	87.26	76.40	86.31	97.95	87.90
Standard deviation for H-channel	94.39	87.26	76.42	86.34	97.80	88.44
Contrast S- channel	96.01	90.31	80.35	91.07	98.05	91.16
Variance for S-channel	78.14	23.20	53.44	76.28	88.89	63.99
Standard deviation for S-channel	58.91	44.11	51.41	57.04	72.52	56.80
Contrast Intensity channel	96.01	90.31	80.35	91.07	98.05	91.16
Variance for Intensity channel	91.62	87.36	75.88	86.21	97.10	87.63
Standard deviation for I channel	94.51	87.36	75.91	86.24	97.61	88.33
Variance without border for I channel	92.49	89.81	78.40	89.92	97.61	89.65
Standard deviation without border for I channel	95.72	89.69	78.67	89.82	97.95	90.37
Entropy for Intensity channel	94.51	87.36	75.89	86.24	97.61	88.32
Contrast L- channel	96.01	90.31	80.35	91.07	97.60	91.07

Variance for L-channel	94.51	87.36	75.89	86.24	97.60	88.32
Standard deviation for L-channel	94.51	87.36	75.89	86.24	97.60	88.32
Entropy for L- channel	94.51	87.36	75.88	86.24	97.60	88.32
Contrast a- channel	72.26	47.28	80.35	88.70	97.35	77.19
Variance for a-channel	95.22	89.93	79.32	90.29	97.80	90.51
Standard deviation for a-channel	94.81	88.91	77.33	88.55	97.65	89.45
Entropy for a- channel	77.91	68.54	75.89	78.00	95.60	79.19
Contrast b- channel	96.01	90.31	80.35	91.07	98.05	91.16
Variance for b-channel	94.51	87.36	75.89	86.24	97.60	88.32
Standard deviation for b-channel	94.51	87.36	75.95	86.24	97.60	88.33
Entropy for b- channel	94.51	87.36	75.89	86.24	97.60	88.32
Contrast l- channel	71.68	60.90	59.10	75.31	62.56	65.91
Variance for l-channel	91.86	87.36	75.88	86.21	97.15	87.69
Standard deviation for l-channel	94.51	87.36	75.91	86.24	97.65	88.33
Entropy for l- channel	94.51	87.36	75.89	86.24	97.60	88.32
Contrast u- channel	68.67	58.23	61.90	78.32	53.75	64.17
Variance for u-channel	88.55	86.42	75.82	85.24	95.15	86.24
Standard deviation for u-channel	94.47	87.36	75.91	86.24	97.60	88.32
Entropy for u- channel	94.51	87.36	75.89	86.24	97.60	88.32
Contrast v- channel	67.95	55.46	52.32	66.97	51.15	58.77
Variance for v-channel	89.14	87.48	70.82	86.19	96.80	86.09
Standard deviation for v-channel	72.84	87.21	56.82	80.44	89.64	77.39
Entropy for v- channel	94.51	87.36	75.89	86.24	97.60	88.32

5.1.1 Input features for FCM

The four features used for FCM clustering are: Hue channel, entropy for intensity channel, standard deviation for intensity and Y-channel, these are

experimentally selected. The reason for selecting these features is explained in this section.

The first input feature to FCM is Hue, which is extracted from HSI color space; it gives chrominance or color information, which showed good results by itself.

Entropy of intensity band, it is the second input for FCM clustering, where the intensity band is extracted from HSI space. The concept of entropy describes how much randomness there is in an image, it is used because it gives contrast from one pixel to the next, which means when the value of entropy is high this represents pixels are different from a rounding ones, on the other hand, if the value of entropy is low then pixels nearby are randomly distributed around it.

While third and fourth inputs are the standard deviation of intensity and Y-channel, standard deviation shows how much variation exists from the mean. On other words, distribution measurement of pixel values would differentiate exudate from non-exudate areas.

The features are shown in Fig.5.1.1: (b), (c), (d), (e) below:

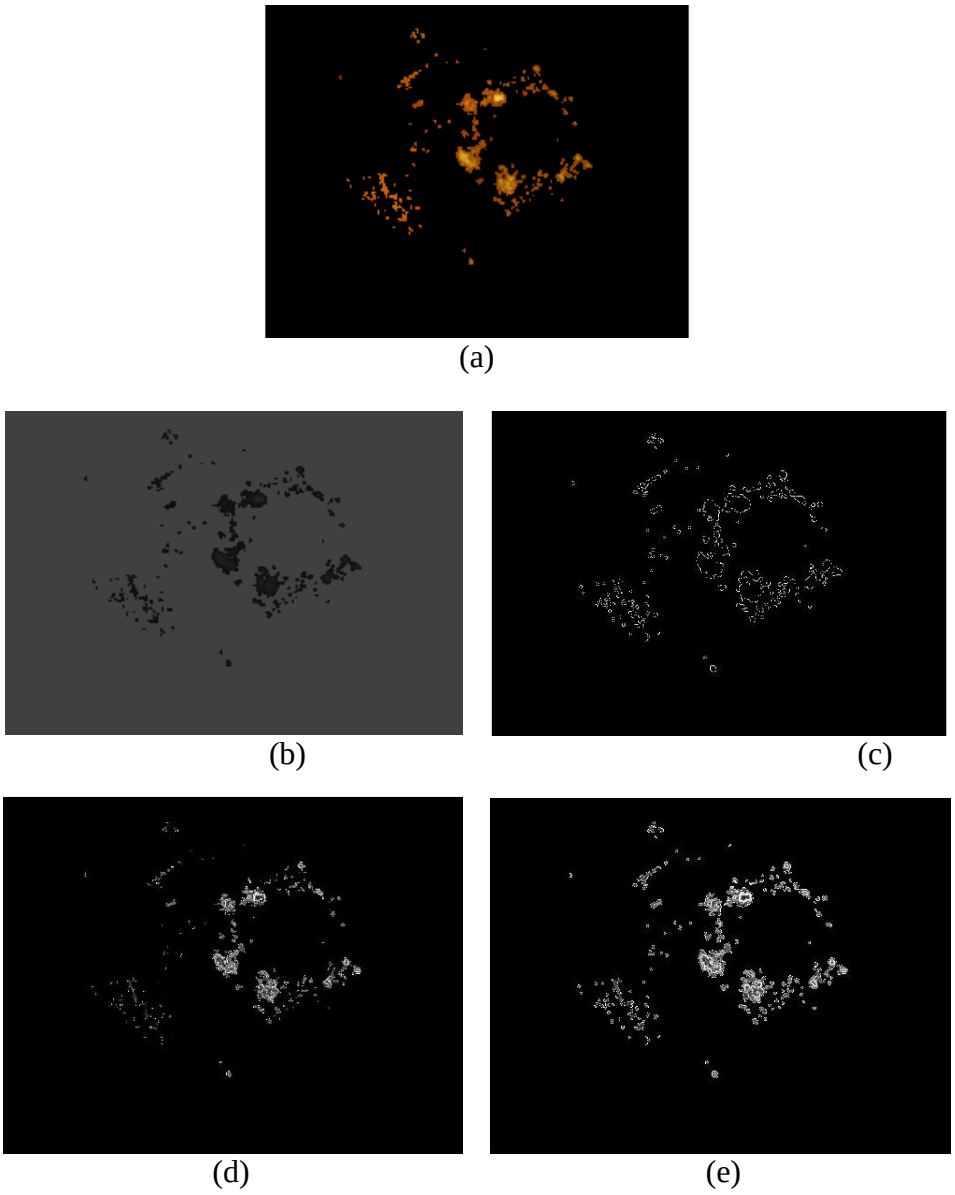

(a) (b) (c) (d) (e)

Fig.5.1.1: Hue, entropy and standard deviation of intensity, standard deviation of Y-channel of an RGB image: (a) Input retinal RGB image, (b) Hue component, (c) Entropy of intensity channel, (d) Standard deviation of intensity, (e) Standard deviation of Y- channel.

5.1.1.1 Data Set

A data set is typically a number of observations of some process. Each observation consists of $\boldsymbol{n}$ measured variables, grouped into an $\boldsymbol{n}$-dimensional

column vector $z_k = [z_{1k}, \ldots, z_{nk}]^T$, $z_k \in \mathbb{R}^n$. An $\boldsymbol{N}$ observations data set is denoted by $\boldsymbol{Z} = \{z_k \mid k = 1, 2, \ldots, N\}$, it is represented as an $n \times N$ matrix:

$$\boldsymbol{Z} = \begin{bmatrix} z_{11} & z_{12} \cdots & z_{1N} \\ z_{21} & z_{22} \cdots & z_{2N} \\ \vdots & \vdots & \vdots \\ z_{n1} & z_{n2} \cdots & z_{nN} \end{bmatrix}$$

$\boldsymbol{Z}$ is called the pattern or data matrix, the rows are called patterns or objects, and the columns are called the features or attributes [11]. The meaning of the columns and rows of $\boldsymbol{Z}$ depends on the context, for example when clustering is applied to the identification of retinal image, the columns of $\boldsymbol{Z}$ may contain image features, and the rows are variables observed in the system.

5.1.2 FCM Clustering Results

After features selection, we applied the FCM clustering algorithm to images for detecting exudates, this technique can be used to identify how much exudates are present in the retinal fundus image, and results are shown in Fig.5.1.2 and Table 5.2.1.

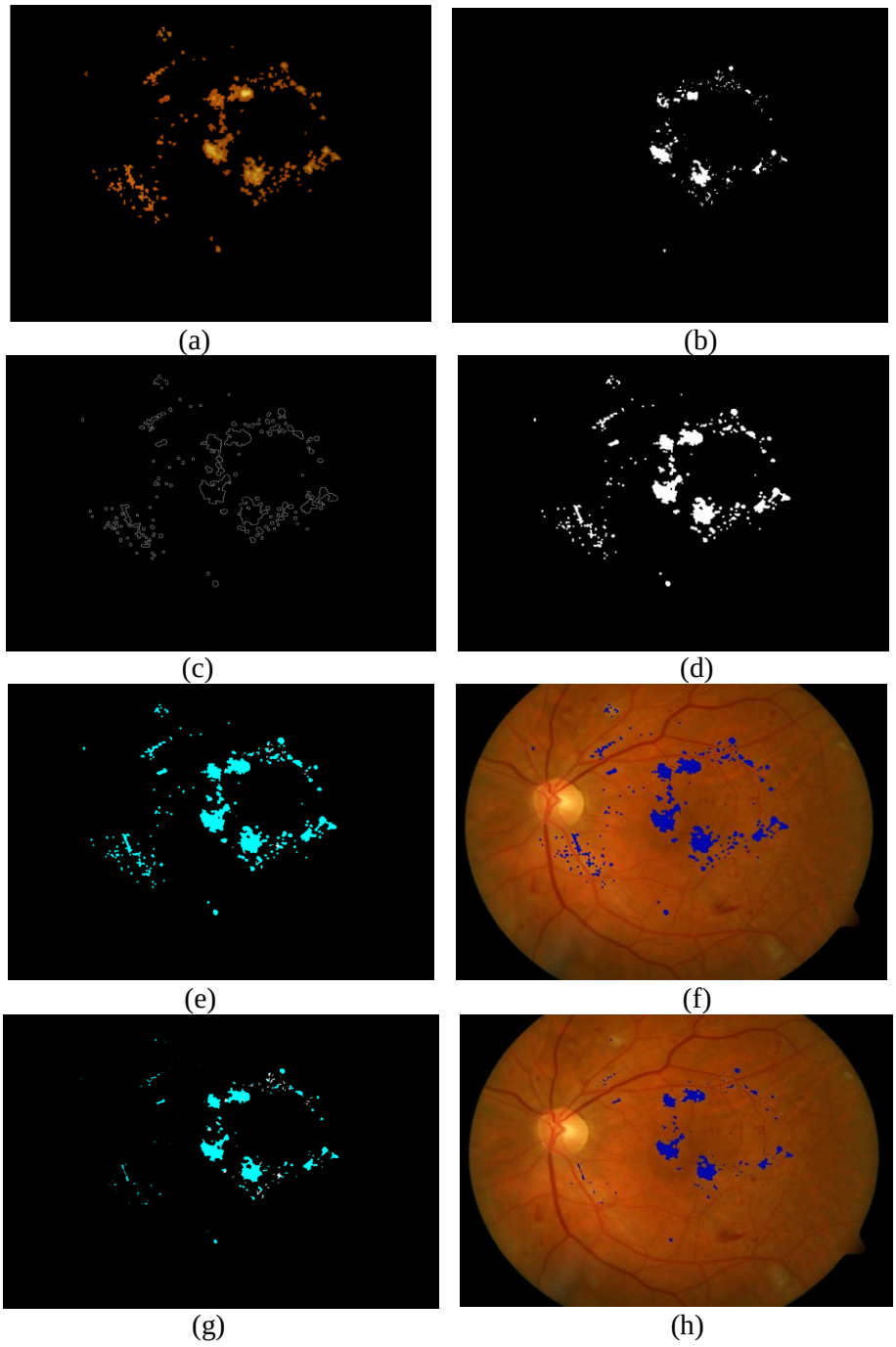

Fig.5.1.2: FCM clustering results with n=2: (a) Expected exudate areas for RGB retinal image, (b) GT, (c) cluster 1 (d) cluster 2, (e) extracted exudates compared with GT, where blue color refer to the extracted exudates and white refer to the GT, (f) FCM clustering results superimposed on original retinal image, (g) extracted exudates after morphological processing, (h) FCM clustering results superimposed on original retinal image after applied mathematical morphology.

In Fig.5.1.2 two candidate clusters were used for exudates detection; which means that the number of clusters equals 2. The first cluster (Fig.5.1.2: (c)) contains non exudate areas, but the second cluster contains most of the exudate areas (Fig.5.1.2: (d)), where the true positive value is high in second cluster and the false negative value is low compared with the first cluster. We note the false positive value would also be very high due to misclassified non-exudate pixels.

From the experimental results, we notice that the FCM clustering technique gives a high true positive value, in addition to false positive values as pixels are located around the OD, this is shown in Fig.5.1.2: (f).

To overcome this difficulty; we used mathematical morphology process to reduce the false positive pixels, after this implementation results are shown in Fig.5.1.2: (h).

5.2 System Evaluation

To evaluate the performance of our technique, we compare the results of the extracted exudates with ophthalmologist's hand-drawn GT images (Fig.5.1.2: (b)), the result is shown in Fig.5.1.2: (e). This approach aims to measure the correctness of the algorithm at the pixel level by using equations 4.5.1, 4.5.2, 4.5.3 and 4.5.4 in chapter four.

Using the FCM clustering algorithm with $n = 2$ on training and testing images, the maximum value of sensitivity, specificity and accuracy are 97.60%, 99.87% and 99.86% respectively. Detailed results of performance measurement are presented in Tables 5.2.1 and 5.2.2.

In exudates detection the sensitivity (true positive rate) is the most important parameter as it measures the potential of FCM to do correct clustering which is positively detecting the exudates. We note in equation (4.5.1); if TP is increasing the sensitivity will increase, and if FN is decreasing the sensitivity will increase and gives the best result, so the FN value must be decreased to improve the sensitivity.

We note if TP is high and FP is low the PPV will be high, but in our work the FP is high so the value of PPV is low. To increase the PPV value we used morphological process.

Another important parameter which measures the potential of FCM clustering to get accurate results, while detecting exudates and non-exudates is accuracy which is increased when TP increases. However, the PPV and PLR values are low. Using FCM clustering followed by morphological process, we have higher accuracy with a lower false positive value.

In Fig.5.1.2: (h); when applying the morphological process after FCM clustering, we have higher accuracy and PPV with a lower FP value, as well as we have lower sensitivity with lower TP value, the results are shown in Tables 5.2.3 and 5.2.4.

Table 5.2.1. Exudates detection results using FCM on training images, for n=2

24-bit images	TP	FP	FN	TN	Sensitivity (%)	Specificity (%)	PPV (%)	PLR	Accuracy (%)
Image 1	12244	25973	714	1689069	94.49	98.49	32.04	62.576	98.46
Image 2	1950	25927	48	1700075	97.60	98.50	6.99	65.067	98.49
Image 3	1826	3116	260	1722798	87.54	99.82	36.95	486.333	99.80
Image4	845	2204	199	1724752	80.94	99.87	27.71	622.615	99.86
Image 5	3930	12597	843	1710630	82.34	99.27	23.78	112.795	99.22

Table 5.2.2. Exudates detection results using FCM on testing images, for n=2.

24-bit Images	TP	FP	FN	TN	Sensitivity (%)	Specificity (%)	PPV (%)	PLR	Accuracy (%)
Image 1	19095	26752	2763	167939	87.36	98.43	41.65	55.643	98.29
Image 2	3465	21551	553	1702431	86.23	98.75	13.89	68.984	98. 72
Image 3	11166	63772	3547	1649515	75.89	96.27	14.90	20.346	96.10
Image4	3411	7790	351	1716448	90.67	99.55	30.45	201.489	99.53
Image 5	452	15434	43	1712071	91.31	99.11	2.84	102.595	99.10

Table 5.2.3. Exudates detection results using FCM, for n=2 after applying morphological processing on training images.

24-bit images	TP	FP	FN	TN	Sensitivity (%)	Specificity (%)	PPV (%)	PLR	Accuracy (%)
Image 1	11152	7917	1806	1707125	86.06	99.54	58.48	187.087	99.44
Image 2	1827	5261	171	1720741	91.44	99.70	25.78	304.8	99.68
Image 3	1713	934	373	1724980	82.12	99.95	64.71	1642.4	99.92
Image4	783	1597	261	1725359	75.00	99.90	32.89	750	99.89
Image 5	3345	5127	1428	1718100	70.08	99.70	39.48	233.6	99.62

Table 5.2.4. Exudates detection results using FCM, for n=2 after applying morphological processing on testing images.

24-bit images	TP	FP	FN	TN	Sensitivity n (%)	Specificity (%)	PPV (%)	PLR	Accuracy (%)
Image 1	16908	10484	4950	1695658	77.35	99.39	61.73	126.803	99.11
Image 2	2875	5766	1143	1718216	71.55	99.67	33.27	216.818	99.60
Image 3	8694	18449	6019	1694838	59.09	98.92	32.03	54.713	98.58
Image4	3031	3223	731	1721015	80.57	99.81	48.47	424.053	99.77
Image 5	364	1478	131	1726027	73.54	99.91	19.76	817.111	99.91

5.3 Tuning the Parameters

In this thesis; many important parameters are used; these parameters are directly affecting the exudates detection, so we have to understand how they affect the results therefore tune these parameters to get the best performance. These parameters are: number of clusters (n), windows size of standard deviation, windows size of entropy and the size of the area around the OD (the size of the structure elements used for the dilation operation on OD).

5.3.1 Number of Clusters (n)

First, we used $n = 2$ to have two clusters; exudates and non-exudates, then we changed the number of clusters into 3; in this case the data is divided into three groups; exudates, non-exudates and else, we note that most of the classified exudate regions are true exudate pixels, giving a smaller TP value; however, it also reduces the FP value because misclassification of non-exudate pixels is also lower.

We noticed that the TP value will be reduced for $n = 3$ clusters; consequently reducing the sensitivity values from 94.49% to 80.42%, so we fix the number of clusters to 2, we introduce a comparison where $n = 2$ and $n = 3$ in Fig.5.3.1: (c).

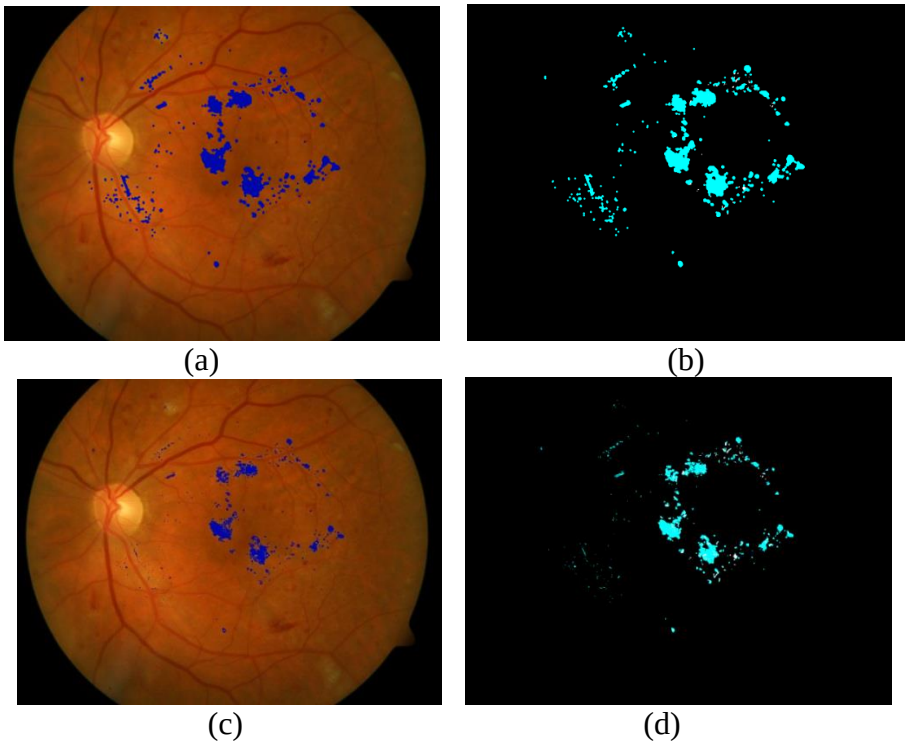

(a) (b)

(c) (d)

Fig.5.3.1: Exudates for 2 and 3 clusters: (a) Results of FCM with $\boldsymbol{n = 2}$ for a retinal image, (b) Extracted exudates for $\boldsymbol{n = 2}$ compared with GT, (c) Results of FCM with $\boldsymbol{n = 3}$ for retinal image, (d) Extracted exudates for $\boldsymbol{n = 3}$ compared with GT.

5.3.2 Windows size of standard deviation

To get the best result of detection we optimized the size of standard deviation window, the following sizes were used 3*3, 7*7, 11*11, 15*15 and 17*17, results are shown in Fig.5.3.1. An experimental result of FCM clustering with 3*3 window for standard deviation gives the highest TP and FP values. We notice that when the window size of standard deviation increases, the small exudate areas are not detected, so this reduces the sensitivity of the system (see Table 5.3.1) consequently reduces the efficiency of exudates detection. Hence, we used standard deviation with 3*3 window size.

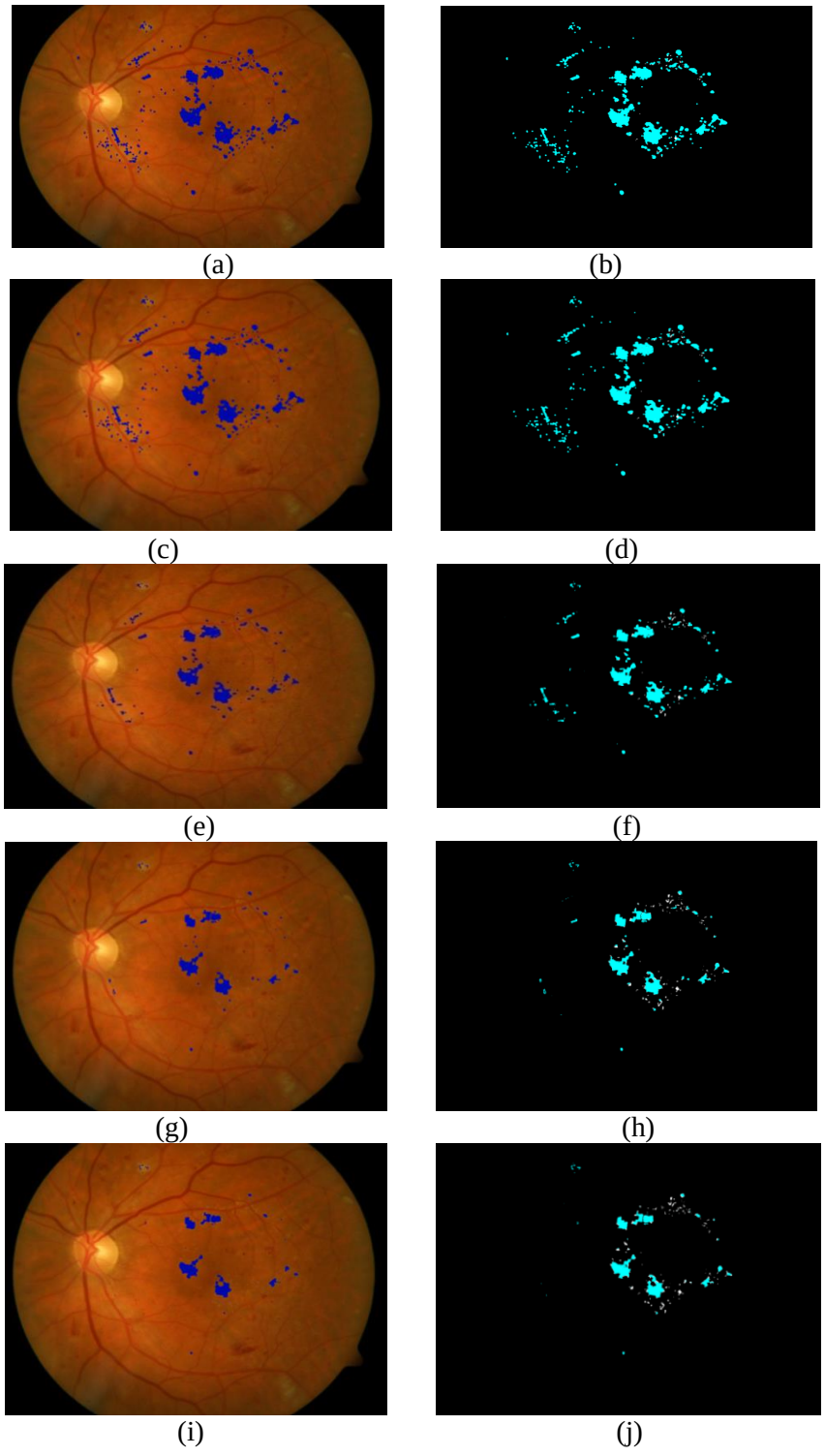

Fig.5.3.2: The result of FCM with variant window size of standard deviation: colored extracted exudates with window size: (a) 3*3, (c) 7*7, (e) 11*11, (g) 15*15 (i) 17*17, extracted exudates compared with GT for window size (b) 3*3, (d) 7*7, (f) 11*11, (h) 15*15, (j) 17*17.

Table 5.3.1. The results of FCM exudates detection for training image 1 of standard deviation with different window size.

Window size	TP	FP	FN	TN	Sensitivity (%)	Specificity (%)	PPV (%)	PLR	Accuracy (%)
3*3	12244	25973	714	1689069	94.49	98.49	32.038	62.576	98.46
7*7	12159	24258	799	1690784	93.83	98.59	33.39	66.546	98.55
11*11	11515	12266	1443	1702776	88.86	99.28	48.42	123.417	99.21
15*15	9981	2977	4711	1710331	77.03	99.73	77.03	285.296	99.56
17*17	9201	2954	3757	1712088	71.01	99.83	75.70	417.706	99.61

5.3.3 Size of Entropy Window

Another important parameter (feature) can be optimized to improve the performance of the system is the size of entropy window. We changed the size between 3*3 and 17*17, it is noticed that increasing the size of the window effects on small exudate areas which are not detect, so TP values will be decreased, this effects on sensitivity value. Also FP value will be decreased which mean the misclassification data will be decreased; the results are shown in Table 5.3.2 and Fig.5.3.3.

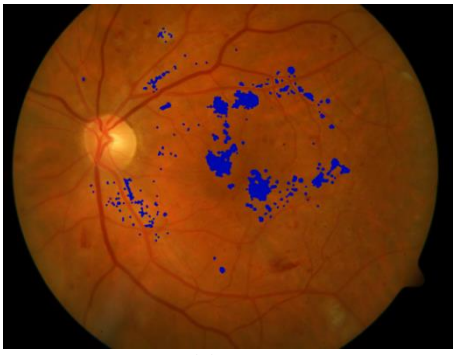

(a)

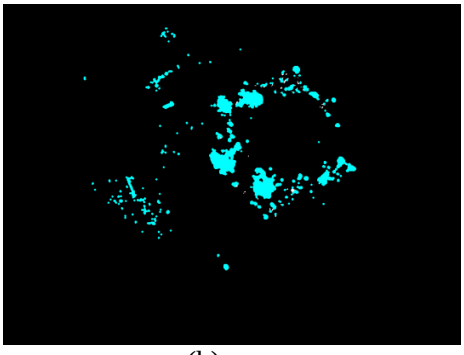

(b)

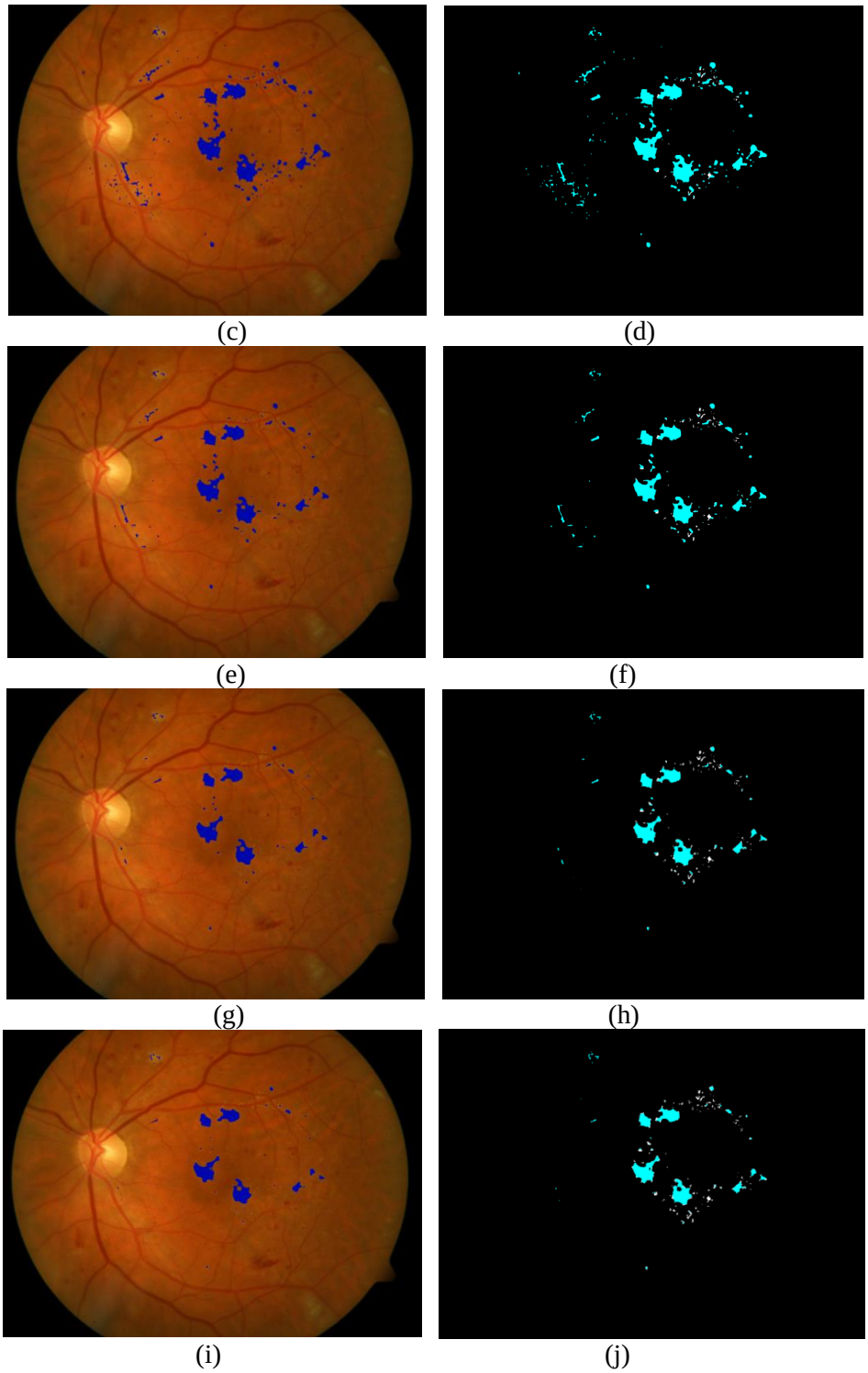

Fig.5.3.3: Resulting extracted exudates for a retinal image using FCM with different size for entropy window: colored extracted exudates with window size: (a) 3*3, (c) 7*7, (e) 11*11, (g) 15*15, (i) 17*17, Extracted exudates compared with GT for: (b) 3*3, (d) 7*7, (f) 11*11, (h) 15*15, (j) 17*17.

Table 5.3.2. Extracting exudates using FCM for training image 1 with different size for entropy windows

Window size	TP	FP	FN	TN	Sensitivity (%)	Specificity (%)	PPV (%)	PLR	Accuracy (%)
3*3	12244	25973	714	1689069	94.49	98.49	32.04	62.576	98.46
7*7	11827	15770	1131	1699272	91.27	99.08	42.86	99.207	99.02
11*11	11205	8679	1753	1706363	86.47	99.49	56.35	169.549	99.40
15*15	10118	5117	2840	1709925	78.08	99.70	66.41	260.266	99.54
17*17	9515	4256	3443	1710786	73.43	99.75	69.09	293.720	99.55

5.3.4 The area size around OD

The area around the OD has in general similar color as OD and exudates; this area doesn't contain the exudates, but effect on exudates detection, so we have to extract this area and eliminate it to reduce artifacts.

In this part we eliminate this area by dilating the OD with a SE between 0 and 45; samples of the results are shown in Fig.5.3.4.

When the SE size increases the FP value will be reduced, as a result the artifacts will be reduced. This will be reflected of the efficiency of the system by getting better and more accurate detection. Though the TP and sensitivity values do not change (see Table 5.3.3).

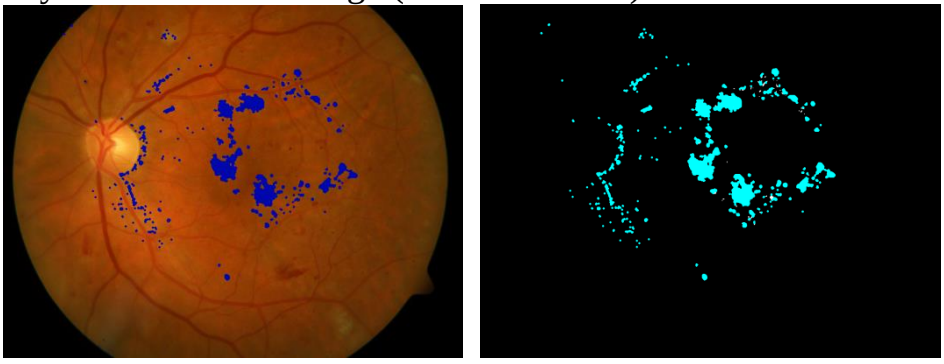

(a) (b)

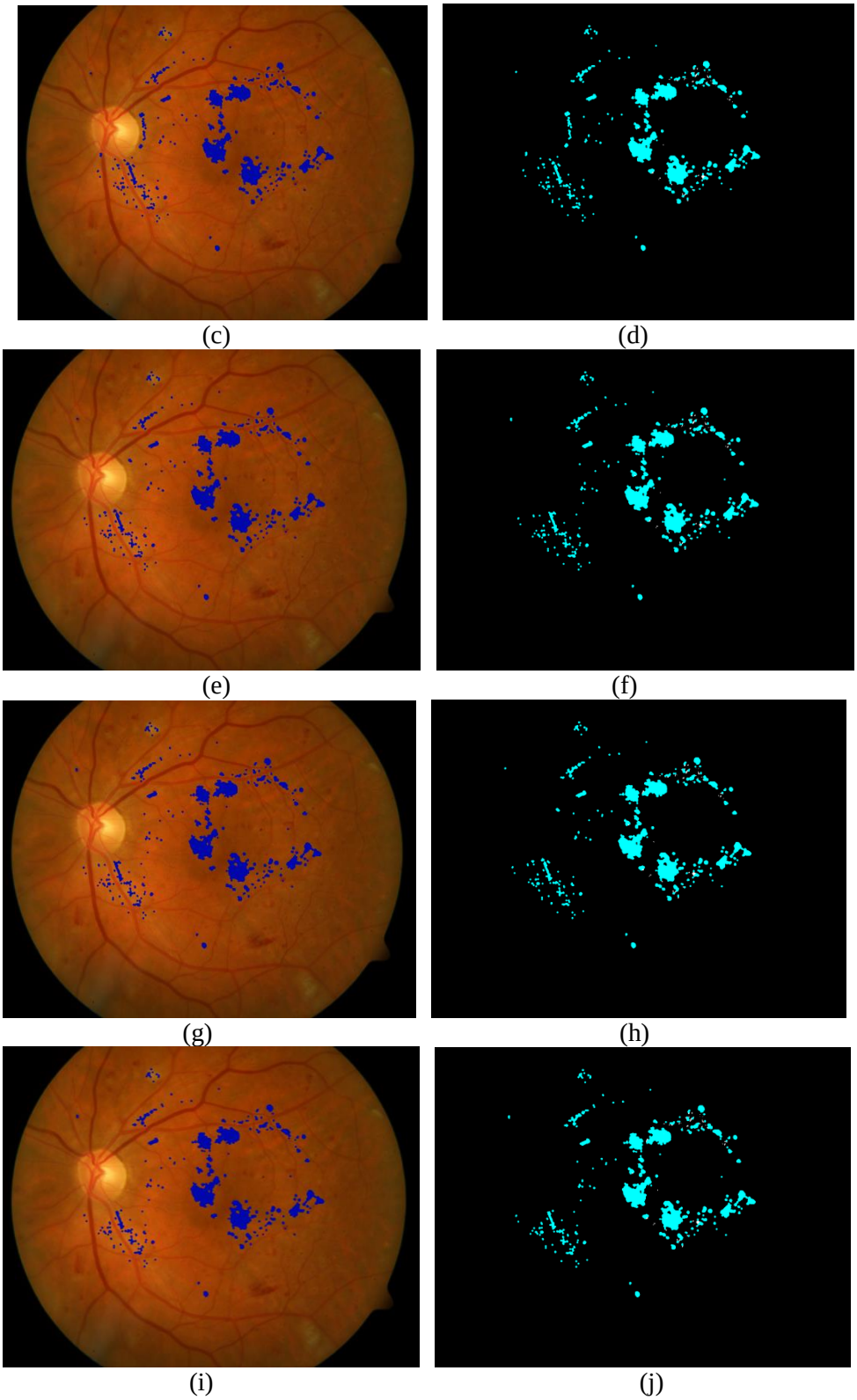

Fig.5.3.4: Dilating the OD with different SE: colored extracted exudates with different size: (a) SE=0, (c) SE=10, (e) SE=25, (g) SE=35, (i) SE=45. Extracted exudates compared with GT for: (b) SE=0, (d) SE=10, (f) SE=25, (h) SE=35, (j) SE=45.

Table 5.3.3. The results of FCM exudates detection for training image 1 for different size of area around the OD.

Size of SE	TP	FP	FN	TN	Sensitivity (%)	Specificity (%)	PPV (%)	PLR	Accuracy (%)
0	12260	26168	698	1688874	94.61	98.47	31.90	64.359	98.45
10	12275	26568	683	1688474	94.73	98.45	31.60	63.516	98.42
25	12244	25973	714	1689069	94.49	98. 49	32.04	65.225	98.46
35	12240	25336	718	1689706	94.45	98.52	32.57	66.568	98.49
45	12204	25709	754	1689333	94.18	98.50	32.19	65.667	98.47

5.4 Conclusions

DR disease is the main cause of blindness, so the early detection of the disease can potentially reduce the risk of blindness. Current methods of detection of DR are expensive, manual, time consuming, and require trained ophthalmologists.

In this research, we proposed a method to detect exudate areas automatically, the development of exudates detection will help the doctors in screening process of DR to detect symptoms faster.

The method is based on the FCM clustering algorithm, OD and blood vessels are removed to prevent misclassification and facilitate exudate detection. Four features are used as input data for FCM: hue, standard deviation for intensity, standard deviation for Y and entropy.

Experimental results showed that when the FCM clustering technique is applied combined with morphological processes the accuracy, PPV and PLR values increases. But when FCM clustering is applied without morphological processes the sensitivity and FP values increases.

One of the major obstacles for identification of retinal exudates is the wide variability in the color of the fundus images from different patients. Moreover, some areas which are similar to exudates, called artifacts, cause incorrect detections. These pixels may have no effect on sensitivity; these patches are known as ambiguous regions.

The method has been evaluated and compared on the DIARETDB1 database images. To evaluate the overall performance it is found that the proposed method detects exudate areas successfully with average sensitivity,

specificity, and accuracy of 86.29%, 98.42%, and 98.35% respectively on the testing used images.

5.5 Future Work

In this section, we present some future work which might improve the performance of the algorithm and overcome some difficulties the algorithm faces, new approaches might be included to the proposed approach as follows:

1. Increasing the number of retinal images, and performing more experiments.
2. Improve methods to localize and segment the OD and blood vessels more accurately.
3. Extending the proposed approach to detect spot lesions, namely micro-aneurysms and hemorrhages.
4. Improving the performance of the system by finding more specific characteristics of exudates which could distinguish them more effectively.

References

[1] A. Agrawal, R.C. Tripathi, E. Yi-Luen Do and M. D. Tiwari, ***Intelligent Interactive Technologies and Multimedia*****:** Second International conference**,** IITM 2013.

[2] A. Ford, A. Roberts, ***Color Space Conversions***, UK, August 11, 1998.

[3] A. Guyton and J. Hall, ***Textbook of Medical Physiology*****, Elsevier Inc**., International Edition ISBN 0-8089-2317-X, 2006.

[4] A. Mohan and K. Mouthy, ***Early Detection of Diabetic Retinopathy Edema using FCM***, **International Journal of Science and Research,** ISSN: 2319-7064, Vol. 2 Issue 5, 2013.

[5] A. Osareh, M. Mirmehdi and B. Thomas, ***Classification and Localizations of Diabetic- Related Eye Disease,*** European Conf. on Computer Vision (ECCV), pp. 502-516, 2002.

[6] A. Osareh, M. Mirmehdi, B. Thomas and R. Markham, ***Automated identification of diabetic retinal exudates in digital colour images*****,** 87:1220–1223, 2003.

[7] A. Sopharak, B. Uyyanonvara and S. Barman, ***Automatic Exudate Detection from Non-dilated Diabetic Retinopathy Retinal Images Using Fuzzy C-means Clustering***, ISSN 1424-8220, UK, 2009.

[8] A. Sopharak, B. Uyyanonvara and S. Barman, ***Automatic exudates detection for diabetic retinopathy Screening***, doi: 10.2306/scienceasia1513-1874.2009.35.080, 2009.

[9] A. Sopharak, B. Uyyanonvara, S. Barman and T. Williamson, ***Automatic Micro-aneurysm Detection from Non-dilated Diabetic Retinopathy***

Retinal Images, Proceedings of the World Congress on Engineering, London, U.K, July, 2011.

[10] A. Ye and Y. Xian Jin, ***A Fuzzy C-Means Clustering Algorithm Based on Improved Quantum Genetic Algorithm***, **International Journal of Database Theory and Application Vol. 9, No.1**, pp.227-236, China, 2016.

[11] B. Balasko, J. Abonyi and B. Feil, ***Fuzzy Clustering and Data Analysis Toolbox For Use with Matlab***, Department of Process Engineering University of Veszprem, 2002.

[12] C. Hsieh, C. Ming Kuo and C. Chao, ***Image Segmentation based on fuzzy clustering algorithm***, Workshop on Machine Vision Applications Dec. 13-15, 1994.

[13] C. Kondermann, D. Kondermanna and M. Yanb, ***Blood Vessel Classification into Arteries and Veins in Retinal Images***, Interdisciplinary Center for Scientific Computing (IWR), Germany, Michelle Yan, Siemens Corporate Research, USA, 19 Feb 2008.

[14] C. S. McCaa, ***The Eye and Visual Nervous System: Anatomy***, Physiology and Toxicology, Environmental Health Perspectives Vol. 44, pp. 1-8, 1982.

[15] C. Sinthanayothin, J. Boyce, H. Cook and T. Williamson, ***Automated localization of the optic disc, fovea and retinal blood vessels from digital color fundus images***, Br. J. Opthalmol. 83:231–238, 1999.

[16] C. Thanapong, W. Watcharachai and R. Somporn, ***Extraction Blood Vessels from Retinal Fundus Image Based on Fuzzy C-Median Clustering Algorithm***, **IEEE**, 0-7695-2874-0/07, 2007.

[17] D. Dubois and H. Prade, ***Operations on fuzzy numbers***, Pages 613-626 | Received 14 Jul 1977, Published online: 27 Apr 2007.

[18] D. Patil, R. Manza and G. Bedke, ***Diagnose Glaucoma by Proposed Image Processing Methods***, **International Journal of Computer Applications** (0975 – 8887) Vol. 106 – No.8, 2014.

[19] DIARETDB1 database,http://www2.it.lut.fi/project/imageret/diaretdb1/.

[20] F. Amel, M. Mohammed and B. Abdelhafid, ***Improvement of the Hard Exudates Detection Method Used For Computer- Aided Diagnosis of Diabetic Retinopathy***, doi: 10.5815, I.J. Image, Graphics and Signal Processing, Algeria, 2012.

[21] F. Dernoncourt, ***Introduction to fuzzy logic***, MIT, January, 2013.

[22] F. W. Wellmer***, Statistical Evaluations in Exploration for Mineral Deposits,*** ISBN978-3-642-64325-5, Springer-Verlag Berlin Heidelberg 1998.

[23] G. B. Kande, P. V. Subbaiah, T. S.Savithri, ***Segmentation of Exudates and Optic Disk in Retinal Images***, Sixth Indian Conference on Computer Vision, Graphics & Image Processing, pp.535-542,**ISBN:** 978-0-7695-3476-3, 2009.

[24] G. Chandel, R. Kumar, D. Khare and S. Verma, ***Analysis of Image Segmentation Algorithms Using MATLAB***, **International Journal**

of Engineering Innovation & Research, Vol. 1, Issue 1, ISSN 2277 – 5668, 2012.

[25] G. Chen and T. Pham, ***Introduction to Fuzzy Sets, Fuzzy Logic and Fuzzy Control Systems***, University of Houston, Texas, ISBN 0-8493-1658-8, 2001.

[26] G. Tortora, and B. Derrickson, ***Principles of anatomy and physiology,*** 12th ed. Chichester: Wiley, 2009.

[27] G.T. Shrivakshan, Dr.C. Chandrasekar, ***A Comparison of various Edge Detection Techniques used in Image Processing*****, International Journal of Computer Science Issues (IJCSI)**, Vol. 9, Issue 5, No 1, ISSN (Online): 1694-0814, September 2012.

[28] H. F. Jelinek and M. J. Cree, ***Automated Image Detection of retinal pathology***, ISBN: 978-0-8493-7556-9 (Hardback), 2010.

[29] H. Jafariani, and H. Tabatabaee, ***Retinal Identification System using Fourier-Mellin Transform and Fuzzy Clustering***, **Indian Journal of Science and Technology**, Vol 7(9), 1289–1296, September 2014.

[30] H. Mohammed, H. Alnoamani and A. AbdulZahraa, ***Improved Fuzzy C-Mean Algorithm for Image Segmentation***, **International Journal of Advanced Research in Artificial Intelligence (IJARAI)**, Vol. 5, No.6 Iraq, 2016.

[31] J. Irani, N. Pise and M. Phatak, ***Clustering Techniques and the Similarity Measures used in Clustering: A Survey***, **International Journal of Computer Applications** (0975 – 8887) Vol. 134 – No.7, January 2016.

[32] J. Mendel, ***Fuzzy logic systems for engineering: A tutorial***, **Proceedings of the IEEE**, Vol. 83, No. 3, pp. 345–377, 1995.

[33] J. Patra, A. Kanti Manna, H. Moulick and A. kumar**, *Segmentation techniques used image reconigation and SAR Image Processing***, **IOSR Journal of Computer Engineering (IOSR-JCE)** e-ISSN: 2278-0661, p- ISSN: 2278-8727, Vol. 16, Issue 2, 2014.

[34] J. V. Oliveira, W. Pedrycz, ***Advances in Fuzzy Clustering and its Applications,*** ISBN: 978-0-470-06118-3. 454 pages, Wiley, June 2007.

[35] K. Saladin, ***Anatomy and Physiology: The Unity of Form and Function,*** (3rd edition), McGraw-Hill, New York, 2004.

[36] K. Wisaeng, N. Hiransakolwong and E. Pothiruk, ***AutomaticDetection of Optic Disc in Digital Retinal Images***, **International Journal of Computer Applications** (0975 – 8887) Vol. 90 – No 5, Thailand, March 2014.

[37] K. Kansal, E. Nishi, ***Automated Detection of Exudates for Diabetic Retinopathy Screening in Fundus Images Using CS-ACO Optimization Approach***, **International Journal of Bio-Science and Bio-Technology** Vol. 8, No.3, pp. 323-340, ISSN: 2233-7849, 2016.

[38] L .A. Zadeh, ***Fuzzy sets***, Department of Electrical Engineering and Electronics Research Laboratory, University of California, Berkeley, California, Vol. 8, Issue 3, USA, June 1965.

[39] L. Sherwood, ***Human Physiology: From Cells to Systems,*** (5^{th} edition), Belmont: Brooks Cole Thomson Learning, 2004.

[40] M. Gandhi**,** D. Raghavan, ***Detection and localization of retinal exudates for diabetic retinopathy***, DOI: 10.1142/S0218339015500102, April 2015.

[41] M. Hellmann, ***Fuzzy Logic Introduction***, LaboratoireAntennes Radar Telecom, F.R.E CNRS 2272, Equipe Radar Polarimetrie, Universit´e de Rennes 1, UFR S.P.M, Campus de Beaulieu - Bat. 22, 263 Avenue General Leclerc, CS 74205, 35042 Rennes Cedex, France, 2001.

[42] M. Yasuda, ***Fuzzy C-Means Clustering, Entropy Maximization, and Deterministic and Simulated Annealing***, doi: 10.5772/48659, 2012.

[43] Ministry of Health, ***Health Annual Report Palestine 2016***, General Directorate of Health Policies and Planning, Palestinian Health Information Center, July 2017.

[44] N. Efford, ***Digital Image Processing: A Practical Introduction Using JavaTM***, Pearson Education, http://www.cs.auckland.ac.nz/courses/compsci773s1c/lectures/ImageProcessing-html/topic4.htm. 2000,

[45] N. El Abbadi and E. Al Saadi, ***Blood Vessel Extraction Using Mathematical Morphology***, Journal of Computer Science 9 (10): 1389-1395, ISSN: 1549-3636, Iraq, 2013.

[46] N. Pattona, T. Aslamc, T. Gillivrayd and et al, ***Progress Retinal image analysis: Concepts, applications and potential in Retinal and Eye Research***, 2006.

[47] National Diabetes Information Clearinghouse (NDIC), ***Your Guide to Diabetes***, **NIH Publication** No. 14–4016, 2013.

[48] National Eye Institute, National Institutes of Health. Available **online at:** ***http://www.nei.nih.gov/***, referred September 2015.

[49] O. Kaya, ***Hnman Resource Performance Clustering by Using Self Regulating Clustering Method***, T.C. BAHÇEŞEHİR ÜNİVERSİTESİ Institute of Science Computer Engineering, Istanbul, 2008.

[50] O. Phyo and A. Khaing, ***Automatic Detection Of Optic Disc and Blood Vessel From Retinal Images Using Image Processing Techniques***, **IJRET: International Journal of Research in Engineering and Technology** EISSN: 2319-1163 | PISSN: 2321-7308, Vol: 03 Issue: 03, Mar-2014.

[51] P. Saine and M. Tyler, ***Ophthalmic Photography: Retinal Photography, Angiography, and Electronic Imaging,*** (2nd Edition), Butterworth-Heinemann Medical; ISBN: 0750673729, 2011.

[52] P. Szczepaniak and P. Lisboa, ***Fuzzy Systems in Medicine***, ISBN: 978-3-662-00395-4, Vol. 41, 2000.

[53] R. Akhavan and K. Faez, ***A Novel Retinal Blood Vessel Segmentation Algorithm using Fuzzy segmentation***, pp. 561~572, ISSN: 2088-8708. 561, Vol. 4, No. 4, Iran, August 2014.

[54] R. Aliev, ***Fundamentals of the Fuzzy Logic-Based Generalized Theory of Decisions***, ISBN:3642443435, Springer-Verlag Berlin and Heidelberg GmbH & Co. KG, USA, 2013.

[55] R. Bock, J. Meier, L. Nyúl, J. Hornegger, and Michelson, ***Glaucoma risk index: Automated glaucoma detection from color fundus images***, pp.471-481, 2010.

[56] R. C. Gonzalez, R. E. Woods and S. L. Eddins, ***Morphological Reconstruction from Digital Image Processing Using MATLAB,*** MATLAB Digest | Academic Edition.

[57] R. Dass, Priyanka and S. Devi, ***Image Segmentation Techniques***, ISSN: 2230-9543, IJECT Vol. 3, Issue 1, 2012.

[58] R. Gonzalez and R. Woods, ***Digital Image Processing (Third Edition)***, Upper Saddle River, New Jersey 07458, 2008.

[59] R. L. Burden, J. D. Faires, ***Numerical Analysis***, Ninth Edition, Cengage Learning, USA, 2010.

[60] R. Muthukrishnan and M. Radha, ***Edge Detection Techniques for Image Segmentation***, **International Journal of Computer Science & Information Technology (IJCSIT)** Vol 3, No 6, 2011.

[61] R. S. Jaiswal and M. V. Sarode, ***An Overview on Fuzzy Logic & Fuzzy Elements***, **International Research Journal of Computer Science (IRJCS)** ISSN: 2393-9842, Issue 2, Vol. 3, 2015.

[62] R. Sandhu, ***http://www.ranjitsandhu.co.uk/***, Consultant Ophthalmic Surgeon.

[63] R. Sharma, P. Mohindru and Pooja, ***Review of Segmentation Techniques for Melanoma Detection***, ISSN: 2277 128X **International Journal of Advanced Research in Computer Science and Software Engineering Research** ,Vol. 6, Issue 7, 2016.

[64] R. Li and Ch. Lu, ***Attribute Weighted Optimization of Fuzzy C-Means Clustering Algorithm***, College of Mathematics and Information Science, China, No. 6, 2015.

[65] S. Babu, S. Vijayan, A. Susan and et al, ***Automatic Segmentation of fovea and classification of different stages of diabetic retinopathy***, Hindusthan College of Engineering and Technology, Coimbatore, Surya Engineering College, Vol. 10, No. 7, India, 2015.

[66] S. Dastgheib, H. Oulia, H. Gholamishiri and A. Ebrahimi, ***A proposed fuzzy method to detect faulty nodes in wireless sensor network clustering structure***, Young Researchers Club, Shiraz Branch, Islamic Azad University, ISSN 2077-3528, Iran, 2012.

[67] S. Habashy, ***Identification of Diabetic Retinopathy Stages using Fuzzy C-means Classifier***, Electronic and Communication Department, Engineering Collage, Helwan University,International Journal of Computer Applications (0975 – 8887) Vol. 77 – No.9, Egypt, 2013.

[68] S. Mirajkar, M. Patil, ***Feature Extraction of Diabetic Retinopathy Images***, **International Journal of Computer Applications (IJCA)** (0975 – 8887) Proceedings on Emerging Trends in Electronics and Telecommunication Engineering (NCET), 2013.

[69] S. Rashid and Shagufta, ***Computerized Exudate Detection in Fundus Images Using Statistical Feature based Fuzzy C-mean Clustering***, No. 3, 135-145, 2013.

[70] S. Sawyer, ***The Method of Lagrange Multipliers***, October 25, 2002.

[71] T. Mapayi, J. Tapamo and S. Viriri, ***Retinal Vessel Segmentation: A Comparative Study of Fuzzy C-means and Sum Entropy Information on Phase Congruency***, doi: 10.5772/60581, University of Kwazulu-Natal, South Africa, 2015.

[72] V. V. Kumar and N. S. Yanan, ***Blood Vessel Extraction Using Wiener Filter and Morphological Operation***, **International Journal of Computer Science & Emerging Technologies** (E-ISSN: 2044-6004) 7 Vol. 1, Issue 4, India, December 2010.

[73] W. J. Chen, M. L. Giger, and U. Bick, ***A fuzzy c-means (FCM)-based approach for computerized segmentation of breast lesions in dynamic contrast enhanced MRI images,*** Acad. Radiol, Vol. 13, pp. 63-72, 2006.

[74] W. Pedrycz and F. Gomide, ***An Introduction to Fuzzy Sets: Analysis and Design***, London, England, 1998.

[75] www.researchgate.net.

[76] W. Yun, U. Acharya, Y. Venkatesh, C. Chee, L. Min and E. Ng, ***Identification of different stages of diabetic retinopathy using retinal optical images***, 2007.

[77] X. Bai and F. Zhou, ***Analysis of different modified top-hat transformations based on structuring element construction***, Image Processing Center, Beijing University of Aeronautics and Astronautics, 100191 Beijing, China, 2010.

[78] X. Wang, R. Hansch, L. Ma and O. Hellwich, ***Comparison of Different Color Spaces for Image Segmentation using Graph-cut***, Germany, 2014.

[79] Y. Yang and Sh. Huang, ***Image Segmentation by Fuzzy C-Means Clustering Algorithm with A Novel Penalty Term***, China, 2006.

Appendices

A-1: Sobel Filter

The Sobel operator or Sobel filter is a filter used in image processing to detect the edges by performing a 2-D spatial gradient measurement on an image. It is known that the image gradient defines the change in the intensity (or color) of an image. An edge in an image occurs when the gradient is remarkable and the Sobel operator makes use of this fact to find the edges in an image [27].

The Sobel operator calculates the approximate gradient of each pixel in an input image by convolving the image with a pair of square filters (for instance 3×3 as shown in Fig.A.1). The filter can be applied separately to the input image to produce separate measurements of the gradient component in each orientation; call these S_x and S_y (see Fig. A.2). One filter is simply the other one rotated by 90°. These can then be combined together to find the absolute magnitude of the gradient at each point and the orientation of that gradient.

The labeling of neighborhood pixels about the pixel $[i, j]$ are illustrated in Fig.A.1:

a_0	a_1	a_2
a_7	$[i,j]$	a_3
a_6	a_5	a_4

Fig.A.1: The labeling of neighborhood pixels [27].

The convolution masks of the Sobel detector are given in Fig.A.2 [27]:

-1	0	$+1$
-2	0	$+2$
-1	0	$+1$

S_x

$+1$	$+2$	$+1$
0	0	0
-1	-2	-1

S_y

Fig.A.2: Masks used by Sobel Operator [27].

The magnitude of the Sobel operator equals the computed gradient in equation (A.1):

$$S = \sqrt{S_x^2 + S_y^2} \qquad (A.1)$$

where the partial derivatives are computed in equations A.2 and A.3:

$$S_x = (a_2 + ca_3 + a_4) - (a_0 + ca_7 + a_6) \qquad (A.2)$$

$$S_y = (a_0 + ca_1 + a_2) - (a_6 + ca_5 + a_4) \qquad (A.3)$$

where c is a constant equals 2 for this case,

A-2: Color Space Overview

Visible light ranging with wavelengths between 400 and 700 nanometers as shown in Fig.A.3 is a small part of the electromagnetic spectrum; human eye can only detect visible light. The color of visible light depends on its wavelength. For instance, violet has a wavelength of 400 nanometers, on the other hand, red color has a wavelength of 700 nanometers [26].

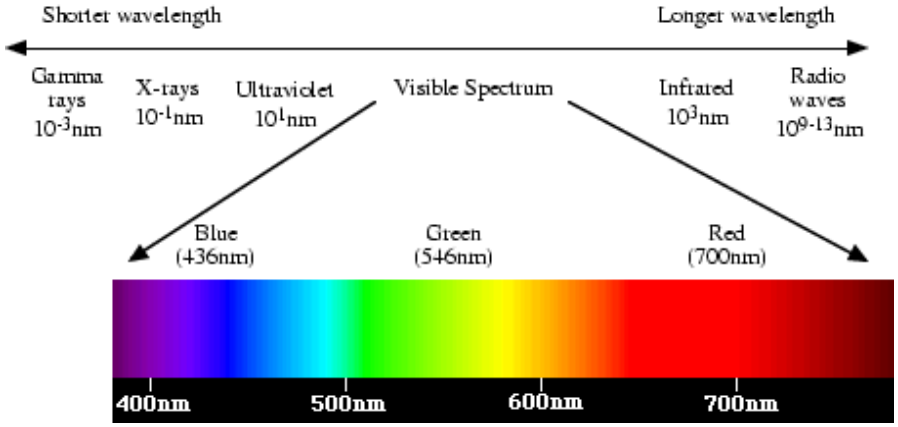

Fig.A.3: Electromagnetic spectrum [26].

Color spaces are different types of color modes, used in image processing. The color space aims to aid the process of describing color, either between people, machines or programs. The RGB, XYZ, HSI, Lab and Luv are examples of color spaces that can be used as features for FCM clustering [75].

A-2.1 Common Color Space Types

RGB color space is simple and most common type of color spaces, which consists of three channels Red, Green and Blue respectively [75], this is shown in Fig.A.4: (b-d).

Since the RGB color space can't produce a color equivalent to any wavelength; in converting the red color components into the corresponding wavelength value it might be negative, hence in 1931 the International Commission on Illumination (CIE) defined three standard primaries: X, Y, and Z, to replace red, green, and blue [75, 2].

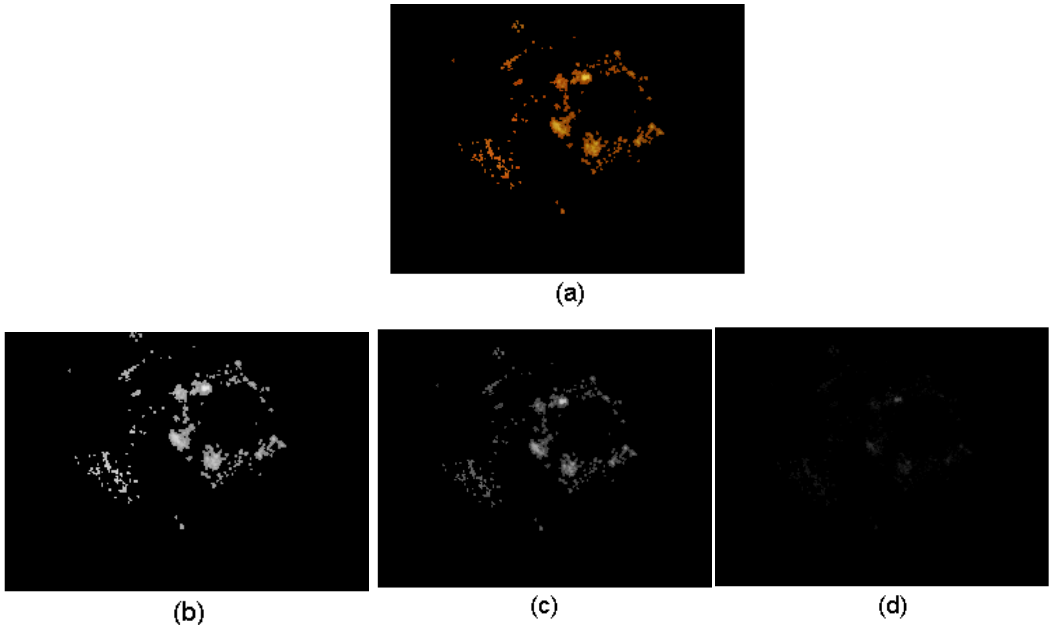

Fig.A.4: RGB channels: (a) Retinal RGB image, (b) Red, (c) Green, (d) Blue.

The **XYZ color space** can produce every color with positive tristimulus values and display color differences more conveniently. It consists of three component X, Y and Z, these components are shown in Fig.A.5. The matrix

equation (eq.A.4) is used in transforming an image from RGB to XYZ, shown in the equation below:

$$\begin{bmatrix} X \\ Y \\ Z \end{bmatrix} = \begin{bmatrix} 0.412435 & 0.357580 & 0.180423 \\ 0.212671 & 0.715160 & 0.072169 \\ 0.019334 & 0.119193 & 0.950227 \end{bmatrix} * \begin{bmatrix} R \\ G \\ B \end{bmatrix} \qquad (A.4)$$

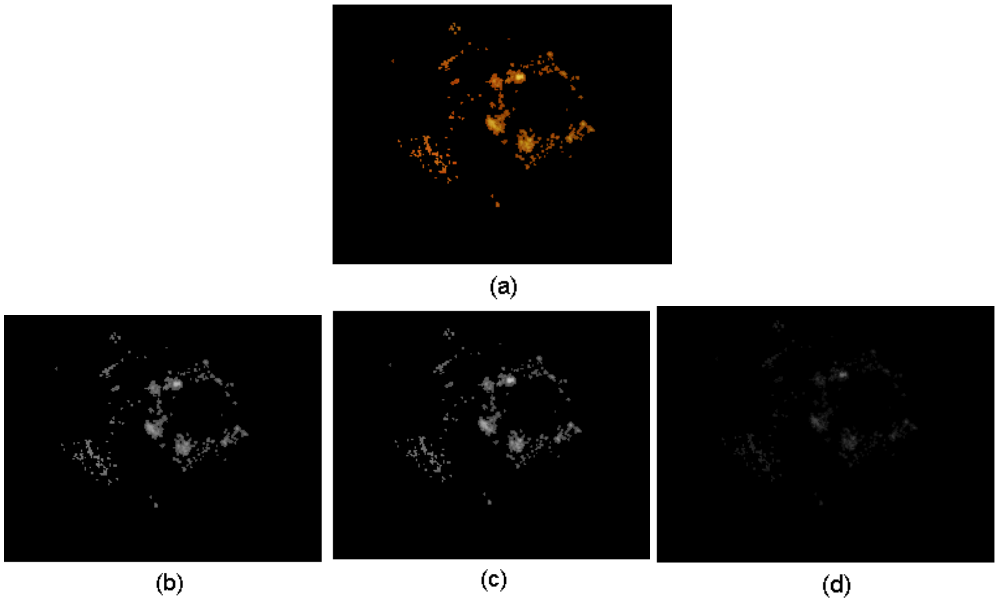

Fig.A.5: XYZ color space: (a) Retinal RGB image, (b) X, (c) Y, (d) Z, components.

HSI color space is very attractive color space, it is important in image processing applications because it represents colors in a similar way how the human eye senses colors. HSI consist of three components: hue (H), saturation (S) and intensity (I) [75]. Fig.A.6 illustrates how the HSI color space represents colors.

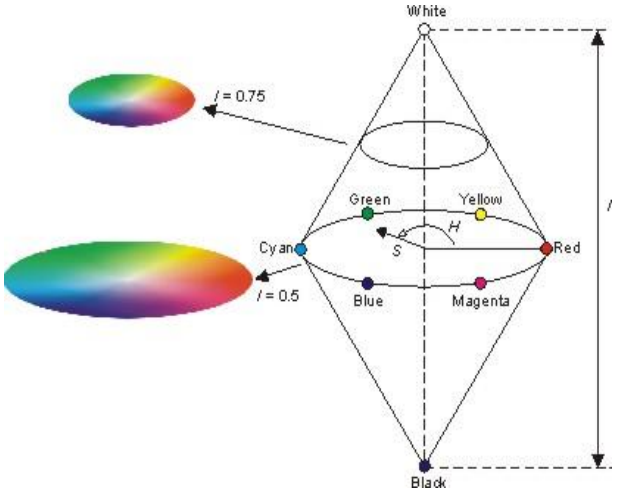

Fig.A.6: The HSI color space [50].

We notice in Fig.A.6 that the Hue component represents the color between 0 and 360 degrees, the saturation component has the range between 0 and 1, where saturation refers how much the color is polluted with white color. The Intensity range is between 0 and 1, where 0 means black, and 1 means white, a retinal RGB image is represented in HSI color components shown in Fig.A.7.

The equations used to convert RGB to HSI are described here; Hue component of each RGB pixel is obtained using the following equation [15,50]:

$$H = \begin{cases} \theta, B \leq G \\ 360 - \theta, B > G \end{cases} \qquad (A.5)$$

where θ is:

$$\theta = \cos^{-1}\left\{\frac{\frac{1}{2}[(R-G)+(R-B)]}{[(R-G)^2+(R-B)(G-B)]^{\frac{1}{2}}}\right\}. \qquad (A.6)$$

The saturation component is defined by equation (A.7):

$$S = 1 - \frac{3}{(R+G+B)}[\min(R,G,B)]\,. \qquad (A.7)$$

Finally, the intensity component is defined by equation (A.8):

$$I = \frac{1}{3} * (R + G + B). \qquad (A.8)$$

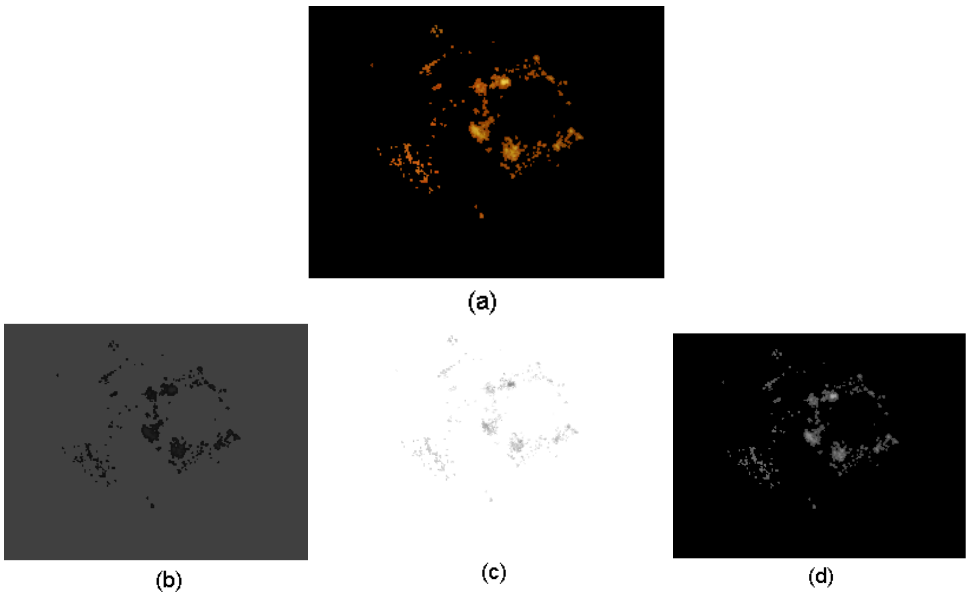

Fig.A.7: HSI channels: (a) Retinal RGB image, (b) Hue,

(c) Saturation, (d) Intensity components.

The **L*a*b color space** is the most beneficial and widely utilized color space; it was developed as a refinement of the XYZ color space. In L*a*b model the color is represented into three components and it is device independent (see Fig.A.8).

Where: L is the luminance and it varies in uniform step from 0 for black to 100 for white. The (a) is expressed as $+a/-a$ and (b) is expressed as $+b/-b$ denotes red-green and blue-yellow respectively. This color space is used in color faxing and JPEG compression [75].

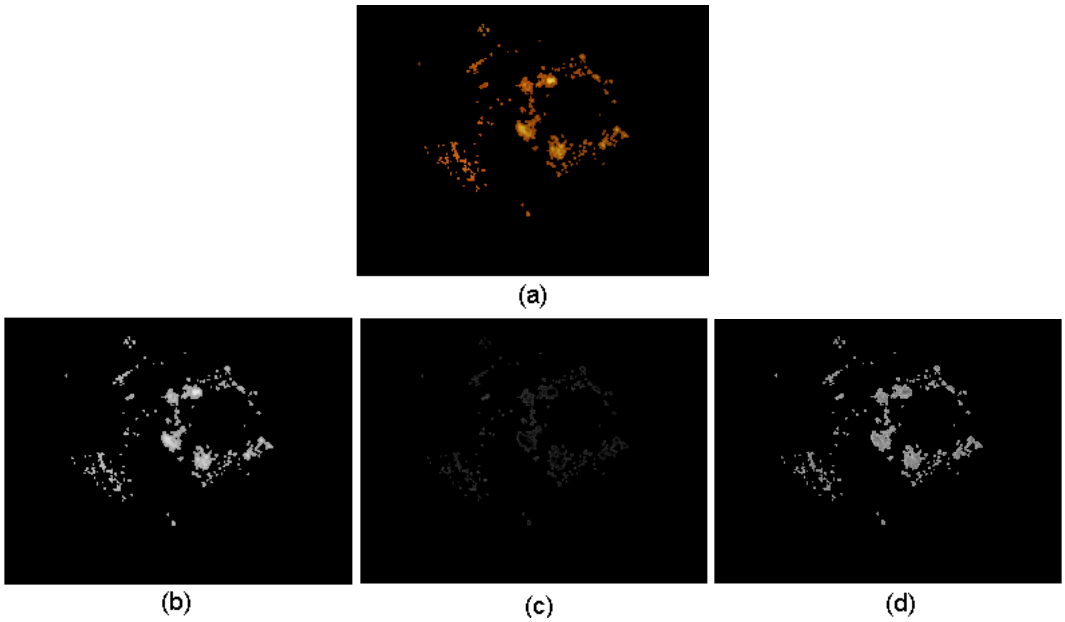

Fig.A.8: Lab channels: (a) Retinal RGB image, (b) L component, (c) a component, (d) b component.

The equations used to convert Lab to XYZ are shown here [2]:

$$\mathrm{L} = \begin{cases} 116 * f(\mathrm{Y}/\mathrm{Y_n}) - 16, \mathrm{Y}/\mathrm{Y_n} > 0.008856 \\ 903.3 * (\mathrm{Y}/\mathrm{Y_n}), \qquad otherwise \end{cases} \tag{A.9}$$

$$a = 500 * (f(\mathrm{X}/\mathrm{X_n}) - f(\mathrm{Y}/\mathrm{Y_n})) \tag{A.10}$$

$$b = 200 * (f(\mathrm{Y}/\mathrm{Y_n}) - f(\mathrm{Z}/\mathrm{Z_n})) \tag{A.11}$$

where

$$f(\mathrm{X}/\mathrm{X_n}) = \begin{cases} (\mathrm{X}/\mathrm{X_n})^{\frac{1}{3}}, \qquad (\mathrm{X}/\mathrm{X_n}) > 0.008856 \\ 7.787 * (\mathrm{X}/\mathrm{X_n}) + 16/116, otherwise \end{cases} \tag{A.12}$$

$$f(\mathrm{Y}/\mathrm{Y_n}) = \begin{cases} (\mathrm{Y}/\mathrm{Y_n})^{\frac{1}{3}}, \qquad (\mathrm{Y}/\mathrm{Y_n}) > 0.008856 \\ 7.787 * (\mathrm{Y}/\mathrm{Y_n}) + 16/116, otherwise \end{cases} \tag{A.13}$$

Here X_n, Y_n and Z_n are the tristimulus values of the reference white [75].

The **Luv color space** is especially useful for additive mixtures of lights, due to its linear addition properties, it is based on XYZ color space, it contains three components: L, u and v. An example is shown in Fig.A.9: (b-d); the L component means brightness or luminance, it has the range $[0,100]$, the u component seems to mimic mostly shifts from green to red, which has the range $[-134,220]$, and the v component seems to mimic mostly blue and purple type colors, it has the range $[-140,122]$.

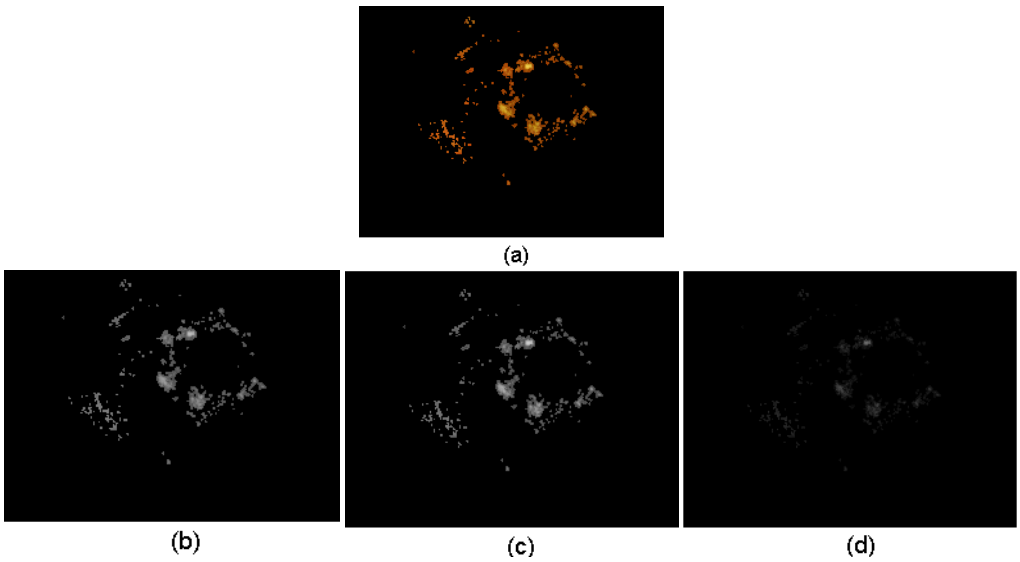

Fig.A.9: Luv channels: (a) Retinal RGB image, (b) L, (c) u, (d) v components.

The transformation formulas between XYZ and Luv color space are following below [2]:

$$L = 116 * \left(\frac{Y}{Y_n}\right)^{\frac{1}{3}} - 16 \qquad (A.14)$$

$$u = 13 * L * (u' - u'_n) \qquad (A.15)$$

$$v = 13 * L * (v' - v'_n) \qquad (A.16)$$

where

$$u' = 4 * \frac{X}{X + 15 * Y + 3 * Z} \quad (A.17)$$

$$v' = 9 * \frac{Y}{X + 15 * Y + 3 * Z} \quad (A.18)$$

$$u'_n = 4 * \frac{X_n}{X_n + 15 * Y_n + 3 * Z_n} \quad (A.19)$$

$$v'_n = 9 * \frac{Y_n}{X_n + 15 * Y_n + 3 * Z_n} \quad (A.20)$$

where X_n, Y_n and $Z_n$are the tristimulus values of the reference white [75].

A-3: Lagrange multiplier

The method of Lagrange multipliers allows us to maximize or minimize functions with constraints by only considering points on a certain surface.

In general, the Lagrangian is the sum of the original objective function added to a term that involves the functional constraint multiplied by a Lagrange multiplier λ [70].

The following steps explain the Lagrangian method:

1. Introduce a new variable λ, and define a new function L as follows:

$$L(x, \lambda) = f(x) + \lambda\big(b - g(x)\big) \quad (A.21)$$

where $f(x)$ is a function, $g(x) = b$ is the constraint, L called Lagrangian function and λ called Lagrange multiplier.

1 Find the critical points by setting the gradient of L to be equal to zero:

$$\frac{\partial}{\partial x} L(x, \lambda) = 0 \quad (A.22)$$

2 Remove the value λ by substituting their value resulting from the previous step in function $f(x)$, since $f(x)$ doesn't have λ as an input.

Whichever give the greatest (or smallest) value is the maximum (or minimum) point you are seeking.

We explained the method by solving an example, in this example we wish to minimize the $f(x, y) = x^2 + y^2$ subject to the constraint $x + y = 1$.

Let us first define the new function called L, new variable λ and rewrite the constraint as $x + y - 1 = 0$

$$L(x, y, \lambda) = x^2 + y^2 + \lambda(\, x + y - 1)$$

After that, take the partial derivatives of the Lagrange function and set them to zero:

$$\frac{\partial L}{\partial x} = 2x + \lambda = 0, \quad \frac{\partial L}{\partial y} = 2y + \lambda = 0, \qquad \frac{\partial L}{\partial \lambda} = \; x + y - 1 = 0.$$

Now, solve the resulting equation:

$$\lambda = -1, \quad x = y = \frac{1}{2}$$

$p = \left(\frac{1}{2}, \frac{1}{2}\right)$ gives the minimum value $\left(\frac{1}{2}\right)^2 + \left(\frac{1}{2}\right)^2 = \frac{1}{4} + \frac{1}{4} = \frac{1}{2}$ in the constrained subspace.

A-4: FCM clustering Example

To illustrate how the FCM clustering algorithm works, we propose here a simple example:

Let A be the features matrix of size 3×3, A is input for FCM, which means 3 input elements have 3 distinct features. After applying FCM algorithm the output is the list of cluster centers (v), and membership grade (μ) for each element.

Suppose we have:

$A = \begin{bmatrix} 220 & 190 & 210 \\ 150 & 130 & 200 \\ 170 & 202 & 100 \end{bmatrix}$, number of clustering = 2, $\varepsilon = 0.00001$ starting with random values of the membership such as:

$\boldsymbol{U}^{(0)} = \begin{bmatrix} 0.4869 & 0.6241 & 0.2680 \\ 0.5131 & 0.3759 & 0.7320 \end{bmatrix}$.

We apply these inputs in the FCM , then:

Iteration #1:

$$\boldsymbol{U}^{(1)} = \begin{bmatrix} 0.6328 & 0.8298 & 0.1851 \\ 0.3672 & 0.1702 & 0.8149 \end{bmatrix}$$

$$\boldsymbol{V}^{(1)} = \begin{bmatrix} 175.8181 & 157.7698 & 193.1133 \\ 180.9923 & 187.8244 & 145.8159 \end{bmatrix}$$

$$J(1) = 5.9271 * 10^3$$

Iteration #2:

$$\boldsymbol{U}^{(2)} = \begin{bmatrix} 0.7413 & 0.9047 & 0.0410 \\ 0.2587 & 0.0953 & 0.9590 \end{bmatrix}$$

$$\boldsymbol{V}^{(2)} = \begin{bmatrix} 175.5659 & 153.5863 & 200.5160 \\ 177.4425 & 197.5262 & 121.4128 \end{bmatrix}$$

$$J(2) = 4.6156 * 10^3$$

Iteration #3:

$$\boldsymbol{U}^{(3)} = \begin{bmatrix} 0.8043 & 0.9093 & 0.0061 \\ 0.1957 & 0.0907 & 0.9939 \end{bmatrix}$$

$$\boldsymbol{V}^{(3)} = \begin{bmatrix} 178.1094 & 154.1612 & 203.8892 \\ 173.1782 & 200.5367 & 108.3056 \end{bmatrix}$$

$$J(3) = 3.8971 * 10^3$$

Iteration #4:

$$\boldsymbol{U}^{(4)} = \begin{bmatrix} 0.8331 & 0.8978 & 0.0021 \\ 0.1669 & 0.1022 & 0.9979 \end{bmatrix}$$

$$\boldsymbol{V}^{(4)} = \begin{bmatrix} 180.7280 & 156.3397 & 204.3871 \\ 171.6921 & 200.9826 & 104.8687 \end{bmatrix}$$

$$J(4) = 3.7861 * 10^3$$

Iteration #5:

$$\boldsymbol{U}^{(5)} = \begin{bmatrix} 0.8470 & 0.8887 & 0.0014 \\ 0.1530 & 0.1113 & 0.9986 \end{bmatrix}$$

$$\boldsymbol{V}^{(5)} = \begin{bmatrix} 182.3850 & 157.7587 & 204.6261 \\ 171.1456 & 200.9494 & 103.9746 \end{bmatrix}$$

$$J(5) = 3.7620 * 10^3$$

Iteration #6:

$$\boldsymbol{U}^{(6)} = \begin{bmatrix} 0.8542 & 0.8832 & 0.0012 \\ 0.1458 & 0.1168 & 0.9988 \end{bmatrix}$$
$$\boldsymbol{V}^{(6)} = \begin{bmatrix} 183.3184 & 158.5587 & 204.7596 \\ 170.8932 & 200.8651 & 103.6911 \end{bmatrix}$$

$$J(6) = 3.7550 * 10^3$$

Iteration #7:

$$\boldsymbol{U}^{(7)} = \begin{bmatrix} 0.8579 & 0.8801 & 0.0011 \\ 0.1421 & 0.1199 & 0.9989 \end{bmatrix}$$
$$\boldsymbol{V}^{(7)} = \begin{bmatrix} 183.8300 & 158.9972 & 204.8328 \\ 170.7658 & 200.8016 & 103.5871 \end{bmatrix}$$

$$J(7) = 3.7529 * 10^3$$

Iteration #8:

$$\boldsymbol{U}^{(8)} = \begin{bmatrix} 0.8599 & 0.8783 & 0.0011 \\ 0.1401 & 0.1217 & 0.9989 \end{bmatrix}$$
$$\boldsymbol{V}^{(8)} = \begin{bmatrix} 184.1080 & 159.2355 & 204.8725 \\ 170.6991 & 200.7621 & 103.5446 \end{bmatrix}$$

$$J(8) = 3.7523 * 10^3$$

Iteration #9:

$$\boldsymbol{U}^{(9)} = \begin{bmatrix} 0.8610 & 0.8774 & 0.0011 \\ 0.1390 & 0.1226 & 0.9989 \end{bmatrix}$$
$$\boldsymbol{V}^{(9)} = \begin{bmatrix} 184.2586 & 159.3646 & 204.8940 \\ 170.6637 & 200.7392 & 103.5255 \end{bmatrix}$$

$$J(9) = 3.7521 * 10^3$$

Iteration #10:

$$\boldsymbol{U}^{(10)} = \begin{bmatrix} 0.8616 & 0.8769 & 0.0011 \\ 0.1384 & 0.1231 & 0.9989 \end{bmatrix}$$
$$\boldsymbol{V}^{(10)} = \begin{bmatrix} 184.3401 & 159.4344 & 204.9056 \\ 170.6448 & 200.7264 & 103.5164 \end{bmatrix}$$

$$J(10) = 3.7521 * 10^3$$

We note in iteration 10 the condition in equation (4.4.4) is satisfied, where $J(10) - J(9) < 10^{-5}$; (in this example we used 5 digits format to display the results; hence it is not clear that the difference between iterations 10 and

9 is 10^{-5}, but in computer it is evident), hence stop. $\boldsymbol{U}^{(10)}$and $\boldsymbol{V}^{(10)}$ are the output of the FCM clustering algorithm, which means that the elements 1 & 2 belong to first cluster group with degree of membership equal 0.8616 and 0.8769 respectively, we note also that the elements 1 & 2 belong to the second cluster group with 0.13840 and 0.1231, while element 3 belongs to the second cluster group with degree of membership 0.9989, this is shown in Fig.A.10, results explain how data distributes around the clustering centers.

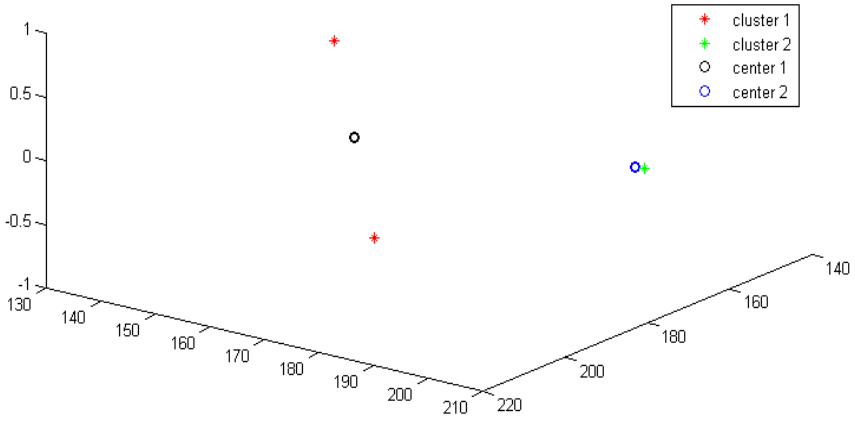

Fig.A.10: FCM clustering data, and data distribution around the clustering centers

However, to understand FCM clustering, and how data is distributed around the centers based on number of cluster (c); see Fig.A.11.

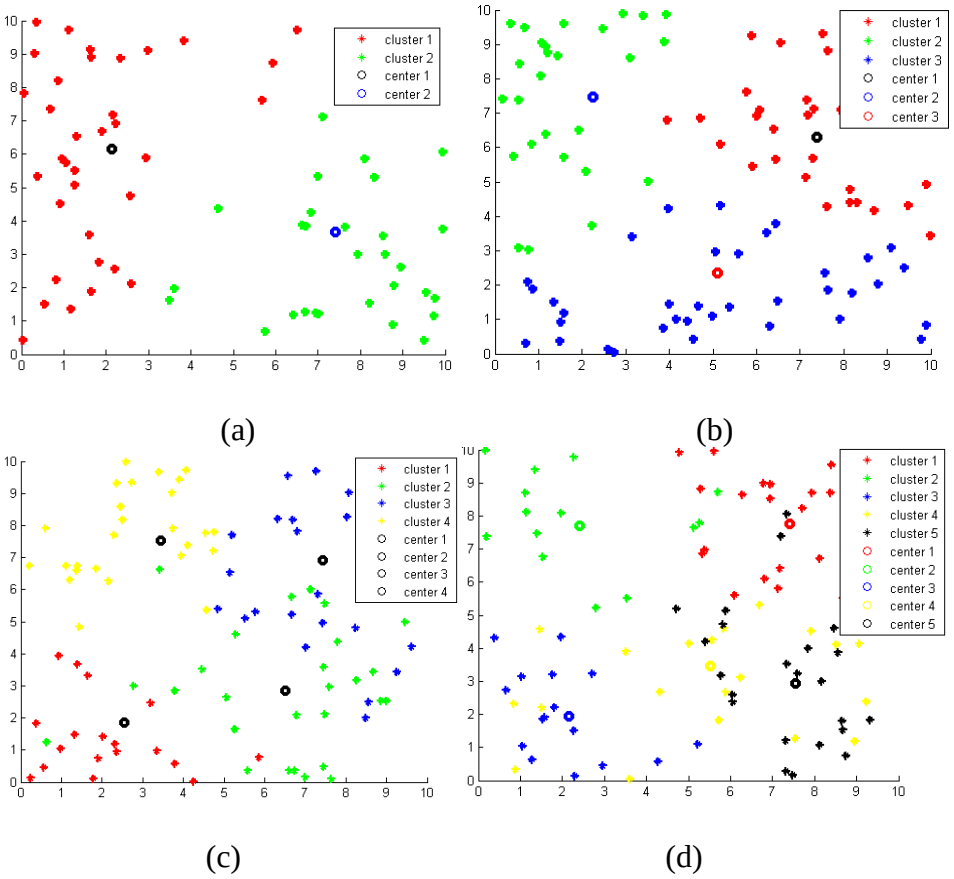

Fig.A.11: Changing the number of cluster in FCM using random data with: (a) c= 2, (b) c=3, (c) c= 4, (d) c=5.

A-5: Exudates Detection from Retinal Images

In this part we display the exudates detection results for testing retinal image number (5), compare it with GT of the image before and after applying mathematical morphology and explain the difference between detection and GT.

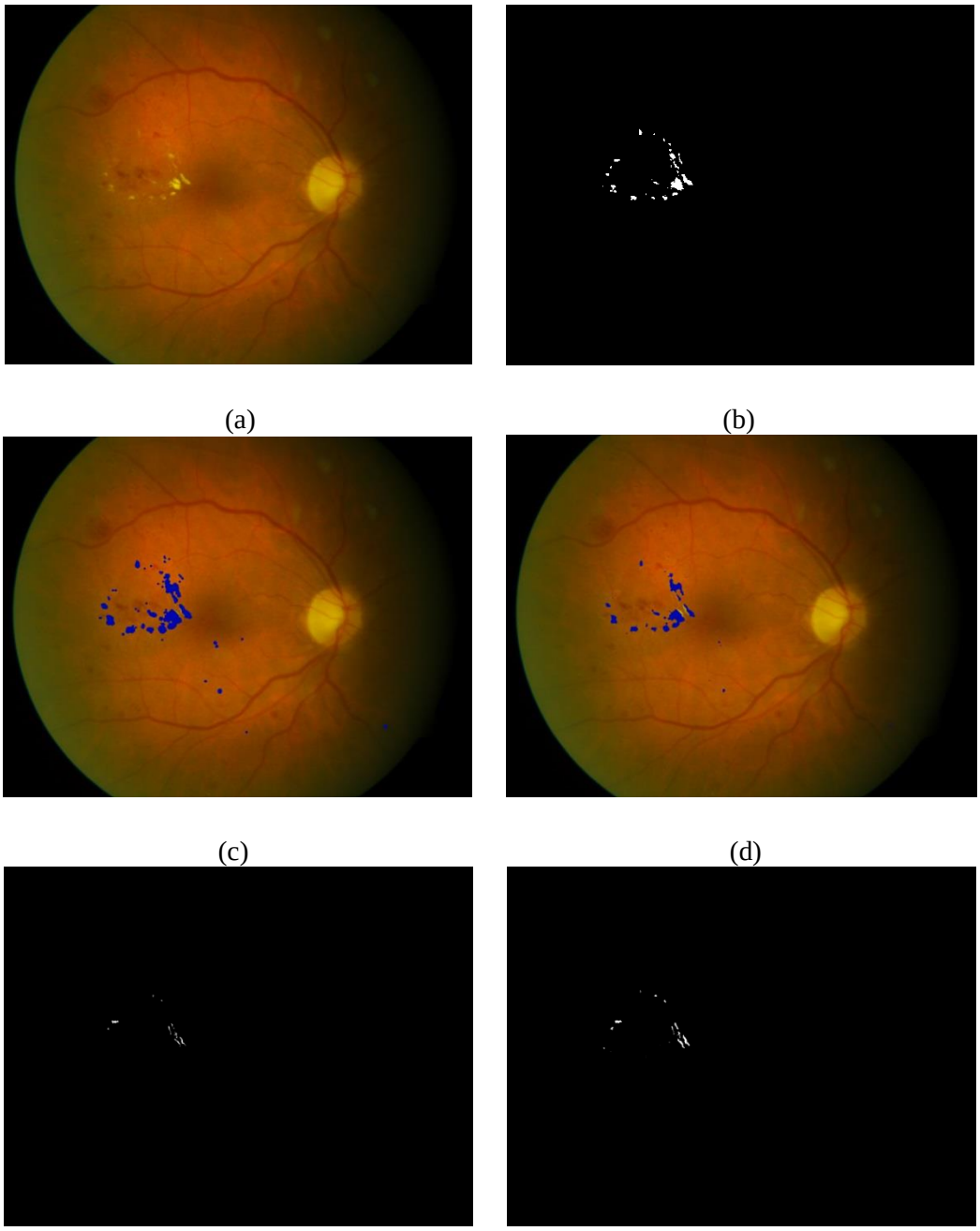

Fig.A.12: Exudates detection for testing retinal image number (5) :(a) RGB retinal image, (b) ground truth (GT) image, (c) exudates detection using FCM clustering, (d) exudates detection using FCM clustering after applied mathematical morphology, (e) the difference between GT and extracted exudates images, (f) the difference between GT and extracted exudates images after applying mathematical morphology.

A-6: MatlabCodes

%matlab code for detection the exudate from retinal images using FCM clustering algorithm

```
Clc
Clear
Close all
format long
tic
i=2;   % image number
switch i
case 1
RGB = imread('image005.png');
TargetImg=imread('GT_5.png');

case 2
RGB = imread('image015.png');
TargetImg=imread('GT_15.png');

case 3
RGB = imread('image016.png');
TargetImg=imread('GT_16_n.png');

case 4
RGB = imread('19.png');
```

```
TargetImg=imread('GT_19.png');

case 5
RGB = imread('image008.png');
TargetImg=imread('GT_8.png');

case 6
RGB = imread('image025.png');
TargetImg=imread('GT_25_n.png');

case 7
RGB = imread('image021.png');
TargetImg=imread('GT_21.png');

case 8
RGB = imread('image018.png');
TargetImg=imread('GT_18_n.png');

case 9
RGB = imread('image003.png');
TargetImg=imread('GT_3.png');

case 10
RGB = imread('image012.png');
```

```
TargetImg=imread('GT_12_nn.png');
    end

% Extract the Optic Disc (OD)
[OD_1,centers]=od_detection(RGB);

% extract the blood vessels network
vessel=vessel_e_fun(OD_1);

% Extract expected exudates from retinal image
pre_expected_exudate=pre_exudate_detection_fn(vessel,TargetImg);

% Feature extraction functions for RGB retinal image
feature_matrix=feature_function(pre_expected_exudate,centers);
[a,b]=size(feature_matrix);

% Apply fuzzy c-mean (FCM) clustering algorithm  using one feature
as input, then evaluate the system
for f=1:b
feature_matrix_in=feature_matrix(:,f);
num_of_cluster=2;
perfo_table=fcm_function_new_2(feature_matrix_in,pre_expected_exudate
,num_of_cluster,TargetImg);
performance_1(f,:)=[0 0 0 0 f perfo_table];
```

```
end
performance_1
% Apply FCM clustering using two features together as input
count=f;
for f1=1:b-1
    for f2=f1+1:b
count=count+1;
feature_matrix_in=[feature_matrix(:,f1);
feature_matrix(:,f2)];
num_of_cluster=2;
perfo_table=fcm_function_new_2(feature_matrix_in,pre_expected_exudate
,num_of_cluster,TargetImg);
performance_1(count,:)=[0 0 0 f1 f2 perfo_table];
end
    end
performance_1;
% Apply FCM clustering using three features together as input
count=count;
for f3=1:b-2
    for f4=f3+1:b-1
        for f5=f4+1:b
count=count+1;
feature_matrix_in=[feature_matrix(:,f3) feature_matrix(:,f4)
feature_matrix(:,f5)];
```

```
num_of_cluster=2;
perfo_table=fcm_function_new_2(feature_matrix_in,pre_expected_exudate
,num_of_cluster,TargetImg);
performance_1(count,:)=[0 0 f3 f4 f5 perfo_table];
end
    end
        end
performance_1;
```

% Apply FCM clustering using four features together as input

```
count=count;
for f6=1:b-3
    for f7=f6+1:b-2
        for f8=f7+1:b-1
            for f9=f8+1:b
count=count+1;
feature_matrix_in=[feature_matrix(:,f6)                feature_matrix(:,f7)
feature_matrix(:,f8) feature_matrix(:,f9)];
num_of_cluster=2;
perfo_table=fcm_function_new_2(feature_matrix_in,pre_expected_exudate
,num_of_cluster,TargetImg);
performance_1(count,:)=[0 f6 f7 f8 f9 perfo_table];
end
     end
         end
```

جامعة النجاح الوطنية
كلية الدراسات العليا

الكشف التلقائي لاعتلال شبكية العين بمرض السكري باستخدام خوارزمية متوسطات المراكز الضبابية

إعداد
تحرير نبيل دويكات

إشراف
د. هادي حمد

قدمت هذه الأطروحة استكمالا لمتطلبات الحصول على درجة الماجستير في الرياضيات المحوسبة بكلية الدراسات العليا في جامعة النجاح الوطنية في نابلس، فلسطين.
2018م

الكشف التلقائي لاعتلال شبكية العين بمرض السكري باستخدام
خوارزمية متوسطات المراكز الضبابية

إعداد
تحرير نبيل دويكات
إشراف
د. هادي حمد

الملخص

اعتلال الشبكية بمرض السكري يعتبر من أكثر الأمراض خطورة على العين؛ التي تؤدي الى فقدان البصر الذي يصاب فيه مرضى السكري. تعتبر الافرازات من أولى العلامات الدالة على الاصابة بالمرض، لذلك من المهم اكتشافها واحصائها، من أجل العلاج والوقاية من تفاقم المرض وفقدان البصر.

في هذه الرسالة قمنا باقتراح طريقة تلقائية (اوتوماتيكية) للكشف عن الافرازات من صور شبكية العين لمرضى السكري، وذلك باستخدام خوارزمية متوسطات المراكز الضبابية بالاضافة الى مجموعة من تقنيات معالجة الصور باستخدام برنامج الماتلاب.

لقد قمنا بعرض بعض المفاهيم الهامة عن أجزاء العين، مرض اعتلال الشبكية بالسكري، تقنيات وطرق معالجة الصور وكذلك الانظمة الضبابية، ونخص بالذكر خوارزمية متوسطات المراكز الضبابية. بعد ذلك قمنا بالتطبيق على صور شبكية العين لمرضى السكري، وكانت الخوارزمية تعتمد اولا على استخراج قرص العين والاوعية الدموية وذلك لتحسين عملية اكتشاف الافرازات، ثم قمنا بتعيين وتحديد الافرازات.

في النهاية تم تقييم النتائج عن طريق حساب الحساسية، النوعية والدقة بمقارنتها بالصور التي تم رسمها عن طريق الاخصائيين والأطباء، وكانت متوسطات النتائج كما يلي: 86.29 %, 98.42% و 98.35% على التوالي.